Department of
Mineral and Petroleum Resources

REPORT
82

GEOLOGY OF THE SHOEMAKER IMPACT STRUCTURE WESTERN AUSTRALIA

by F. Pirajno

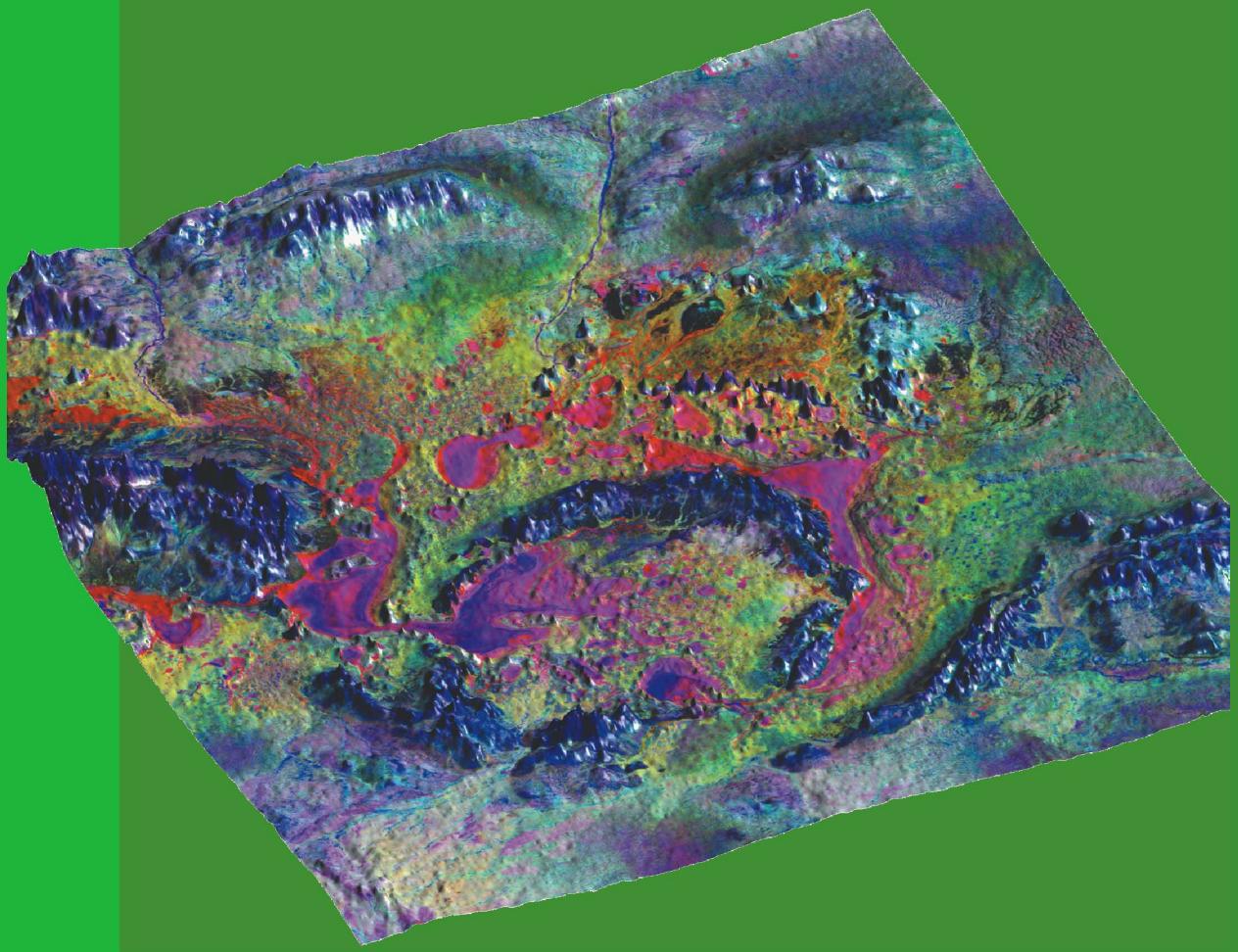

Geological Survey of Western Australia

GEOLOGICAL SURVEY OF WESTERN AUSTRALIA

REPORT 82

GEOLOGY OF THE SHOEMAKER IMPACT STRUCTURE, WESTERN AUSTRALIA

by
F. Pirajno

with contributions from
A. Y. Glikson[1], D. Phillips[2], and T. Uysal[3]

[1] Research School of Earth Sciences, Australian National University, Canberra, A.C.T.
[2] School of Earth Sciences, University of Melbourne, Melbourne, Victoria
[3] Department of Earth Sciences, University of Queensland, Brisbane, Queensland

This Report is dedicated to Eugene and Carolyn Shoemaker as a tribute to their work on meteorite impact structures in Australia

Perth 2002

REFERENCE
The recommended reference for this publication is:
PIRAJNO, F., 2002, Geology of the Shoemaker impact structure, Western Australia: Western Australia Geological Survey, Report 82, 52p.

National Library of Australia
Cataloguing-in-publication entry

Pirajno, Franco, 1939–
Geology of the Shoemaker impact structure, Western Australia

Bibliography.
ISBN 0 7307 5722 6

1. Geology — Western Australia — Earaheedy Basin.
2. Earaheedy Basin (W.A.).
I. Glikson, A. Y. (Andrew Yoram).
II. Uysal, T.
III. Phillips, D. (David), 1961–.
IV. Geological Survey of Western Australia.
V. Title. (Series: Report (Geological Survey of Western Australia); 82).

559.41

ISSN 0508–4741

Grid references in this publication refer to the Geocentric Datum of Australia 1994 (GDA94). Locations mentioned in the text are referenced using Map Grid Australia (MGA) coordinates, Zone 50. All locations are quoted to at least the nearest 100 m.

Copy editor: D. P. Reddy
Cartography: Lisa Cosgrove
Desktop publishing: K. S. Noonan
Printed by Haymarket Printing, Perth, Western Australia

Published 2002 by Geological Survey of Western Australia

Copies available from:
Information Centre
Department of Mineral and Petroleum Resources
100 Plain Street
EAST PERTH, WESTERN AUSTRALIA 6004
Telephone: (08) 9222 3459 Facsimile: (08) 9222 3444
This and other publications of the Geological Survey of Western Australia are available online through the Department's bookshop at www.mpr.wa.gov.au

Cover photograph:
Landsat image of the Shoemaker impact structure; principal components 1, 2, and 3 (all bands) as RGB over DEM (data from Geoscience Australia). Vertical exaggeration is 1500: view looking northeast.

Contents

Appendices

Plate

Figures

Tables

Geology of the Shoemaker impact structure, Western Australia

by
F. Pirajno

with contributions from
A. Y. Glikson[1], D. Phillips[2], and T. Uysal[3]

Abstract

The Shoemaker impact structure, on the southern margin of the Palaeoproterozoic Earaheedy Basin, consists of two well-defined concentric ring structures surrounding a basement uplift. The concentric structures include a ring syncline and a ring anticline, formed in sedimentary rocks of the Earaheedy Group, with an outer diameter of about 30 km. Aeromagnetic data indicate that the Shoemaker impact structure is deeply eroded and tilted to the east, and combined with morphometric calculations indicate a 30 km-diameter impact structure, partly surrounded by a 90 km-diameter ring fault. The central basement uplift, with a diameter of 12 km, consists of fractured Archaean granitoids of overall syenitic composition belonging to the Teague Granite.

The precise age of the impact is not known, but recent dating of the Teague Granite of the central uplift indicates a maximum age of c. 1300 Ma (Ar–Ar determinations on K-feldspar) and a minimum age of c. 568 Ma (K–Ar on illite–smectite). Shock metamorphic features include shatter cones in sedimentary rocks and planar deformation features in quartz crystals of the Teague Granite. Pseudotachylite veins have not been recognized with certainty during the present investigation, although they were previously reported.

The Teague Granite consists principally of albite, quartz, and K-feldspar with subordinate amounts of alkali pyroxene. The alkali-rich syenitic composition of the Teague Granite suggests that it could be either one of a late Archaean suite of alkaline plutons that intruded the Yilgarn Craton, or the product of alteration of a granite by alkali metasomatism related to an impact-generated heat source. Locally, the Teague Granite exhibits partial to pervasive silicification, is fractured, and contains hydrothermal minerals, such as fibrous amphibole, garnet, sericite, and prehnite, consistent with metasomatism. The illite–smectite K–Ar age of 568 Ma probably represents hydrothermal activity triggered by impact-related heat energy.

KEYWORDS: impact structure, Earaheedy Basin, Teague Granite, alkali metasomatism, shatter cones, hydrothermal alteration.

Introduction

The Shoemaker impact structure, formerly known as the 'Lake Teague Ring Structure', is about 30 km in diameter and one of the oldest known impact features in Australia, with a possible age between 1300 and 568 Ma. The structure is on the southern margin of the Palaeoproterozoic Earaheedy Basin, Western Australia, with the centre at 25°52'S, 120°53'E (MGA 258820E 7137600N; Figs 1 and 2, Plate 1). The nearest town is Wiluna, about 110 km to the southwest. Western Australia is well endowed with meteorite impact structures (Fig. 1), which range in age from about 0.3 to 1000 Ma (Glikson, 1996). More impact structures may be discovered as detailed geophysical data become available and geoscientists become increasingly aware of impact structures.

The results of field, geophysical, geochronological, remote sensing, and laboratory investigations of the Shoemaker impact structure, carried out to date, constitute the subject of this Report. The geology and structure of the Shoemaker impact structure and surrounding areas, and the petrography and geochemistry of the crystalline rocks from the central uplift are discussed in some detail. The Report concludes with a synthesis of the geological events that led to the present-day morphological expression of the Shoemaker impact structure.

[1] Research School of Earth Sciences, Australian National University, Canberra, A.C.T.
[2] School of Earth Sciences, University of Melbourne, Melbourne, Victoria.
[3] Department of Earth Sciences, University of Queensland, Brisbane, Queensland.

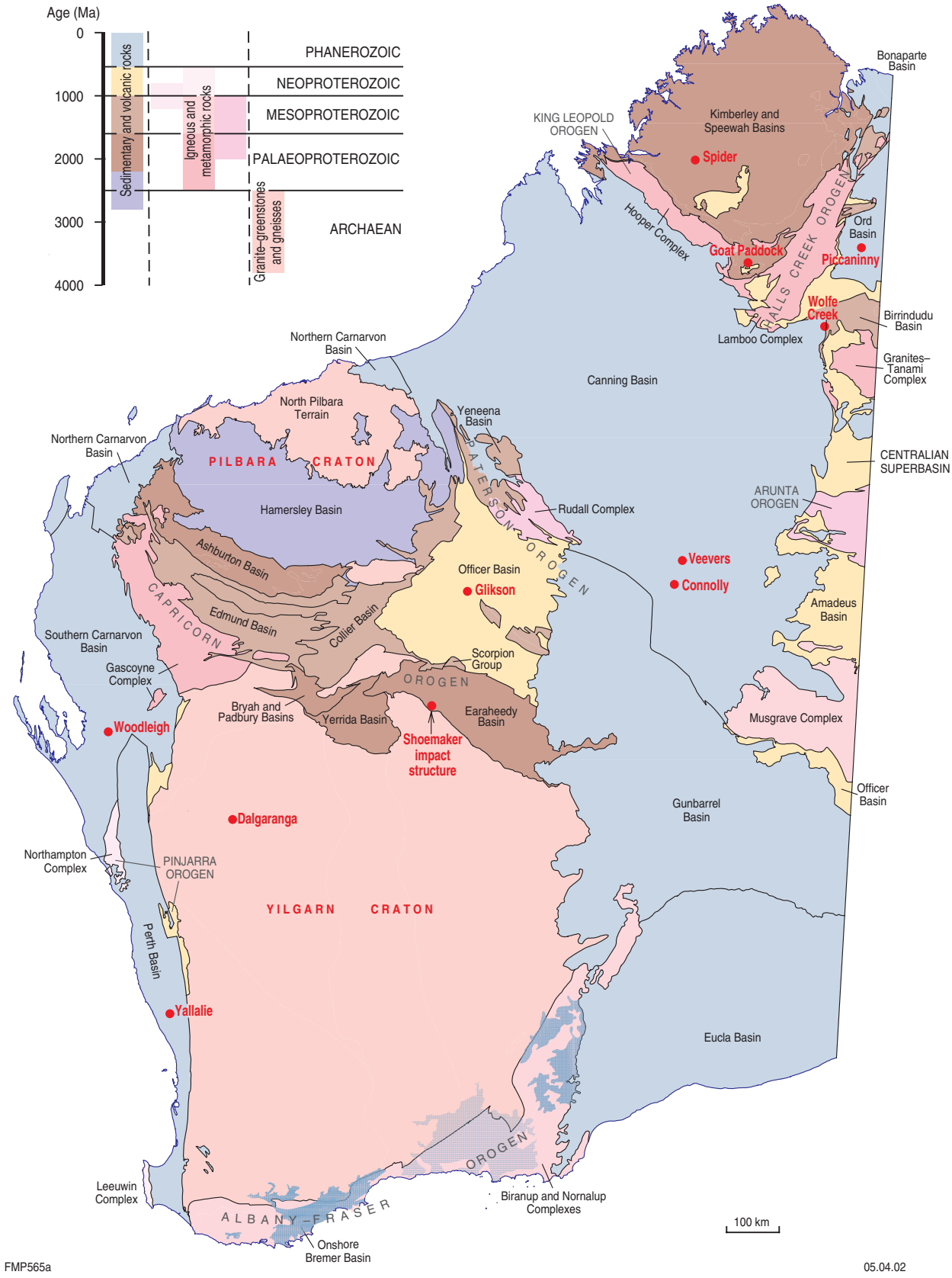

Figure 1. Simplified geological map of Western Australia, showing the locations of impact structures

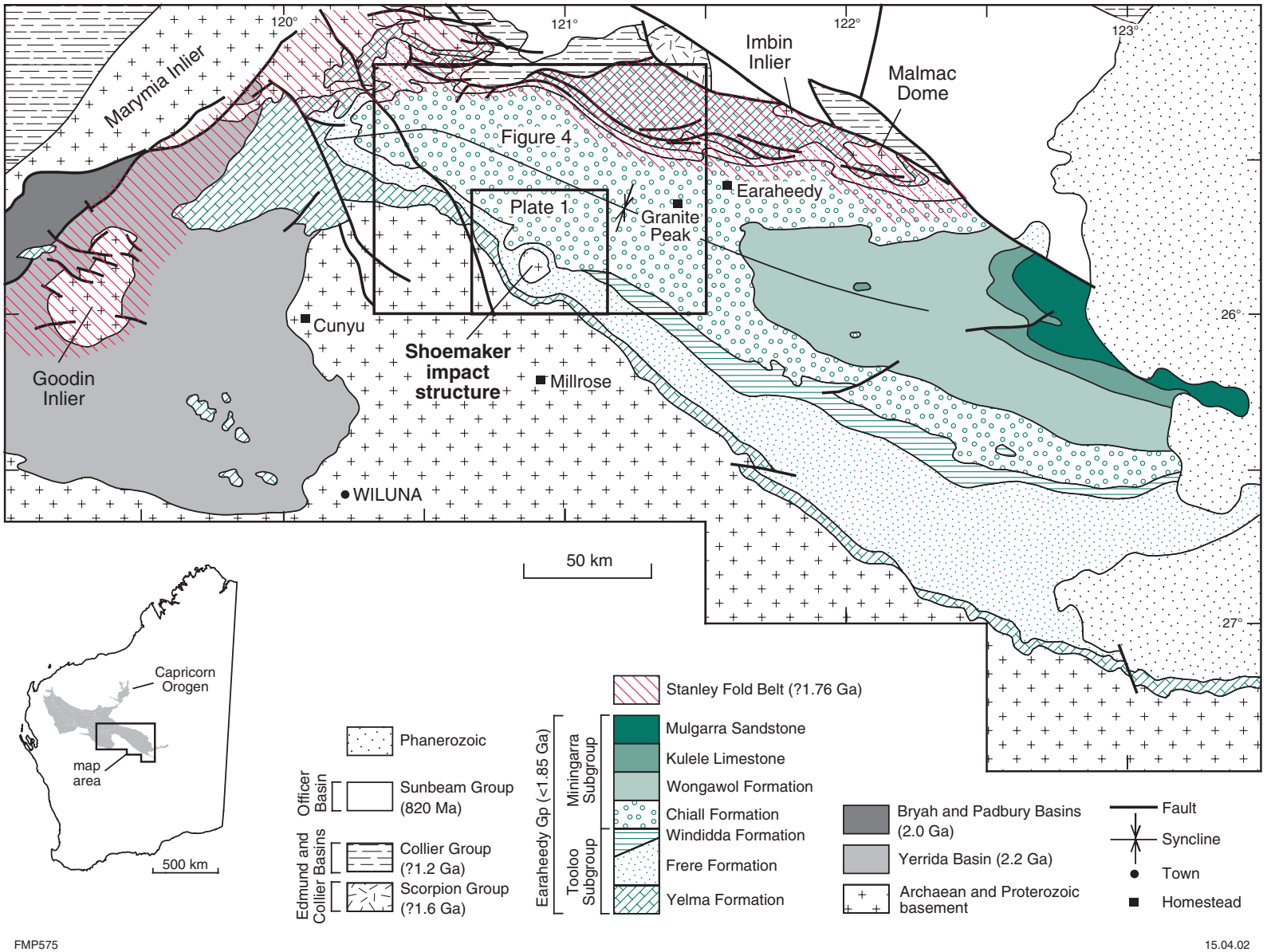

Figure 2. Simplified geological map of the Earaheedy Basin, showing the location of the Shoemaker impact structure and Plate 1

Shoemaker and Shoemaker (1996), on the basis of their fieldwork in 1986 and 1995, concluded that although it is deeply eroded, the Shoemaker impact structure meets most of the diagnostic criteria for the recognition of impact structures. Their conclusion is confirmed in this Report.

Previous work

The Shoemaker impact structure was initially investigated by Butler (1974), who named it the 'Lake Teague Ring Structure' and suggested that it formed either as a result of a granitic intrusion or a meteorite impact. Butler's cross sections clearly showed the uplift of the Archaean basement rocks in the centre of the structure surrounded by a syncline (rim syncline). The Shoemaker impact structure and surrounding areas were mapped in more detail by Bunting et al. (1977, 1980), who recognized planar deformation features (PDFs) in quartz crystals and shatter cones. However, these authors considered the structure to be the result of a cryptoexplosive event (which is a non-genetic term to designate an endogenic explosion; Nicolaysen and Ferguson, 1990), but lacking any direct evidence for volcanism (Jackson, 1997). The granitic rocks that outcrop in the eastern parts of the Shoemaker impact structure were part of a regional study of felsic alkaline rocks of the Yilgarn Craton by Johnson (1991), who concluded that the granitoids are syenitic in composition, but have been subsequently modified by alkali metasomatism.

Shoemaker and Shoemaker (1996) recorded the presence of a negative gravity anomaly over the Archaean crystalline rocks of the central structural uplift. This gravity anomaly is based on a reconnaissance survey carried out by the Shoemaker team in 1986, and was later confirmed by other gravity surveys conducted in 1996 (Plescia, 1999) and 2001 (Hawke, in prep.). From 1996 to 1998, further work was conducted on the Shoemaker impact structure within the framework of the geological mapping of the Earaheedy Basin by the Geological Survey of Western Australia (GSWA; Jones et al., 2000a,b; Pirajno et al., 2000). During this work the NABBERU* and GRANITE PEAK 1:100 000 map sheets, within which the Shoemaker impact structure is contained, were mapped at 1:25 000 scale and published as 1:100 000 geological series maps (Pirajno, 1998; Jones, 2000). In a preliminary account of the structure, Pirajno and Glikson (1998) renamed the 'Lake Teague Ring Structure' the Shoemaker impact structure in honour of the late Eugene Merle Shoemaker†.

Physiography and access

The Shoemaker impact structure is well defined physiographically and topographically by two concentric rings of upland areas and low hills (Fig. 3). The highest point in the region is Mount Teague (600 m above sea level), in the Frere Range, which trends west-northwest from the Shoemaker impact structure. The ephemeral Lake Nabberu, on the southern side of the Frere Range, passes into a series of smaller playa lakes in the centre, and between the inner and outer rings, of the Shoemaker impact structure (Fig. 3). One of these smaller lakes on the northern side of the impact structure is Lake Teague. The lakes contain saline silt and mud, and are surrounded by sand dunes, gypsiferous calcrete, and saline bedded deposits. To the east, between the inner and outer rings, is the newly named Lake Shoemaker (Fig. 3).

Access to the Shoemaker impact structure can be gained by four-wheel drive vehicles, through reasonably well maintained tracks from Cunyu Homestead to the west, from the Canning Stock Route, through Snell Pass in the Frere Range, from Millrose Homestead to the south, or from the Granite Peak Homestead to the east via Madman Outcamp. From these stations tracks, additional four-wheel drive vehicle tracks extend into and across the centre of the Shoemaker impact structure (Fig. 3). It is not advisable to use any of the tracks in wet weather. The station owners should be contacted before gaining access to the area.

Characteristics of impact features

Impacts on planetary surfaces by celestial objects (asteroids, comets), collectively referred to as meteoroids, result in the formation of craters. The morphology of craters is dependent on the nature of the target rocks, pre-impact structures, angle of incidence, and the size and composition of the impactor. Three main types of crater morphologies are recognized: simple, complex, and multi-ringed. Simple impact craters are 'bowl-shaped' depressions, less than 4 km in diameter, with an uplifted rim. They are formed by impactors smaller than about 100 m in diameter. Examples are the Meteor or Barringer Crater (1.2 km diameter) in Arizona, U.S.A. (Shoemaker, 1963), and the Wolfe Creek crater (900 m diameter) in Western Australia (Fig. 1; Guppy and Matheson, 1949; Albritton, 1989). Impacts by kilometre-scale meteoroids result in complex structures consisting of a central structural uplift surrounded by circular breccia troughs and terraced rims (Grieve and Pilkington, 1996). Multi-ringed impact structures, containing internal ring faults and shallow outer-crater aureoles are produced by the largest impacts. Multi-ringed impact structures are characterized by central-peak ring structures (Melosh, 1989; Morgan et al., 2000), and include Chicxulub (Yucatan, Gulf of Mexico; Morgan et al., 1997), Manicouagan (Quebec, Canada; Grieve and Head, 1983), Vredefort (Reimold and Gibson, 1996) and Morokweng (Corner et al., 1997) in southern Africa, and Woodleigh in Western Australia (Mory et al., 2000a,b; Iasky et al., 2001; Mory et al., 2001). Prior to erosion, the Shoemaker impact structure was possibly a multi-ringed structure.

Melosh (1989) and French (1998) provided more details on meteorite impacts as a geological process. Other useful publications include Grady et al. (1998), Koeberl and Anderson (1996), Glikson (1993, 1996), Grieve (1987, 1990, 1994, 1997), and Grieve et al. (1996).

* Capitalized names refer to standard 1:100 000 map sheets unless otherwise indicated.

† Eugene M. Shoemaker died on 18 July 1997, in Australia, in a car accident during fieldwork.

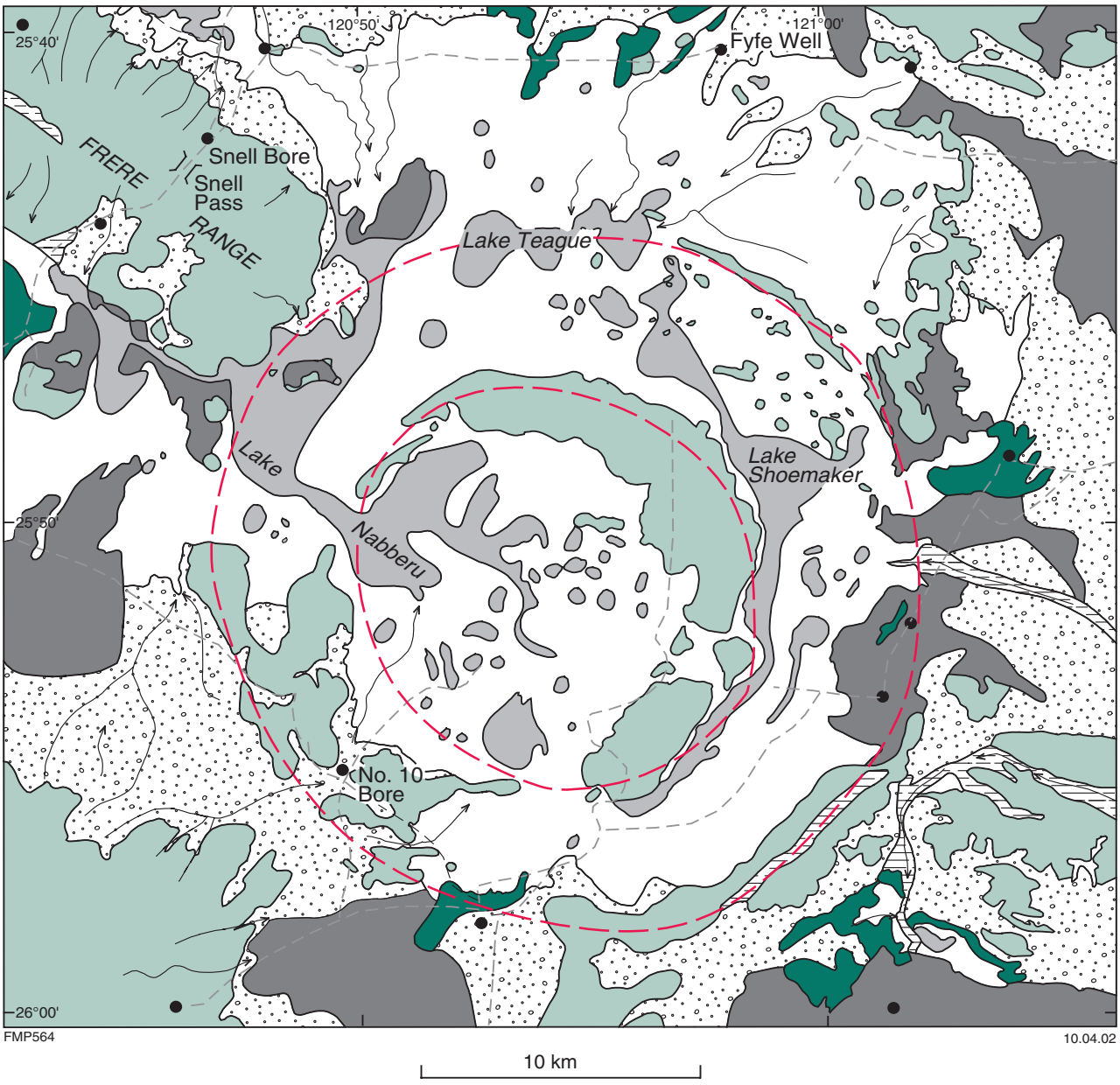

Figure 3. Physiographic map of the area around the Shoemaker impact structure; the map encompasses the area of Plate 1

The term 'hypervelocity impact crater' is defined (French, 1998, p. 17) as the 'structure formed by a cosmic projectile that is large enough and coherent enough to penetrate the Earth's atmosphere with little or no deceleration and to strike the ground at virtually its original cosmic velocity (>11 km/s)'. Diagnostic features of hypervelocity impacts are shatter cones, diaplectic glass, and planar microstructures (Melosh, 1989; French, 1998). Shatter cone fractures form penetrative cone-within-cone patterns; their axes are a few centimetres to tens of metres long, and their surfaces show characteristic penetrative 'horse tail-like' striations radiating from their apices (French, 1998). At the time of their formation the axes of shatter cones point towards the focus of the shock wave, but subsequent post-impact deformation, such as the elastic rebound that forms the central structural uplift, results in changes to the original orientation. Shatter cones form at pressures of 2 to 30 GPa, below the crater's floor. Diaplectic glass refers to solid state loss of crystal structure, or amorphization of minerals 'in which the crystal structure has been affected by the passage of a shock wave' (Jackson, 1997). Diaplectic glass is optically isotropic, preserves the original texture of the affected crystal, and forms at higher shock pressures (35–45 GPa) than planar microstructures (French, 1998). Shock-induced planar microstructures are present in silicate minerals (e.g. quartz, feldspar) in the target rocks. Planar microstructures that are formed in quartz are of two types: planar microfractures and planar deformation features (French, 1998). Shatter cones and PDFs in the Shoemaker impact structure are discussed in **Impact features**.

A non-diagnostic feature of impact structures is pseudotachylite. Pseudotachylite veins are not unique to impact structures because they are also formed by friction related to seismic activity, but they do constitute an important feature of impact structures. Tectonically formed pseudotachylites are mostly composed of breakdown products of the wallrocks (mechanical comminution), whereas impact-related pseudotachylite can contain diaplectic glass as well as extensive resorption related to shock fusion. Pseudotachylite forms irregular veins and dyke-like bodies containing large and small angular to resorbed fragments in an aphanitic, dark, and glassy groundmass. Pseudotachylite is typically present in low-porosity rocks (e.g. granite, gneiss) and is a 'glassy or very fine grained fault rock…..that forms by local melting of the rock along a brittle fault plane, due to heat generated by rapid frictional sliding' (Passchier and Trouw, 1996, p. 99–102). Spray (1998) defined two types: S- and E-type pseudotachylite. S-type pseudotachylite is associated with shock fusion, and the E-type, due to friction-induced comminution, is accompanied by a small amount of fusion. More than one type of pseudotachylite may be present in impact structures. The presence of pseudotachylite veins in the Shoemaker structure, although reported by Bunting et al. (1980), could not be confirmed during this study. The veinlets observed in this study closely resemble pseudotachylites and show extensive recrystallization, probably due to hydrothermal alteration.

An important effect of meteoroid impacts on Earth is rock melting, which results in the emplacement within craters of sheet-like masses, usually containing target rock fragments (Dressler and Reimold, 2001).

Hypervelocity impacts also induce chemical changes in the target rocks, as a result of ensuing hydrothermal activity, as well as minor contamination of the rocks by the impacting meteoroid. Contamination of the target rocks is marked by unusual amounts of siderophile and chalcophile meteoritic elements (e.g. Ir, Ni, Co, As, Sb, Se; Alvarez et al., 1980, 1982; Wang et al., 1994; Pernicka et al., 1996; Glikson et al., in prep.). There is evidence of chemical changes and hydrothermal alteration in the crystalline rocks of the central structural uplift of the Shoemaker impact structure. These topics are discussed in **Geochemistry of the Teague Granite** and **Hydrothermal alteration**.

Regional geological setting

The Shoemaker impact structure is on the southern margin of the Palaeoproterozoic Earaheedy Basin (Bunting, 1986; Pirajno et al., 1999; Pirajno et al., 2000; Jones et al., 2000a,b). The Earaheedy Basin contains the Earaheedy Group (Figs 2 and 4), and lies at the eastern end of the Capricorn Orogen (Fig. 1; Tyler et al., 1998). This basin was probably much larger than its present-day exposure, extending farther to the southeast and north, where it is now concealed by the overlying Edmund, Collier, and Officer Basins. Compressive movements from the northeast created a zone of deformation along the exposed northern margin of the Earaheedy Basin, which is named the Stanley Fold Belt (Jones et al., 2000a,b). This belt forms the northern limb of an east-plunging asymmetric syncline (Fig. 2).

Magnetic and gravity data indicate that most of the basin south of the Stanley Fold Belt is underlain by the Archaean Yilgarn Craton (Shevchenko, 2001; Morris et al., in press). Archaean granite and greenstone rocks of the Yilgarn Craton are exposed to the south, in the Marymia Inlier to the northwest, and in the central structural uplift of the Shoemaker impact structure (Figs 2 and 4). To the west the basement to the Earaheedy Basin is the Palaeoproterozoic Yerrida Basin. In the north, basement rocks are exposed in the Imbin Inlier (Pirajno and Hocking, 2001) and the Malmac Dome, within the Stanley Fold Belt (Fig. 2). Subvolcanic rhyodacite from the Imbin Inlier yielded a sensitive high-resolution ion microprobe (SHRIMP) U–Pb zircon age of 1990 ± 7 Ma (Nelson, 2001), which is close to the age of granitic rocks of the southern Gascoyne Complex at the western end of the Capricorn Orogen (Fig. 1; Tyler, 1999, 2000; Sheppard et al., 1999). Monazite from the monzogranite in the Malmac Dome yielded a SHRIMP U–Pb zircon age of 2611 ± 6 Ma (Nelson, in prep.).

Other rocks in the region include the Mesoproterozoic Scorpion Group, the Collier Group (Collier Basin, Fig. 2), and the Neoproterozoic Sunbeam Group (Officer Basin; Fig. 4).

Archaean Yilgarn Craton

Archaean granitoid and greenstone rocks exposed to the south and west (Figs 2 and 4, Plate 1) of the Shoemaker

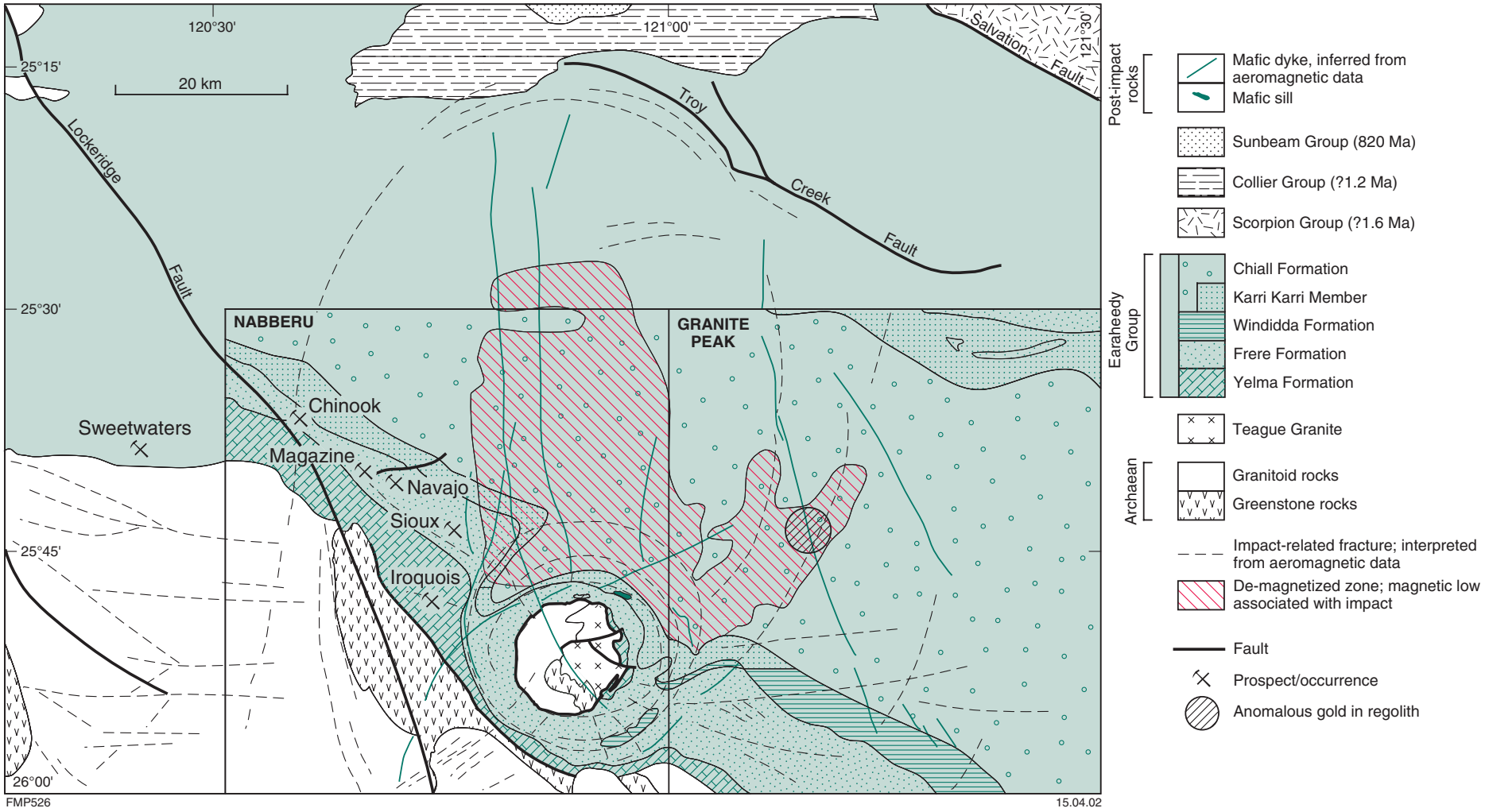

Figure 4. Simplified geological map of the Nabberu and Granite Peak 1:100 000 map sheets and adjacent areas to the north, showing impact-related fractures interpreted from magnetic data. See Figure 2 for location. Geology after Pirajno (1998) and Jones (2000)

impact structure, at the northern margin of the Yilgarn Craton, belong to the Eastern Goldfields Granite–Greenstone Terrane (Griffin, 1990; Wyche and Farrell, 2000).

Granitic rocks are dominantly monzogranite (*Ag*; Plate 1), but south and southwest of the Shoemaker impact structure, granitic rocks are hornblende-bearing quartz monzonite (*Agzq*), for which a SHRIMP U–Pb zircon age of 2664 ± 4 Ma was determined (Nelson, 1999). The hornblende–quartz monzonite intrudes greenstone rocks, as shown by the presence of thermally metamorphosed rocks consisting of quartz–actinolite hornfels that surround the granitic pluton. Granitic rocks of the Teague Granite (*Ægte*) outcrop in the core of the Shoemaker impact structure, and are discussed in **Central structural uplift**. The Teague Granite in the central structural uplift of the Shoemaker impact structure has a SHRIMP U–Pb zircon age of 2648 ± 8 Ma, which is interpreted to be the magmatic age (Nelson, 1997).

Greenstone rocks in the area of Figure 4 are part of the Merrie (Adamides, 2000) and Yandal greenstone belts (Farrell and Wyche, 1999; Pirajno and Jones, in prep.). South and southwest of the Shoemaker impact structure, greenstone rocks (*Ab*) are exposed along the northwest-trending Lockeridge Fault, and aeromagnetic and subsurface data indicate that greenstone rocks continue along and on the northern side of the hornblende–quartz monzonite pluton. The greenstones include mafic, ultramafic (*Ab, Abe*), and felsic volcanic (*Af*) rocks metamorphosed to upper greenschist to lower amphibolite facies. Aeromagnetic data and amphibolite xenoliths within the Teague Granite, suggest the presence of greenstone enclaves within the central structural uplift of the Shoemaker impact structure.

Palaeoproterozoic Earaheedy Basin

The age of the Earaheedy Basin is not precisely known, thereby hindering the accurate placement of the basin within a regional framework. Regional stratigraphic relationships indicate that the Earaheedy Basin is younger than the Yerrida Basin (c. 2200 Ma; Pb–Pb model age from carbonate rocks; Woodhead and Hergt, 1997) and older than the Collier Basin (c. 1211 Ma; Martin and Thorne, 2001). The available isotopic ages for the sedimentary rocks of the Earaheedy Group cluster around 1900–1850 Ma (Pirajno et al., in press). The Earaheedy Basin is apparently unaffected by the c. 1830 Ma Capricorn Orogeny, which records the collision of the Pilbara and Yilgarn Cratons (Tyler and Thorne, 1990), but the basin may have been east of the area affected by the orogeny because the eastern parts of the Yerrida Basin (which are unequivocally older than the orogeny) are also not affected. Deformation in the Stanley Fold Belt is tentatively attributed to the second phase of the Yapungku Orogeny at 1760 Ma (Smithies and Bagas, 1997), which was probably caused by the collision of the North and West Australian Cratons (Tyler, 2000). If this is correct, then 1760 Ma provides a minimum age constraint for the Earaheedy Basin. Based on stromatolite taxa that are similar to those of the (<1840 Ma) Duck Creek Dolomite of the Wyloo Group, Grey (1994) suggested that the age of the Earaheedy Group might be around 1840 Ma.

The Earaheedy Group (Figs 2 and 4) is an approximately 5 km-thick package of shallow-marine clastic and chemical sedimentary rocks that was deposited on a passive continental margin at the northern edge of the Yilgarn Craton. The Earaheedy Group has been divided into two subgroups (Hall et al., 1977). The Tooloo Subgroup consists of the Yelma Formation (base), Frere Formation, and Windidda Formation (top). The overlying Miningarra Subgroup consists of the Chiall Formation (base), Wongawol Formation, Kulele Limestone, and Mulgarra Sandstone (top). The last three units do not outcrop in the area of Figure 4 and Plate 1 and are not discussed further. The local stratigraphy of the Earaheedy Group is shown in Figure 4, and is briefly summarized below after Hocking et al. (2000) and Jones et al. (2000a,b).

The Yelma Formation (*PEy*) consists of between 3 and 500 m of shale, sandstone, and siltstone deposited in shallow-marine and locally fluvial environments. A 100 m-thick stromatolitic carbonate facies in the southwest of the basin is the Sweetwaters Well Member (*PEyw*). The Frere Formation (*PEfg*), with a total thickness of about 600 m, records the onset of iron-oxide precipitation within the basin and consists of up to four major granular iron-formation intervals, separated by up to three major ferruginous shale and siltstone bands, and minor carbonate units. Granular iron-formation horizons consist of jasperoidal granular iron-oxide layers, typically 5 to 20 cm in thickness, and intraclastic breccia interbedded with shale and siltstone beds. Individual granular iron-formation beds consist of chert, iron oxides, peloids (microplaty hematite), and jasper (cryptocrystalline silica with finely disseminated haematite) in a cherty, chalcedonic or jasperoidal cement. The Windidda Formation (*PEd*) is approximately 600 m thick and a lateral facies equivalent of the Frere Formation. It consists of iron-rich shale and siltstone, locally stromatolitic carbonate, minor jasperoidal beds, and granular iron-formation. The shale is interbedded with thin, fine- to medium-grained sandstone beds in the upper part of the formation.

The Chiall Formation (*PEc*; Figs 2 and 4) totals about 1000 m in thickness and contains three member units: the Karri Karri Member (*PEck*), Wandiwarra Member (not present in area of study), and Princess Ranges Member (*PEcp*). The Karri Karri Member consists of reddish to red-brown and purple 'pin-stripe' siltstone and shale in the north and southwest of the Earaheedy Basin. The contact of the Karri Karri Member with the underlying Frere Formation is placed at the top of the last major unit of granular iron-formation or chert (Bunting, 1986). The bulk of the Chiall Formation (including the Wandiwarra and Princess Ranges Members) consists of shale, siltstone, and mudstone intercalated with thick glauconitic sandstone beds and intraclastic breccia, representing a change from combined chemical and clastic sedimentation to dominantly clastic deposition. The base of the formation is a breccia of poorly sorted, angular carbonate clasts in a ferruginized glauconitic sandstone matrix.

Geology and structure of the Shoemaker impact structure

The geology and structure of the Shoemaker impact structure are presented in Plate 1, which is an interpreted bedrock geology map based on outcrop, Landsat, and aeromagnetic data. Outcrop geology is based on the 1:100 000 geological series maps of NABBERU (Pirajno, 1998) and GRANITE PEAK (Jones, 2000). A simplified geological map of the structure and surrounding region is shown in Figure 4.

The Shoemaker impact structure consists of two concentric annular or ring structures (discussed in more detail in **Inner and outer rings**), with an outer diameter of 28 km, and is evident on satellite images (Plate 1). The target rocks shallowly dip to the northeast (about 10–15°), but are essentially undeformed and unmetamorphosed sedimentary rocks of the Earaheedy Group, overlying Archaean granite–greenstone basement of the Yilgarn Craton. The Archaean granite–greenstone basement rocks are only exposed within the eastern side of the central structure, on the inside of the inner ring (Plate 1), but they can be extrapolated across the rest of this central structure (Fig. 4). The presence of diagnostic impact indicators suggest that these rocks form an impact-induced central structural uplift, which has a diameter of about 12 km. The eastern side of the structural uplift is characterized by high total magnetic intensity (TMI; see **Aeromagnetic data**), and the only exposures of granitoid rocks (see **Central structural uplift**). Zones of hydrothermal alteration are present only in rocks of the eastern rings. The TMI pattern suggests not only that the upper parts of the original impact structure were eroded, but also that the entire structure is probably tilted towards the east. Therefore, the present structure exposes deeper levels in the western parts of the structural uplift than in the east. The implications of this tilting and low erosion level are examined again in **Conclusions and discussion** and Appendix 1.

Geophysical signatures

Gravity data

Large impact structures are characterized by negative gravity anomalies due to the lower density of fractured target rocks. This was confirmed by Pilkington and Grieve (1992), who concluded that in most crystalline rocks the contrast between fractured and unfractured target rocks is between 0.13 and 0.17 g/cm^3 (quoted in Plescia, 1999). Iasky et al. (2001) calculated that for the Woodleigh impact structure the density of the basement was reduced from 2.67 to 2.55 g/cm^3.

A gravity survey carried out by Plescia (1999) defined a negative Bouguer anomaly coincident with the core of the Shoemaker impact structure (Fig. 5). The survey was based on 140 stations using a Lacoste Romberg gravity meter with readings spaced about 500 m apart along traverses. Plescia (1999) combined the results of his survey with those of Shoemaker and Shoemaker (1996) in order to obtain a more accurate model. Plescia's (1999) gravity model of the Shoemaker impact structure suggests that the fractured crystalline core extends to a depth of 4–5 km. The negative anomaly is about –120 μm/s^2 (–12 mGal; Fig. 5), which is comparable to anomalies associated with other impact structures, such as Acraman and Tookoonooka (Fig. 6; Iasky et al., 2001). On the basis of the gravity data, Plescia (1999) concluded that the Shoemaker impact structure may have had a diameter slightly larger (up to 42 km) than is presently exposed. This aspect is discussed in Appendix 1.

Aeromagnetic data

A regional airborne magnetic survey over the Shoemaker impact structure and the surrounding region (NABBERU 1:250 000 map sheet), flown with a line spacing of 200 m and at a height of 60 m (dataset from Australian Geological Survey Organisation, AGSO, now Geoscience Australia; Liu, 1997; Liu and Mackey, 1998), clearly displays the outline of the Shoemaker impact structure (Fig. 7a and Plate 1). The TMI image shows that the Shoemaker impact structure has a complex magnetic signature with well-defined circular anomalies along the eastern and southeastern margins.

The magnetic image shows two circular patterns: an outer circular feature, approximately 28 km in diameter and characterized by a magnetic low, and an inner circular magnetic high along the eastern and southeastern rims. There is a pronounced magnetic signature along the eastern and northeastern rims and a low magnetic signature to the west and southwest. The high magnetic intensity in the eastern parts of the structure is spatially associated with extensive quartz veining and hydrothermal alteration of the Frere Formation rocks, and can be explained as due to enhanced magnetic susceptibility associated with a change from hematite to magnetite in the iron formation units, during circulation of hydrothermal fluids. Hydrothermally induced enhanced susceptibility and resulting magnetic anomalies are a common feature of many hydrothermal processes (e.g. porphyry systems; Pirajno, 1992). The high magnetic intensity along the eastern side of the Shoemaker structure, together with the presence of hydrothermal alteration and extensive quartz veining in the same area, indicates that higher levels of the structure are exposed in the east, thereby suggesting a tilt of the Shoemaker impact structure towards the east. It follows that although the amount of tilt is not known, the western and southwestern parts of the structure must be more deeply eroded.

The magnetic data also indicate the presence of dykes, fractures, and faults. Dykes trending north and northeast cut the circular structures. Fractures near the Shoemaker impact structure trend northeast, southeast, and east. The northeast-trending fracture system in the granite–greenstone rocks to the southwest is also clearly displayed on the TMI image (Plate 1). Directly north and northeast of the Shoemaker impact structure are two irregularly shaped zones of low magnetic intensity in basement rocks (Fig. 7a). These zones of low magnetic intensity are interpreted as demagnetized zones (Fig. 4), perhaps

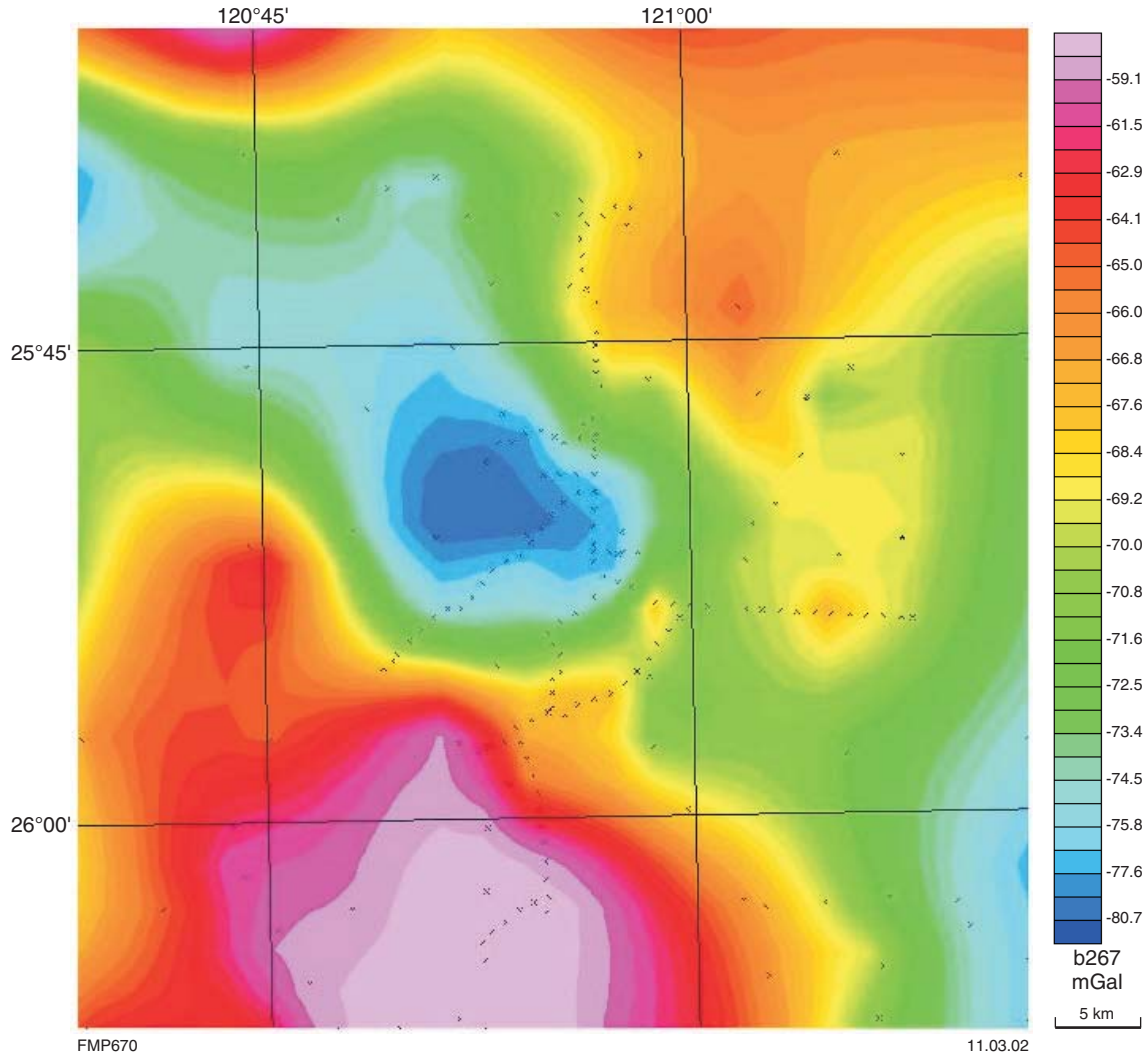

Figure 5. Bouguer gravity image of the Shoemaker impact structure, showing gravity stations; data reprocessed from Plescia (1999); image courtesy of P. Hawke (University of Western Australia)

caused by circulation of fluids within areas of greater permeability created by the impact and resulting in the change of iron oxides to oxyhydroxides (e.g. goethite). This interpretation is supported by the clear spatial association of these zones with the Shoemaker impact structure and absence of similar magnetic features elsewhere in the region.

Total magnetic intensity images of the Yilgarn Craton processed by A. Whitaker (1999, written comm.) from AGSO–GSWA data (Figs 4 and 7a,b) show near-circular patterns, defined by magnetic lows, around the Shoemaker impact structure and extending up to 60 km north and 45–50 km south from the centre of the structure.

The magnetic signatures of the Australian Shoemaker, Acraman, Tookoonooka, and Talundilly impact structures are shown in Figure 6. The magnetic signatures of these other structures appear to be more complex than the Shoemaker impact structure, and are probably due to differences in magnetic susceptibilities and rheology of the target rocks.

Inner and outer rings

The concentric structural elements of the Shoemaker impact structure are an inner ring syncline and an outer ring anticline (or outer collar) affecting sedimentary rocks of the Earaheedy Group (Yelma, Frere, Windidda, and Chiall Formations). These fold structures almost completely surround or collar the central basement uplift or granitic core (Fig. 4 and cross sections on Plate 1). Magnetic and stratigraphic data indicate that folding is more complicated in the eastern parts, with thrusting or sheared limbs (or both). Faults and fractures, some of which are interpreted (from magnetic data) to contain mafic dykes, are locally filled with quartz veins, and have a radial disposition with respect to the centre of the structure. These radial structural elements converge towards the centre of the structure (Plate 1; Fig. 4).

The structural complexity in the eastern part of the rings is accompanied by hydrothermal alteration and associated with discontinuities and irregular high (positive) and low (negative) magnetic intensities. To the north and

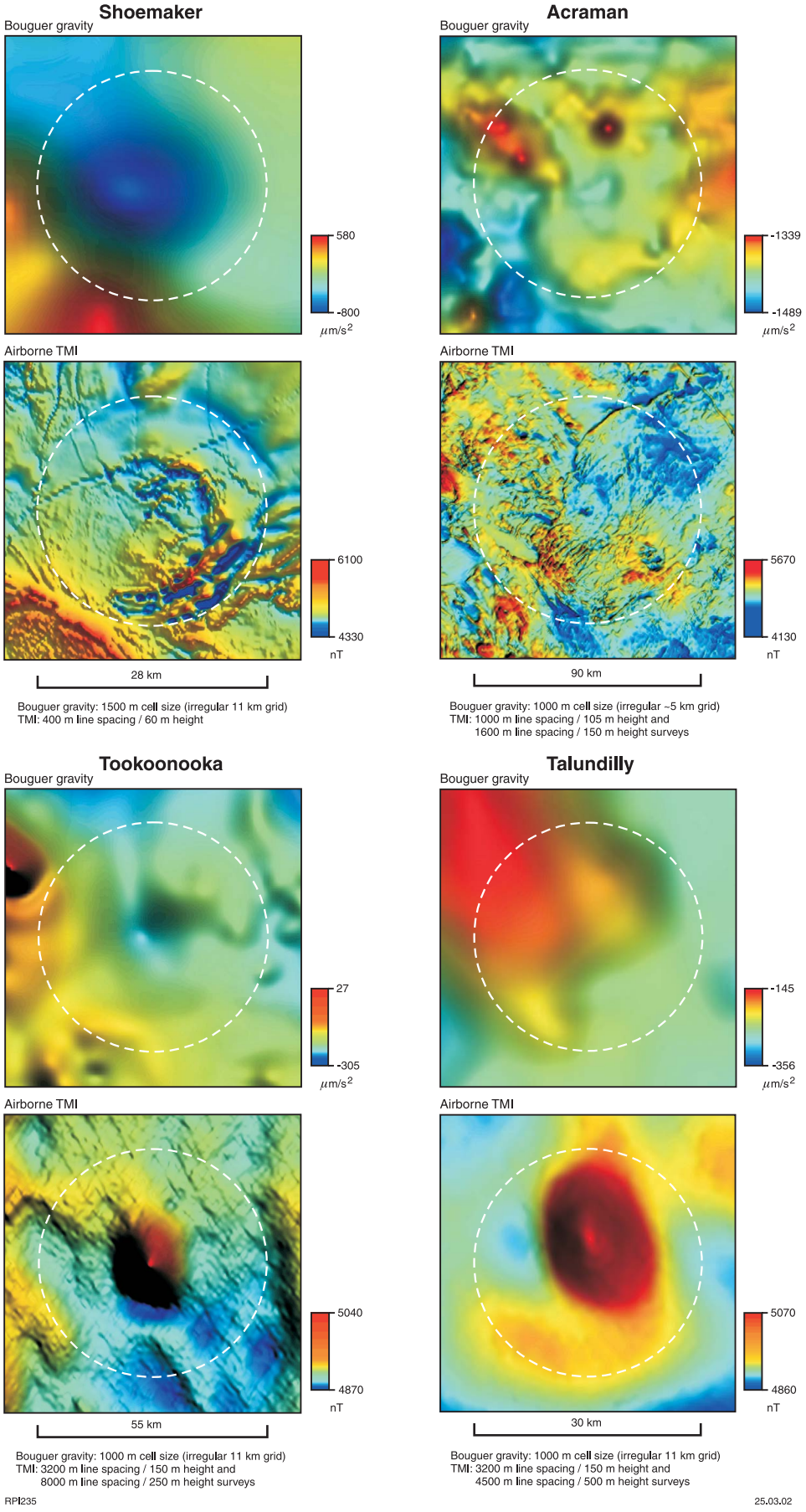

Figure 6. Potential-field images of selected Australian impact structures (note different scales; after Iasky et al., 2001)

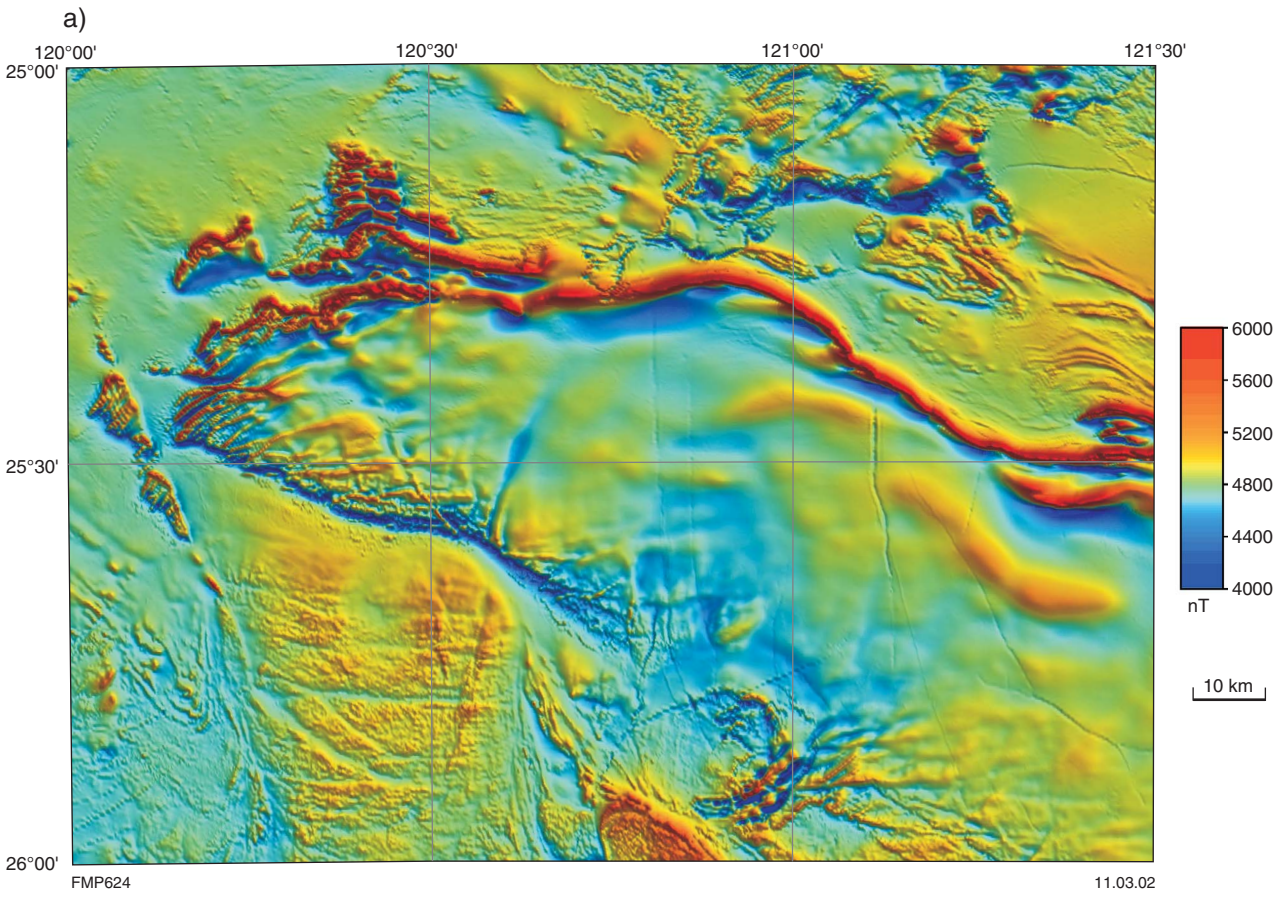

Figure 7. **a) Total magnetic intensity image of the Nabberu 1:250 000 sheet area; b) schematic illustration showing possible original dimensions of the Shoemaker impact structure, based on interpretation of total magnetic intensity map of the Yilgarn Craton (courtesy of A. Whitaker, Geoscience Australia); inset shows interpreted cross section of the structure**

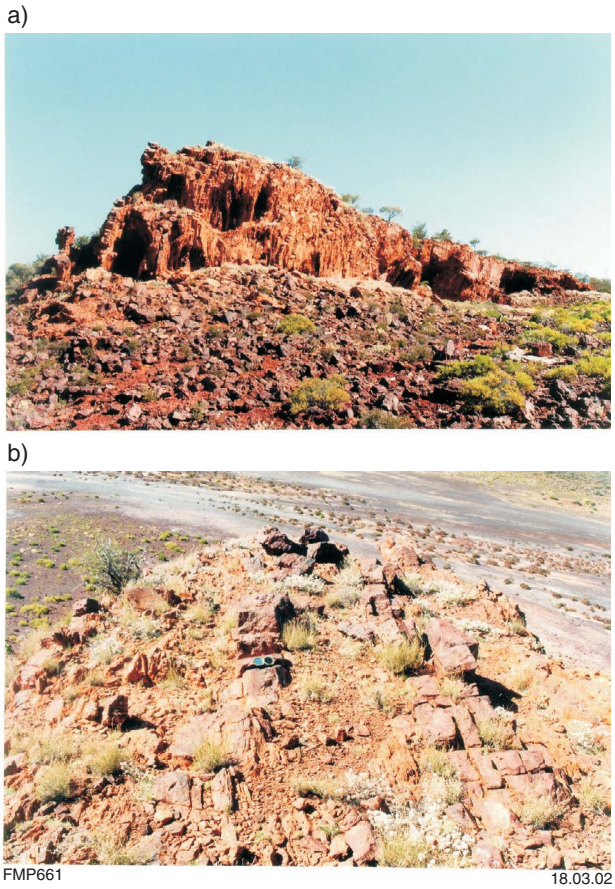

Figure 8. Granular iron-formation beds of the Frere Formation in the inner syncline: a) with a nearly vertical attitude; b) steeply dipping and facing the newly named Lake Shoemaker

west, in contrast, the sedimentary rocks of the inner and outer rings are only gently deformed into synclinal and anticlinal folds (Plate 1, cross section A–B).

In the northeast, the outer ring is within the Chiall Formation, at the contact between the Princess Ranges Member glauconitic sandstone (*PEcp*) and sandstones of undivided Chiall Formation (*PEc*; Plate 1). In the southeast the outer ring is composed of granular iron-formation units of the Frere Formation (*PEfg*). To the east this outer ring is poorly or not exposed, but on the basis of magnetic data is interpreted to be composed of complexly folded shale units of the Windidda Formation (*PEd*) and Karri Karri Member of the Chiall Formation (*PEck*). In the southwest and west, the outer ring is well defined by outcrops of the Frere Formation (*PEfg* and *PEfs*; Plate 1), where they form high ground (50–70 m above the salt lakes in the centre of the Shoemaker impact structure). Frere Formation rocks of the outer ring continue northward, beneath Lake Nabberu (Plate 1).

Rocks of the Frere Formation (*PEfg*) form an almost continuous circular outcrop, defining the limbs of the inner syncline. On the eastern side, granular iron-formation units are contorted and locally enriched by secondary iron oxides, commonly forming prominent ridges (*PEfgi;* Fig. 8). These are discussed more fully in **Mineralization**.

On the northern rim, outcrops of shale units of the Karri Karri Member (Chiall Formation, *PEck*) are intruded by a dolerite sill. This dolerite (*Pd)* is undeformed (possibly post-impact) and composed of plagioclase, augite, brown hornblende, biotite, and accessory quartz, sericite, and ilmenite. Optically determined plagioclase composition is about An_{50} (andesine–labradorite). Hornblende replaces augite along the crystal margins and biotite replaces hornblende. Minor and interstitial granophyric intergrowths (quartz–feldspar) are also present.

The eastern sector of the inner ring contains rocks of the Yelma Formation (*PEy*), which on the inside of the structure are in faulted contact with the Teague Granite. Here the formation consists of quartz sandstone and layers of light-coloured to greenish, laminated cryptalgal chert units. The latter are interpreted to be slivers of silicified stromatolitic dolomite of the Sweetwaters Well Member (*PEyw*; Plate 1). The contact between the Yelma Formation and Frere Formation is locally marked by pods of jasperoidal quartz (*qc*). These pods may have resulted from chemical deposition of silica from hydrothermal fluids, perhaps heated by thermal gradients originating from impact energy. This is discussed further in **Hydrothermal alteration**.

Impact features

Scattered centimetre- to metre-sized, round and angular boulders (*Px*; Fig. 9) about 5 km from the eastern shore of Lake Teague could be a lag deposit of Permian age (Paterson Formation; Bunting et al., 1982; Commander et al., 1982). Alternatively, because of their closeness to the outermost ring and absence of this lithology elsewhere in the Earaheedy Group in the region, it is also possible that they are either lag deposits of reworked lithic breccia ejecta or crater-fill allochthonous breccia. Although these boulders were not examined in detail for shock metamorphic effects, in this work, the former is the preferred interpretation because of the spatial association with the outer ring.

Figure 9. Outcrops of a lag deposit on the northeastern outer ring of the Shoemaker impact structure. These boulders are interpreted to represent reworked allochthonous ejecta material

FMP573A 08.04.02

Figure 10. Shatter cones in granular iron-formation of the Frere Formation on the northern rim of the Shoemaker impact structure (MGA 290424E 7145154N)

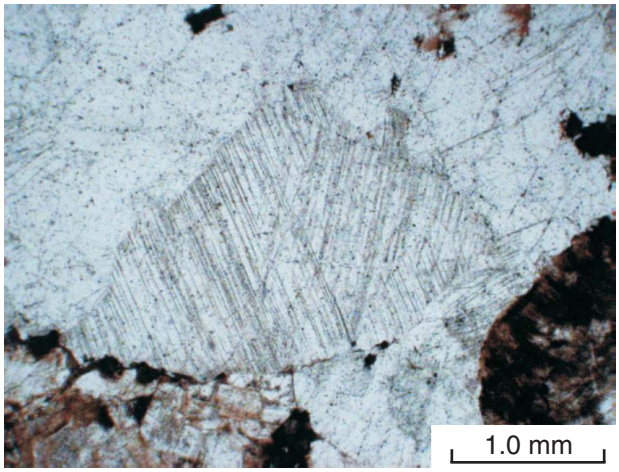

FMP609 19.03.02

Figure 11. Planar deformation features in quartz crystals from the Teague Granite (plane-polarized light)

In the Shoemaker impact structure shatter cones are developed in granular iron-formation of the Frere Formation (Fig. 10), chert units of the Yelma Formation (Plate 1), and sandstone of the Chiall Formation (Wandiwarra Member). The Chiall Formation sandstone units contain 0.5 m-long shatter cones about 15 km northeast of the centre of the Shoemaker impact structure (MGA 297700E 7150200N), and these are the most distal found to date. Shatter cones are present in the silicified rocks of the Yelma Formation, about 7 km east-southeast from the centre of the structure (MGA 294620E 7135100N; photo 2 on Plate 1). Shatter cones in Frere Formation rocks are present in several places on the northern rim (e.g. MGA 290424E 7145154N; Fig. 10); they are smaller (<30 cm long) than those developed in siliciclastic rocks. The size and extent of shatter cone development is related to the rheological properties of the target rock, including grain size (the finer the grain size, the more common and the smaller the cones). Therefore, they are most common in fine- to medium-grained sedimentary rocks, such as quartzite, sandstone, carbonates, and shales.

Planar fractures that may be related to the impact can be seen in quartz grains in sandstone of the Chiall Formation (Wandiwarra Member), near the area with shatter cones. Diagnostic PDFs, with fluid inclusions, are present in quartz crystals of the Teague Granite (Fig. 11, photo 3 on Plate 1).

Central structural uplift

The granitoid rocks that outcrop in the eastern part of the 12 km-diameter inner structure are grouped in the Teague Granite (photo 1 on Plate 1, Fig. 12). The central and western parts of the inner structure are covered by Quaternary lake sediments and sand dunes. However, magnetic data indicate the presence of granitoid (*Ag*; possibly monzogranite) and greenstone (*Ab*) rocks beneath these surficial deposits. These rocks, together with the Teague Granite, are interpreted as the central structural uplift of the impact structure and possibly the basement core of the original crater.

Bunting et al. (1980) recognized two units: a medium-grained leucogranite and a quartz syenite. The petrography and chemistry of the granitic rocks in the core of the Shoemaker impact structure were studied in some detail by Johnson (1991), who subdivided them into syenite and alkali granite. In this study, and on the basis of more detailed field and petrographic studies, the Teague Granite is subdivided into three units (Plate 1):

- aegirine-augite-bearing orthoclase–albite granite or syenite (*Ægtea*), in places cut by pegmatite veins;
- albite–quartz–microcline granite or quartz syenite (*Ægtex*);
- leucocratic alkali-feldspar granite (*Ægte*).

Field relationships between the Teague Granite and the surrounding sedimentary rocks are unclear due to poor

FMP571 19.03.02

Figure 12. Detail of fractured Teague Granite outcrop

outcrops. However, the lack of intrusive features in nearby outcrops of the Yelma Formation indicate that these rocks were originally unconformable on the Teague Granite. Although Bunting et al. (1980) considered the quartz syenite to be intrusive into the leucocratic granite, field evidence suggests that it is more likely that the boundaries between the three units are transitional. Small xenoliths of greenstone rock (amphibolite) are present in the syenite rock (*Ægtea*). Planar deformation features with numerous fluid inclusions, although present, are not common in quartz crystals of the Teague Granite (Fig. 11).

Petrography of the Teague Granite

The syenite (*Ægtea*) unit of the Teague Granite is medium grained and pink to brick-red. This unit contains up to 55% by volume of orthoclase phenocrysts, up to 7 mm long (Fig. 13a), and up to 15% by volume of zoned alkali pyroxene (sodic hedenbergite or aegirine-augite), associated with up to 2% accessory titanite and inclusions of apatite crystals, up to 2.5 mm long (Fig. 13b–e). Albite (25% by vol.) forms small grains (0.1 to 0.8 mm) in the groundmass. Other accessory minerals include green

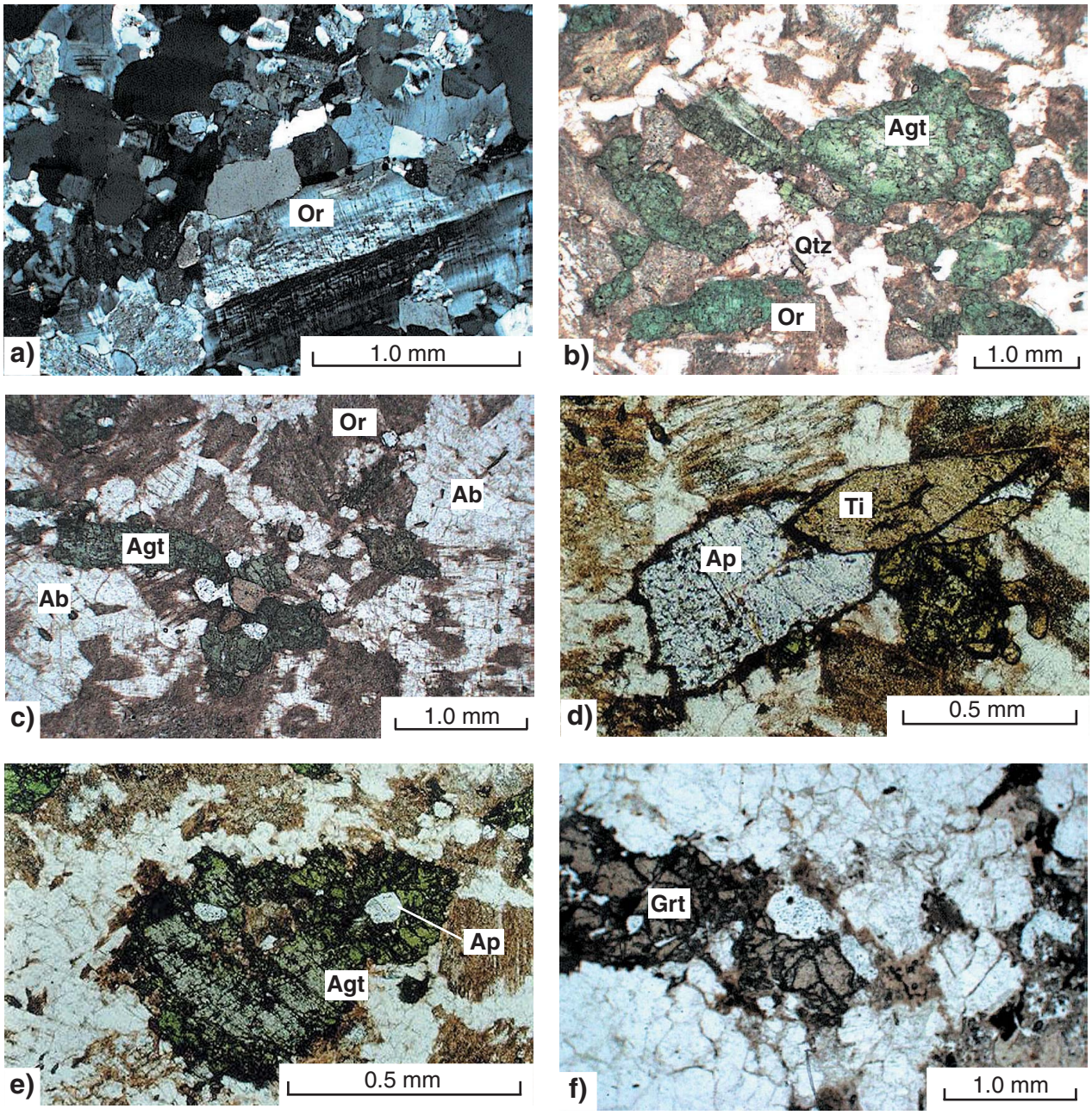

Figure 13. Mineralogical assemblages of the syenite unit of the Teague Granite (*Ægtea*): a) orthoclase (Or) phenocryst in a matrix of quartz–albite; b) orthoclase (Or), aegirine-augite (Agt), and quartz (Qtz); c) orthoclase (Or), aegirine-augite (Agt), and albite (Ab) assemblage; d) apatite (Ap) and titanite (Ti) crystals; e) aegirine-augite crystal (Agt) with apatite (Ap) inclusion; f) garnet (Grt) crystal associated with a quartz–albite assemblage; (a) with crossed polars; (b) to (f) with plane-polarized light

fibrous amphibole, zircon, and andradite garnet (Fig. 13f). The accessory amphibole is an actinolitic to tremolitic hornblende (Johnson, 1991) replacing alkali pyroxene. Quartz is anhedral with PDFs locally. The CIPW normative composition of the syenite is presented in Tables 1 and 2.

The quartz syenite (*Ægtex*) is also medium grained, pink to brick-red, fractured, characterized by a distinct polygonal and granoblastic texture (Fig. 14a,b), and transitional to the syenite discussed above. This rock is dominated by euhedral to subhedral albite and quartz, roughly in equal proportions (Fig. 14a,b; photo 4 on Plate 1), overprinted by perthitic microcline crystals. Accessory minerals include alkali pyroxene, probably aegirine-augite or sodic hedenbergite (brown to bright-green pleochroism), fibrous amphibole (actinolite–tremolite), zircon, and titanite. The alkali pyroxene is interstitial to the albite–quartz–microcline assemblage and is commonly replaced by the fibrous amphibole. Millimetre-wide, anastomosing microbreccias containing grains of fractured quartz, feldspar, fibrous amphibole, prehnite, and minor epidote, cemented by iron oxides, are locally present and could represent pseudotachylite veinlets (Fig. 14c,d). Pseudotachylite veinlets were identified by Bunting et al. (1980), but could not unambiguously be confirmed in this study. Bunting et al. (1980) also reported fluorite along fractures. The CIPW normative composition of the quartz syenite is given in Table 1.

Leucocratic alkali-feldspar granite (*Ægte*) is coarse to medium grained, locally brecciated, and contains the assemblage quartz–K-feldspar(–microcline–albite–biotite–sericite). Where least altered, it contains about 30% by volume of quartz, 40% albite, and 30% K-feldspar (Bunting et al., 1980). In some cases the unit is partially to pervasively silicified and cut by quartz veinlets and microfractures (Fig. 15a,b). In places, this granitoid has a mylonitic fabric or brecciated texture (or both), in which turbid, early, coarse-grained albite crystals are embedded in a foliated quartz-rich matrix (Fig. 15c). The albites are commonly rimmed by quartz with sericitic alteration along crystallographic directions. The turbid albites exhibit stages of replacement by K-feldspar, indicated by the presence of Carlsbad twins or microclines, which impart the turbidity, at a different orientation to the original albite. The turbid albites are surrounded by a fine-grained equigranular quartz–albite–microcline–biotite assemblage, quartz ribbons, and fine microshears containing aegirine-augite–titanite–?mica crystals. Fine veinlets filled with isotropic material cut across the mylonitic fabric (?pseudotachylite). Rare reticulate textures, similar to those in the Woodleigh impact structure (Mory et al., 2000a,b), suggestive of diaplectic glass, are present in potassic–sodic feldspar (Fig. 15d). Diaplectic plagioclase glass is called maskelynite, of which good examples are observed in the shocked granitoid of the Woodleigh structure (Mory et al., 2000a,b; Mory et al., 2001). X-ray diffraction (XRD) analyses indicate that the clay-mineral phases are dominated by vermiculite, which fills microfractures or replaces iron-magnesium silicates (e.g. biotite). In places the overall texture is distinctly cataclastic and fractures are infilled with microcrystalline or fine-grained quartz or, locally, with unidentified dark material or sheaves of fibrous amphibole.

X-ray diffraction analysis of sample GSWA 152614 (*Ægtea*) identified microcline perthite, quartz, albite, and vermiculite. The presence of vermiculite, a trioctahedral sheet silicate similar to smectite, indicates hydrothermal alteration or weathering of biotite. Perthite is a microcline (K-rich phase) in which small domains of albite (Na-rich phase) are present.

Interpretation of petrographic data

The Teague Granite conforms to the overall nature of late Archaean alkaline intrusions in the Yilgarn Craton (Smithies and Champion, 1999). Johnson (1991, p. 120) recognized the unusual features of the alkali granitic and syenitic rocks of the Teague Granite and noted that their fabric is more consistent 'with production via intense alkali metasomatism of the original gneissic granite' and that the 'severe alteration and anhedral character of the quartz syenite…lends support to the suggestion that the former (quartz syenite) is a product of metasomatism'. Johnson (1991 quoting Deer et al., 1966) also drew attention to the presence of andradite garnet, which is typical of metasomatic environments associated with thermal metamorphism.

In agreement with Johnson's (1991) observations, the petrography of the Teague Granite suggests that an original granitoid rock was subjected to intense potassic, sodic–calcic, and silicic alteration, which replaced magmatic silicate minerals and formed a quartz–K-feldspar–albite–aegirine-augite(–titanite–apatite) assemblage (Figs 13a,b and 14a,b). The reddish colouration of the quartz syenite and syenite is probably the result of exsolution of hematite inclusions due to the replacement of quartz and albite by microcline. If the Teague Granite aegirine-augite is a product of alkali alteration, temperatures of between 430 and 460°C can be inferred for its formation (Smith and Wu, 2000).

A more rigorous assessment of stages of replacement of the precursor granitoid by alkali, calcium, and silica-rich fluids is difficult due to a combination of poor exposure and inadequate sampling. Nevertheless, a tentative and combined paragenetic sequence, based on textural relationships, and assuming that the mineral assemblages observed replaced those from an original granitoid (?monzonite), is shown in Figure 16.

Geochemistry of the Teague Granite

Hypervelocity impacts may result in the contamination and alteration of target rocks. For this reason a limited number of whole-rock major and trace element analyses were used in an attempt to quantify the geochemical character of the Teague Granite, to ascertain if traces of meteoritic elements are present, and whether or not this granite is a product of metasomatism or crystallization from a melt. The datasets used include six new analyses (major and trace elements) from this study, performed on three samples (GSWA 152162, leucocratic alkali-feldspar granite, *Ægte*; GSWA 152613, quartz syenite, *Ægtex*; and

Table 1. New chemical analyses of the Teague Granite

GSWA sample *Lithology* *MGA coordinates*	*152612* *Leucocratic alkali-feldspar granite (Ægte)* *294432E 7137221N*	*152613*[(a)] *Quartz–microcline–albite granite (Ægtex)* *293289E 7141449N*	*152614*[(b)] *Quartz–albite–orthoclase granite (Ægtea)* *291616E 7413460N*	*Average high-Ca granite (Champion and Sheraton, 1997)*	*Average trace elements, Claypan Suite (Smithies and Champion, 1999)*
			Percentage		
SiO_2	75.09	75.03	70.84	72.2	–
TiO_2	0.06	0.10	0.22	0.2	–
Al_2O_3	14.20	13.79	14.85	14.7	–
Fe_2O_3	0.84	0.86	1.89	0.6	–
FeO	0.38	0.28	0.29	1.0	–
MnO	0.00	0.00	0.00	0.10	–
MgO	0.09	0.06	0.33	0.6	–
CaO	1.09	0.21	0.61	1.9	–
Na_2O	4.29	4.60	4.60	4.6	–
K_2O	4.19	5.07	5.82	3.1	–
P_2O_5	0.00	0.01	0.03	0.1	–
CO_2	0.02	0.01	0.25	–	–
H_2O-	0.08	0.07	0.18	0.2	–
H_2O+	0.16	0.11	0.26	0.8	–
			Parts per million		
Sc	0.05	1.00	1.30	3	1.7
V	5.60	5.25	7.20	18	18.2
Cr	2.35	1.35	2.20	8	5.8
Ni	1.40	2.10	0.95	5	5.3
Cu	3.15	1.75	1.55	8	5.8
Zn	16.00	10.95	23.80	26	41.8
Ga	15.20	17.35	18.15	40	23.0
Ge	0.65	0.70	0.65	20	–
As	0.30	0.30	0.50	–	–
Se	0.10	0.10	0.20	–	–
Br	0.50	0.50	0.65	–	–
Rb	67.85	191.40	172.30	101	103.0
Sr	433.50	247.30	446.95	403	775.0
Y	2.60	7.70	11.30	6	9.2
Zr	50.00	185.60	724.80	121	116.0
Nb	1.20	6.25	12.40	5	15.7
Mo	0.30	0.35	0.70	–	–
Ag	0.10	0.10	0.10	–	–
Cd	0.05	0.15	0.10	–	–
In	0.10	0.10	0.10	–	–
Sn	0.75	0.80	1.60	–	–
Sb	1.00	0.10	0.75	–	–
Te	1.45	0.20	1.20	–	–
I	1.20	0.35	0.05	–	–
Cs	7.85	3.85	12.40	–	–
Ba	1 608.50	623.90	1 783.50	908	968.5
La	9.80	41.05	134.60	29	45.3
Ce	12.55	62.50	214.75	52	63.8
Pr	16.70	23.50	69.50	–	–
Nd	3.30	6.10	16.85	17	28.5
Hf	0.55	1.20	1.85	–	–
Ta	17.05	22.15	35.05	–	–
Tl	0.20	0.20	0.00	–	–
Pb	1.60	25.90	40.55	26	18.0
Bi	0.45	2.45	–	–	–
CIPW Norms			**Percentage**		
Quartz	30.50	27.43	19.10	–	–
Corundum	0.51	0.30	0.34	–	–
Orthoclase	24.74	30.6	34.72	–	–
Albite	36.28	38.94	39.17	–	–
Anorthite	5.81	1.20	1.82	–	–
Hypersthene	2.23	1.94	4.18	–	–
Ilmenite	0.11	0.20	0.42	–	–
Apatite	0.02	0.02	0.09	–	–
Zircon	0.01	0.04	0.15	–	–
Calcite	0.06	0.03	0.63	–	–

NOTES: Average of two analyses for each sample
(a) quartz syenite
(b) syenite

Table 2. Chemical analyses of the Teague Granite from Johnson (1991)

Sample number	*59*	*226*	*227*	*228*	*230*	*231*	*232*	*234*	*236*
MGA coordinates	*292839E 7142068N*	*291605E 7140817N*	*291605E 7140817N*	*291605E 7140817N*	*291605E 7140817N*	*291826E 7140882N*	*291604E 7140878N*	*291853E 7140913N*	*291825E 7140943N*
					Percentage				
SiO_2	63.34	73.71	71.3	74.24	71.36	68.51	69.03	67.22	68.55
TiO_2	0.5	0.11	0.2	0.08	0.2	0.19	0.19	0.18	0.19
Al_2O_3	16.2	13.72	14.71	13.29	14.6	15.81	15.79	16.72	15.69
Fe_2O_3	3.29	1.76	2.4	1.1	2.03	1.02	1.14	1.32	1.27
FeO	na	na	na	0.48	na	0.2	na	na	na
MnO	0.11	nd	0.01	0.01	0.02	0.09	0.04	0.02	0.05
MgO	0.97	0.2	0.23	0.08	0.1	0.22	0.22	0.26	0.19
CaO	2.27	0.15	0.23	0.13	0.27	0.71	0.65	0.41	0.63
Na_2O	5.47	5.25	4.7	4.54	5.22	5.29	5.46	5.55	5.02
K_2O	6.46	4.42	4.95	5.03	4.89	5.95	5.88	6.4	6.42
P_2O_5	0.43	0.01	0.02	0.01	0.04	0.03	0.03	0.03	0.03
LOI	0.48	0.49	0.59	0.49	0.62	0.95	0.87	0.92	0.97
					Parts per million				
Sc	2.1	0.9	1.2	0.2	1.6	1	1.2	nd	0.8
V	34	7	12	5	9	6	5	6	5
Cr	<5	<5	<5	<5	<5	<5	<5	<5	<5
Ni	15	2	2	2	1	14	8	4	11
Cu	19	4	3	4	3	3	4	4	3
Pb	16	15	20	14	18	12	16	26	14
Zn	82	9	14	7	14	54	43	72	51
Ga	23	22	20	21	21	20	23	22	21
Rb	221	156	169	180	168	192	187	211	208
Sr	303	308	390	293	394	292	312	267	284
Y	65	9.5	12.6	6	10.5	47	51	40	61
Zr	129	280	297	214	295	311	282	71	300
Nb	18.8	8.5	9.9	6.7	10.1	14.2	13.9	15.7	15.4
Ba	1 638	671	1 961	892	2 185	1 830	1 877	2 015	1 923
La	272	82	121	49	113	323	364	294	321
Ce	459	105	169	70	155	254	289	255	256
Nd	228	39	50	24	47	206	222	166	190
Th	15	31	37	28	36	53	52	80	53
F	na	na	na	150	na	200	na	na	na
CIPW Norms					**Percentage**				
Ap	0.93	0.02	0.04	0.02	0.09	0..07	0.07	0.07	0.07
Il	0.94	0.21	0.38	0.15	0.38	0.36	0.36	0.34	0.36
Mt	2.44	1.59	2.02	1.36	1.68	0.39	0.82	0.98	0.99
Or	38	26	29	30	29	35	35	38	38
Ab	46	45	40	39	44	45	47	47	43
An	0.56	0.68	1.00	0.58	1.07	1.82	1.22	1.84	1.32
Di	5.93	–	–	–	–	1.37	1.36	–	1.18
Ne	–	–	–	–	–	–	–	–	–
Hy	–	0.33	0.37	0.13	0.16	–	–	0.43	–
Ac	–	–	–	–	–	–	–	–	–
C	–	0.10	2.49	0.34	0.66	–	–	0.00	–
Q	3.37	26	24	28	22	14	14	9.38	14
Hm	0.61	0.15	0.28	0.17	0.27	0.76	0.24	0.26	0.21
Ru	–	–	–	–	–	–	–	–	–
Wo	0.50	–	–	–	–	0.01	0.14	–	0.14
Total	99	100	99	99	99	99	99	99	99

Table 2. (continued)

Sample number	*239*	*240*	*242*	*245*	*247*	*248*	*249*	*251*
MGA coordinates	*291826E 7140966N*	*291826E 7140966N*	*291798E 7140974N*	*292122E 7141595N*	*292122E 7141595N*	*292150E 7141595N*	*292150E 714159N*	*292178E 7141596N*
				Percentage				
SiO_2	69.72	72.71	72.3	61.98	63.3	63.62	63.54	63.55
TiO_2	0.23	0.1	0.12	0.64	0.49	0.41	0.4	0.41
Al_2O_3	15.37	14.15	14.62	16.12	16.62	16.86	16.8	16.95
Fe_2O_3	1.74	0.94	0.44	4.2	3.27	2.12	3.01	2.89
FeO	na	na	0.41	0.34	na	0.89	na	na
MnO	0.04	0.03	0.03	0.12	0.09	0.08	0.07	0.07
MgO	0.12	0.16	0.16	1.49	0.7	0.65	0.54	0.6
CaO	0.63	0.36	0.39	1.49	2.06	1.81	1.77	1.84
Na_2O	5.16	4.89	5.12	5.88	6.19	6.11	6.04	6.01
K_2O	5.52	5.11	5.22	5.37	6.17	6.37	6.38	6.41
P_2O_5	0.05	0.02	0.02	0.21	0.18	0.19	0.17	0.18
LOI	0.51	0.7	0.88	1.11	0.46	0.5	0.49	0.49
				Parts per million				
Sc	1.3	nd	0.8	2.1	2.3	2.2	2.8	2.5
V	9	3	4	43	32	30	29	26
Cr	<5	<5	<5	<5	<5	<5	<5	5
Ni	3	3	5	13	9	5	7	8
Cu	3	4	4	nd	3	4	4	4
Pb	22	9	9	12	13	8	10	10
Zn	32	21	26	207	88	67	70	72
Ga	21	19	20	27	22	22	24	23
Rb	182	178	177	149	139	148	142	145
Sr	589	133	142	651	1 187	1 142	1 177	1 279
Y	26.9	36	33	64	31	26	26.4	25.6
Zr	359	248	177	1 907	211	230	169	189
Nb	12.8	9.1	8.8	39	21.4	17.4	16.9	17.6
Ba	1 668	1 231	1 328	2 132	3 351	2 063	2 187	2 307
La	285	250	292	217	177	153	160	155
Ce	200	182	202	433	349	294	320	307
Nd	131	159	200	220	178	148	160	147
Th	49	26	30	72	23	22	23	22
F	na	na	200	300	na	200	na	na
CIPW Norms				**Percentage**				
Ap	0.11	0.04	0.04	0.46	0.39	0.42	0.37	0.39
Il	0.44	0.19	0.23	0.99	0.93	0.78	0.76	0.77
Mt	1.35	0.83	0.65	–	2.39	1.95	2.30	2.15
Or	33	30	31	32	36	38	38	38
Ab	44	42	44	50	51	51	51	51
An	2.47	1.59	1.53	1.75	–	–	–	0.33
Di	0.29	0.06	0.24	3.49	4.30	4.00	3.32	3.69
Ne	–	–	–	–	–	–	–	–
Hy	0.12	0.25	0.30	1.54	–	–	–	–
Ac	–	–	–	–	1.10	0.37	0.20	–
C	–	–	–	–	–	–	–	–
Q	17	24	22	3.48	0.95	1.17	1.58	1.37
Hm	0.30	0.09	–	4.26	0.26	0.65	0.45	0.54
Ru	–	–	–	0.33	–	–	–	–
Wo	–	–	–	–	1.75	1.36	1.65	1.45
Total	99	99	100	99	99	99	99	99

NOTE: na: not available

SOURCE: Johnson (1991); by permission

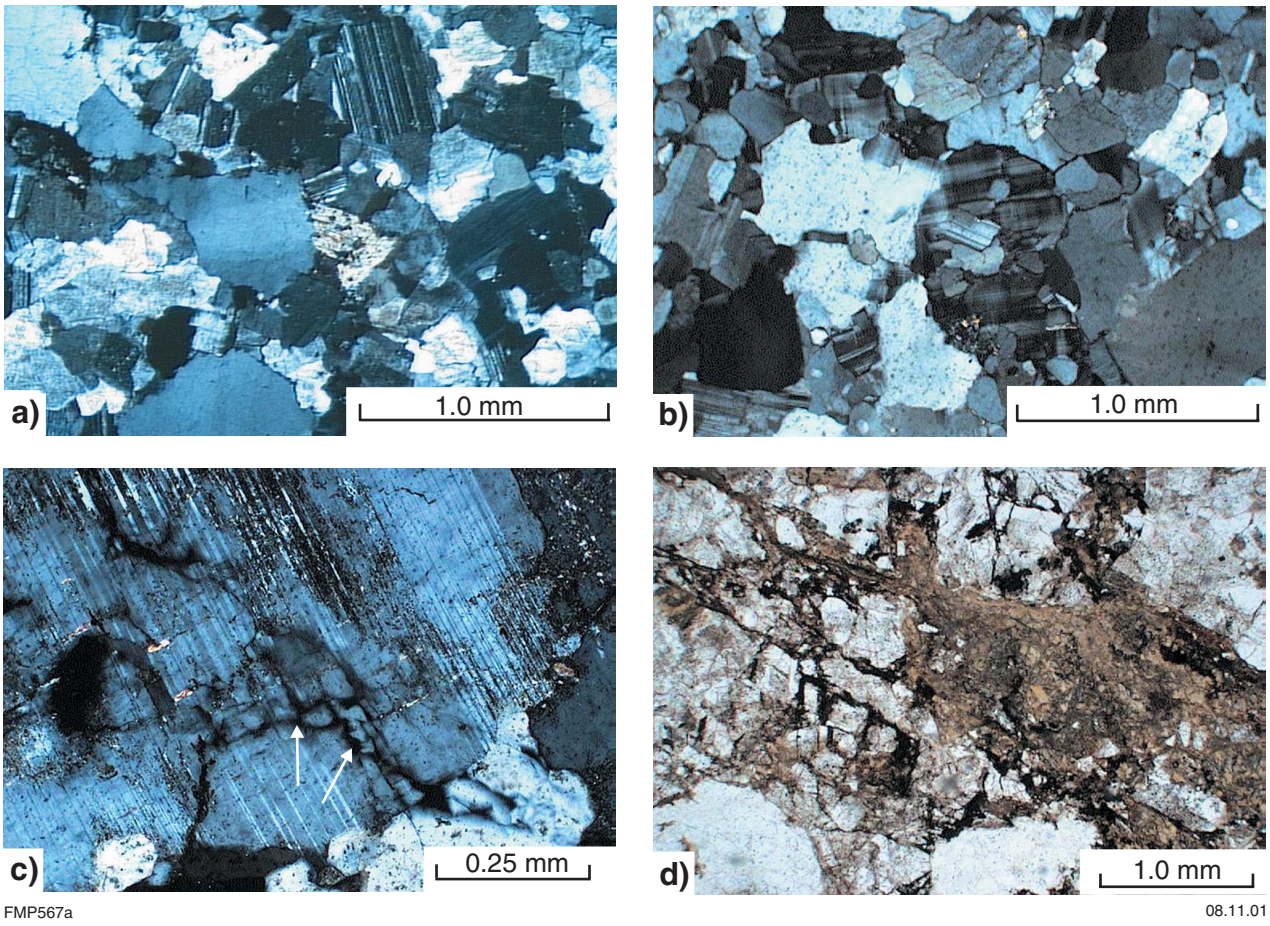

Figure 14. Mineralogical assemblages of the quartz syenite of the Teague Granite (*Ægtex*): a and b) albite–quartz–microcline with granoblastic texture; c) possible pseudotachylite veinlets in feldspar; d) pseudotachylite veinlets cutting across an albite–quartz assemblage and infilled with sericite; (a) to (c) with crossed polars, (d) with plane-polarized light

GSWA 152614, syenite, *Ægtea*; Table 1) and 17 analyses from Johnson (1991; Table 2). In addition, rare earth element (REE) analyses were performed on four samples (GSWA 152612, 152613, 152614, and 120467B; Table 3). Scanning electron microscopy (SEM) and energy dispersive scanning (EDS) analyses of samples GSWA 152162, 152613, and 152614 were carried out at the Australian National University, Canberra, and the analytical techniques and results are discussed in Appendix 2.

Analytical techniques

Major and trace element analyses for this study (six new analyses) were carried out by ANUTECH Pty Ltd at the Australian National University INAX laboratory in Canberra. Major elements were determined by X-ray fluorescence (XRF) using a PW2400 spectrometer. Samples were fused into glass discs using a lithium borate flux consisting of 12 parts lithium tetraborate to 22 parts lithium metaborate, following the method of Norrish and Hutton (1969). Trace elements were analysed using a Phillips PW1400 XRF spectrometer following methods discussed by Chappell (1991) and using energy dispersive X-rays or monochromatic X-rays from secondary targets to achieve low backgrounds and therefore low detection limits. Instrumental neutron activation analysis (INAA) was completed using the method of Chappell and Hergt (1989). Rare earth element analyses were performed by laser ablation inductively coupled plasma mass spectrometry (ICP-MS).

Johnson's (1991) 17 major and trace element analyses, with the exception of Na_2O, FeO, and F, were performed by XRF using a Siemens SRS-1 spectrometer, following the method of Norrish and Hutton (1969) with some modifications by Nesbitt and Stanley (1980). Na_2O concentrations were measured by atomic absorption spectroscopy (AAS) using standard methods (Nesbitt and Stanley, 1980). FeO concentrations were determined by titration. Fluorine was determined by specific ion electrode analysis, following the method of Nicholson (1983). All analytical procedures were calibrated against internal and international standards (Nesbitt and Stanley, 1980).

Major, trace, and rare earth elements

The petrography of the Teague Granite indicates that it is of syenitic composition, with the mineral assemblage and textural relationships suggesting that it is derived from the alteration of a precursor granitoid. The magmatic age of the Teague Granite is 2648 ± 8 Ma (see **Geochronology**),

which is within the age range for other Archaean alkaline rocks in the Yilgarn Craton (e.g. Smithies and Champion, 1999). Thus, the analytical data (Tables 1, 2, and 3) for the Teague Granite are compared with Yilgarn Craton granitoids and syenites. With this purpose in mind both Johnson's (1991) and the new analytical data were normalized against high-Ca granites of the Yilgarn Craton (considered representative of a typical granitoid in the region; Champion and Sheraton, 1997) and late Archaean alkaline intrusions (Smithies and Champion, 1999) of the Yilgarn Craton. The multi-element plots for each of the two datasets used are presented in Figures 17 to 22.

Figures 17 and 18 show sample groups of syenite and quartz syenite from Johnson's (1991) dataset normalized to Yilgarn Craton high-Ca granites. Figure 17 indicates Si and Mn depletion; enrichment in Fe, Ti, Na, K, Al, Mg, Zr, Ce, Th, and P; enrichment in Ni, V, Zn, the large ion lithophile elements (LILE; Rb, Y, Nb, Ba, La, Nd), Ca, and Sr; and depletions in Cu, Pb, and Sc, compared to the high-Ca granites. The enrichment in Ni may indicate the possible addition of meteoritic elements, whereas addition of LILE may be related to alkali alteration. In Figure 18, the alkali (Na and K) enrichment is less pronounced, Ti and P are depleted, as are all of the base metals, whereas Si is practically unchanged. This variation in the chemistry may reflect stages of silicification of the syenitic rock, with destruction of feldspars and Fe–Mg silicates. Figure 19 shows plots of the second dataset (this study; with one sample from each granitoid type; see Table 1), also normalized to high-Ca granites. These plots indicate that for all three granite compositions (*Ægte, Ægtex, Ægtea*), compared to the high-Ca granites, there is depletion in Mn, Ti, Mg, Ca, and P, enrichment in Fe and K, depletion in siderophile and chalcophile elements (V, Cr, Ni, Cu, Zn), Y, Nb and La, and enrichments in Zr and Sr. Cerium is enriched in the quartz–albite–orthoclase granite (quartz syenite, *Ægtea*) and depleted in the leucocratic alkali-feldspar granite (*Ægte*).

Major and trace elements from the new analyses (this study; Table 1) were also compared with 2630–2650 Ma Archaean syenitic intrusions of the Yilgarn Craton (Claypan Suite; Smithies and Champion, 1999). Figure 20 shows that the Teague Granite samples are all depleted in major oxides compared to the Claypan Suite, except for Mn and K. Trace elements also show overall depletions for metallic elements (Sc, V, Cr, Ni, Cu, Zn), but minor

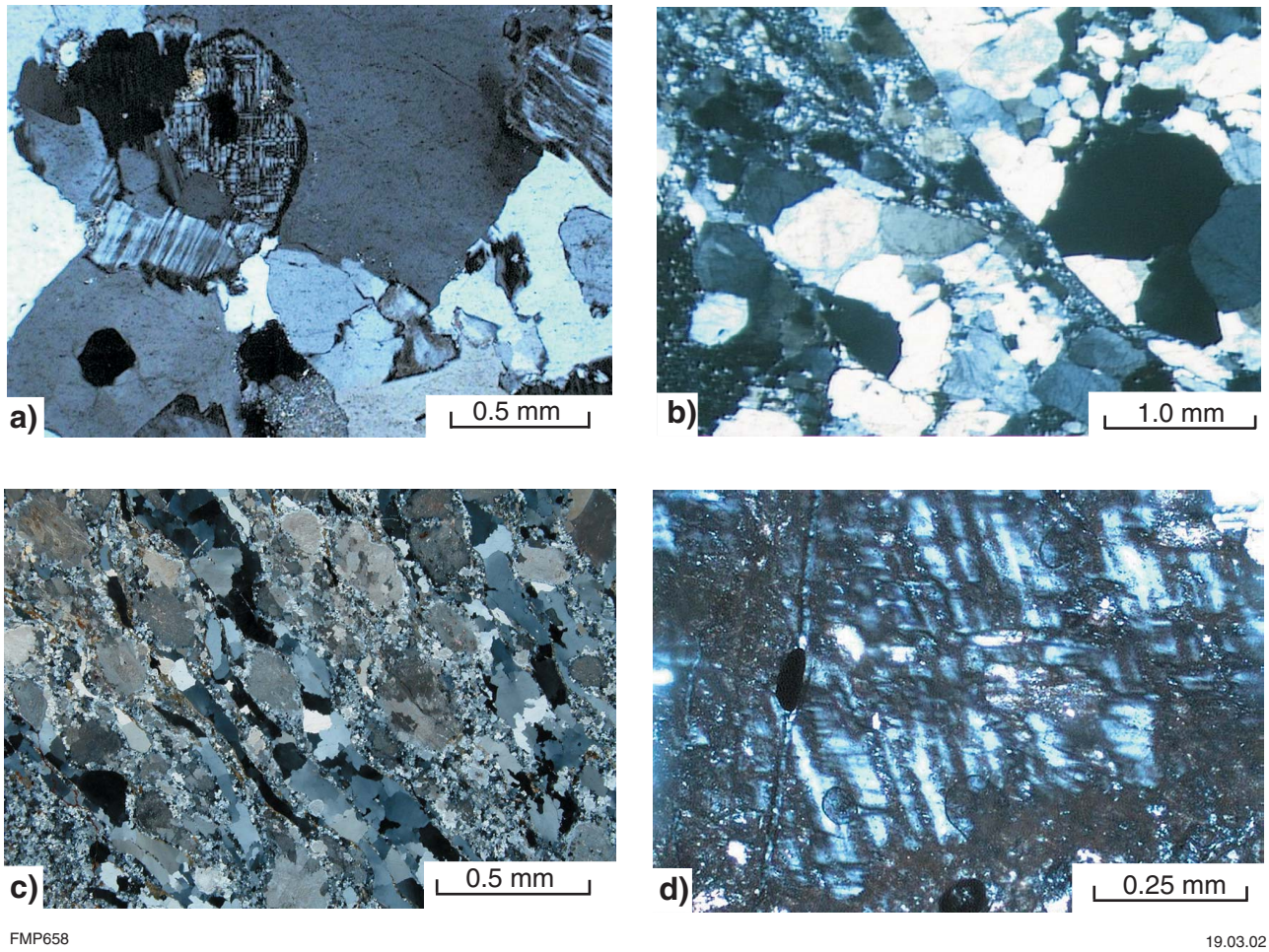

Figure 15. Mineralogical assemblages of the leucocratic alkali-feldspar granite of the Teague Granite (*Ægte*): a) with the assemblage of quartz–microcline(–albite); b) fractured and partly silicified leucocratic granite; c) mylonitic fabric with ribbons of clear quartz and turbid feldspar in a recrystallized quartz matrix; d) reticulate texture in potassic–sodic feldspar, probably diaplectic glass; all with crossed polars

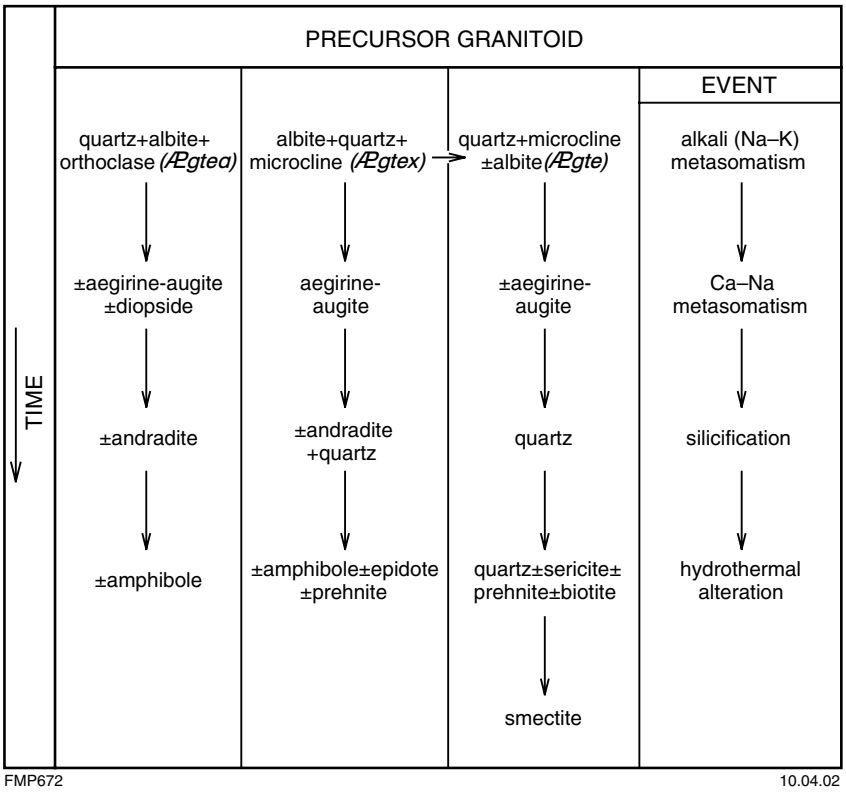

Figure 16. Mineral assemblages of the Teague Granite and tentative paragenesis

Table 3. Rare earth element abundances of the Teague Granite

GSWA sample	*152612*	*152613*	*152614*	*120467B*	*Average*
Lithology	*Leucocratic alkali–feldspar granite (Ægte)*	*Quartz–microcline–albite granite (Ægtex)*	*Quartz–albite–orthoclase granite (Ægtea)*	*Quartz syenite (Ægtex)*	*Morapoi Supersuite (Witt and Davy, 1997)*
MGA coordinates	*294432E 7137221N*	*293289E 7141449N*	*291616E 7413460N*	*289386E 7137253N*	
			Percentage		
La	9.19	42.34	139.65	210.93	31.50
Ce	18.75	71.23	218.72	288.24	59.02
Pr	2.12	6.87	20.71	42.5	7.65
Nd	7.58	21.12	62.67	116.96	29.38
Sm	1.30	2.86	7.96	19.7	4.47
Eu	0.471	0.649	1.635	5.6	1.26
Gd	0.79	1.94	4.57	14.7	2.99
Dy	0.40	1.20	2.51	7.3	1.62
Er	0.19	0.55	1.14	2.7	–
Yb	0.22	0.59	1.21	1.66	0.56
Lu	0.035	0.089	0.176	0.33	0.11
Hf	1.44	4.38	18.65	0.92	–
Ta	0.102	0.721	1.062	–	–
Th	1.47	23.46	40.02	10.3	–
U	0.54	4.20	6.96	2.8	–

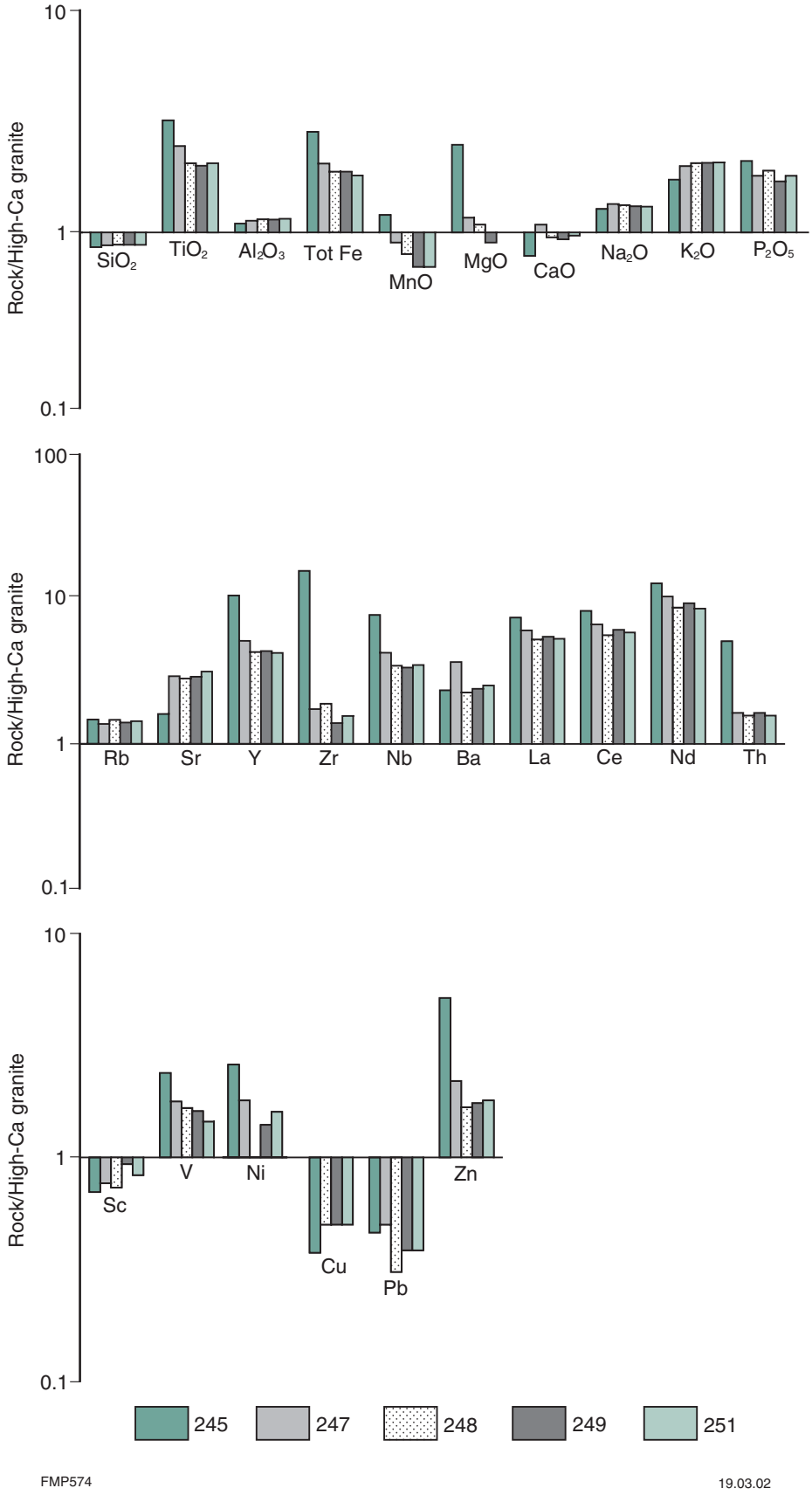

Figure 17. Bar diagrams showing major and trace element variations of syenite of the Teague Granite normalized to average high-Ca granite of the Yilgarn Craton. Dataset from Johnson (1991). Sample numbers from Table 2; collected from the eastern part of the central uplift

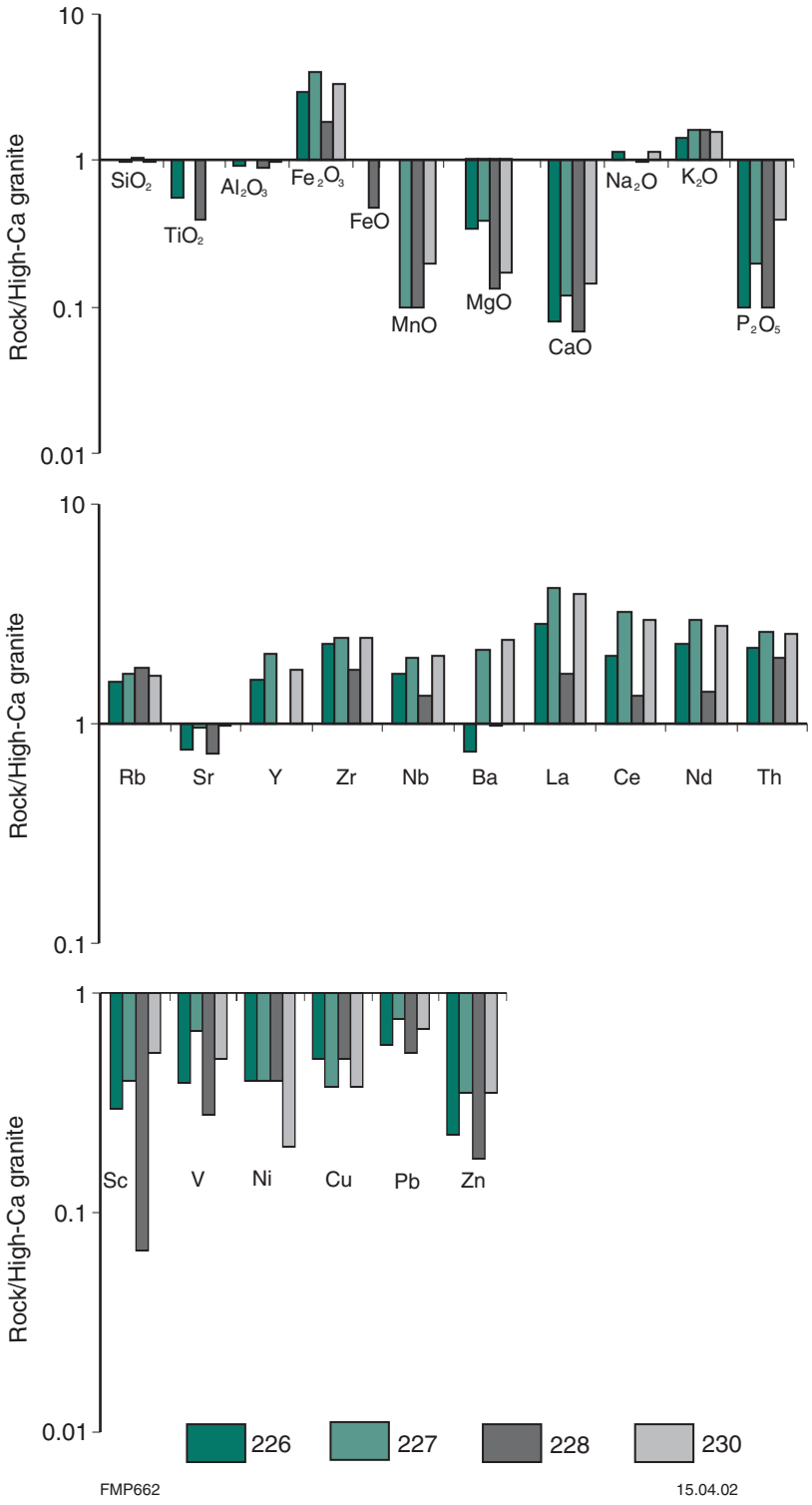

Figure 18. Bar diagrams showing major and trace element variations of quartz syenite of the Teague Granite normalized to average high-Ca granite of the Yilgarn Craton. Dataset from Johnson (1991). Sample numbers from Table 2; collected from the eastern part of the central uplift

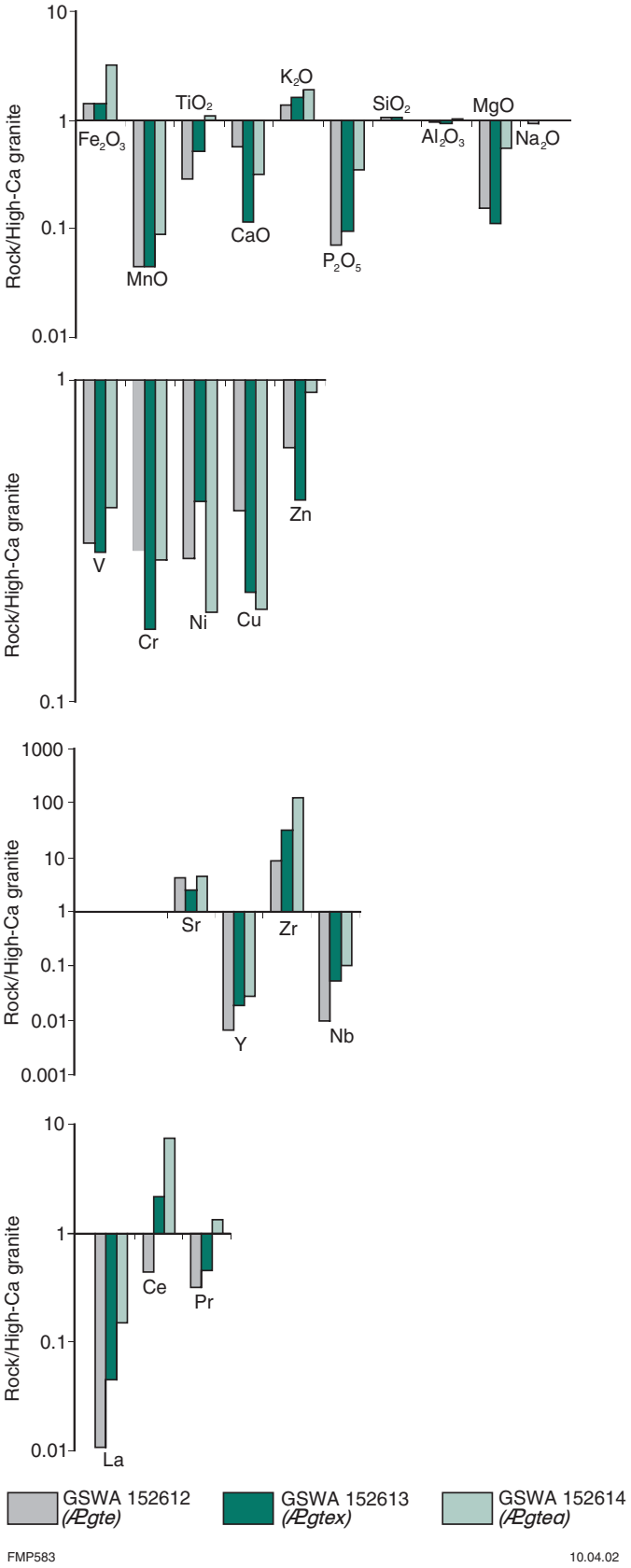

Figure 19. Bar diagrams showing major and trace element variations of new analyses of the Teague Granite (GSWA 152612, leucocratic alkali-feldspar granite; GSWA 152613, quartz syenite; GSWA 152614, syenite), normalized to average high-Ca granite of the Yilgarn Craton (Table 1). Dataset from this study

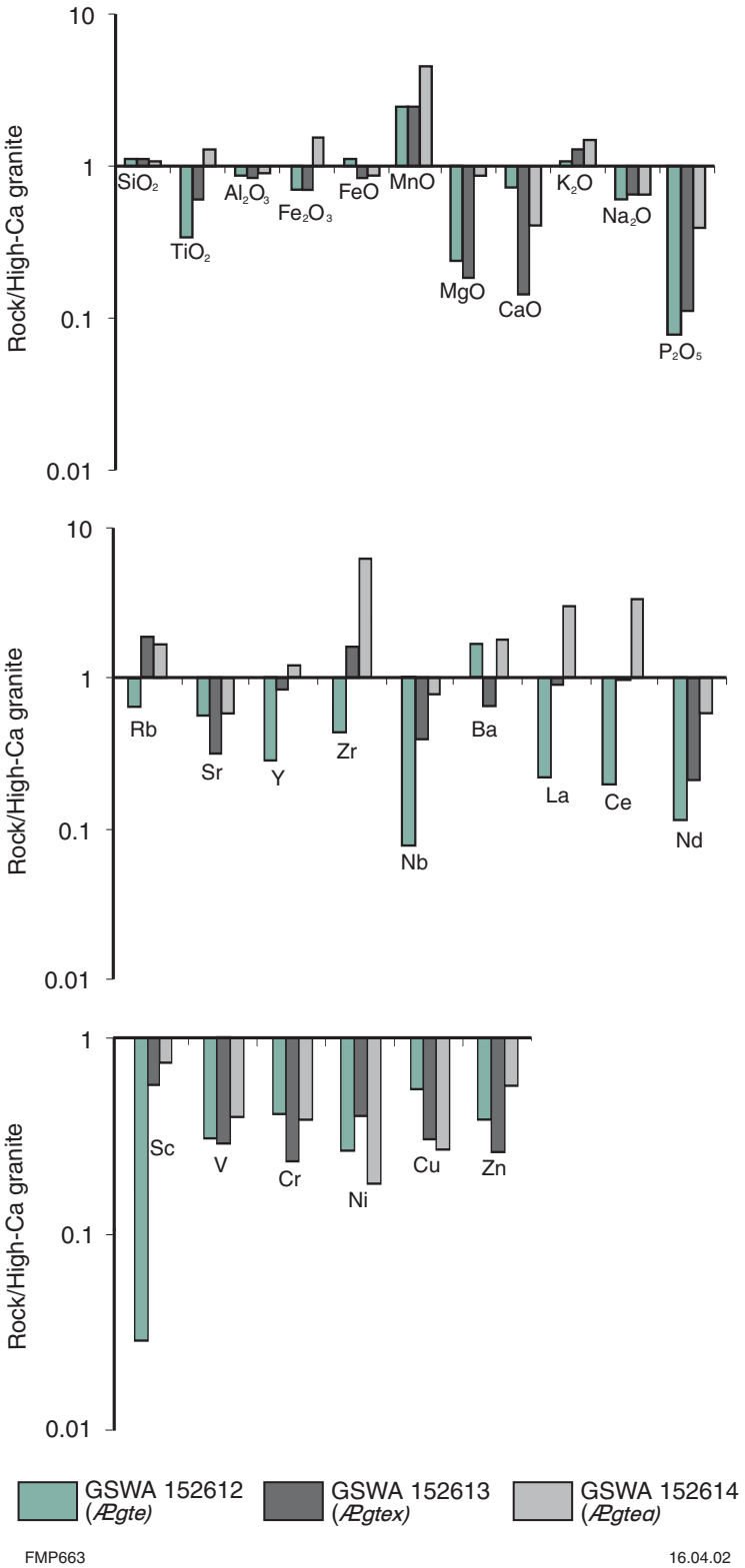

Figure 20. Bar diagram showing major and trace element variations of new analyses of the Teague Granite (dataset from this study; Table 1) normalized to alkaline rocks of the Claypan Suite from the Yilgarn Craton (data from Smithies and Champion, 1999; Table 1)

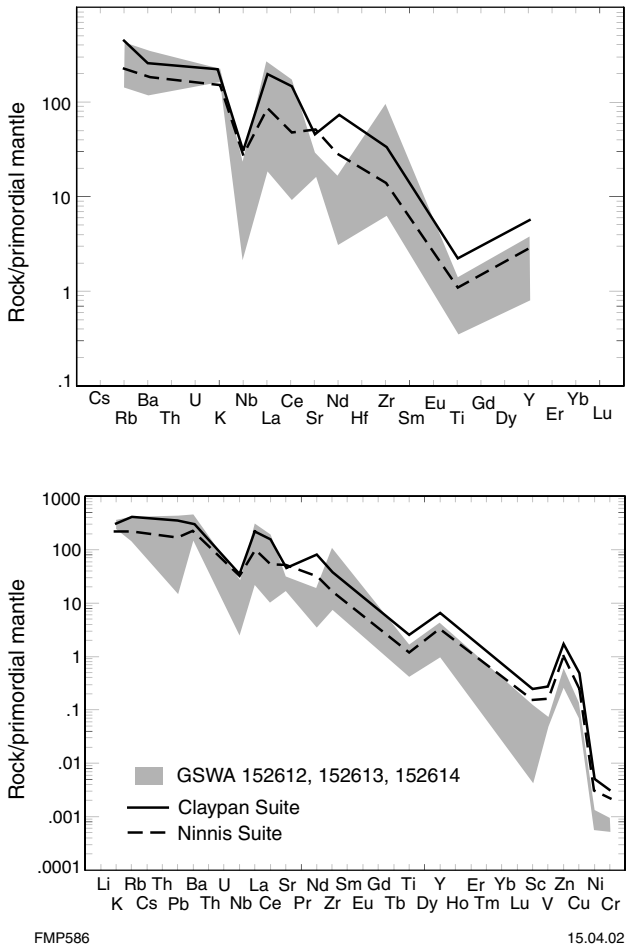

Figure 21. Multi-element spider diagram for Teague Granite samples (dataset from this study) and Yilgarn Craton syenites (data from Smithies and Champion, 1999) normalized to primordial mantle; normalization factors after Sun (1982)

enrichment for Rb, Zr, Ba, La, and Ce, particularly for the syenite unit of the Teague Granite (GSWA 152614). Multi-element spider diagrams (Fig. 21) normalized to primordial mantle reveal parallel patterns, suggesting that the composition of the Teague Granite is broadly similar to that of the syenitic Claypan (A) and Ninnis (B) Suites of Smithies and Champion (1999).

The lack of available REE analyses from the Claypan and other suites in the Smithies and Champion (1999) datasets necessitated comparison of REE data of four Teague Granite samples with REE data from alkaline rocks of the Morapoi Supersuite of the Yilgarn Craton (Witt and Davy, 1997; average of five samples). Figure 22 shows that the syenite unit of the Teague Granite (GSWA 152614 and 120467B) is enriched in REE by almost one order of magnitude compared to the average Morapoi Supersuite (sample 93903-7), whereas the leucocratic alkali granite unit (GSWA 152612) shows a pattern of REE depletion. The quartz syenite unit of the Teague Granite (GSWA 152613) has similar REE values as the average Morapoi Supersuite syenite. The strong REE enrichment of the Teague Granite syenite compared to average Morapoi Supersuite syenite suggests that the precursor granitoid was modified by alkali alteration.

Hydrothermal alteration

Meteoroid impacts induce considerable fracturing and brecciation of the target rocks, thus enhancing their permeability. This promotes hydrothermal circulation within and around the impact structure and can also lead to the subsequent formation of oil and gas traps (Gorter, 1998). In large impact structures, such as Vredefort, Chixculub, Sudbury, and Woodleigh, a thick coherent melt sheet and melt breccia (suevite) would have formed surrounding the central uplift. Although the melt sheet and suevite can be several kilometres thick, their aspect ratio, with respect to the overall crater diameter, is probably around 1:50 (Grieve and Thierriault, 2000).

Melting of the target rocks resulting from the conversion of kinetic to thermal energy causes thermal perturbations and heat release in meteorite impact structures, particularly in the central structural uplifts, because deeper and hotter crust is brought near the surface, and there is an instantaneous formation of a steep inverse thermal gradient, from thousands of degrees centigrade within and immediately around the projectile (resulting in its evaporation) to a few hundred degrees below the crater floor. The melt sheet, suevite, and the conversion of kinetic energy into heat combine to constitute a powerful heat source for a spectrum of phenomena from partial melting to high-temperature metamorphism, as well as the inception of hydrothermal convection cells in the underlying breccias and below the crater floor (McCarville and Crossey, 1996; Grieve and Thierriault, 2000). Impact melt sheets can provide the heat source necessary to drive hydrothermal systems for about 100 000 years (Kring, 1995; McCarville and Crossey, 1996). In general, the transformation of kinetic energy into heat occurs mainly at subcrater levels, where hydrothermal circulation would

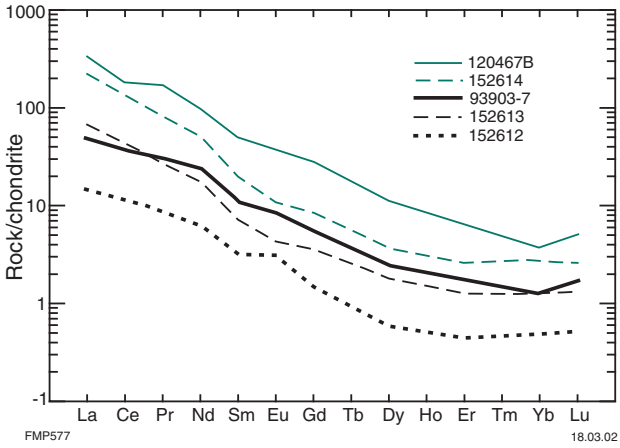

Figure 22. Chondrite-normalized rare earth element plot for the Teague Granite compared with average values for Morapoi Supersuite granitoids (sample 93903-7, data from Witt and Davy, 1997); normalization factors after Sun (1982)

be focused. Impact-related hydrothermal circulation can extend well below the crater floor to depths of several kilometres (Komor et al., 1988), and heated fluids can vent at the surface as hot springs and geysers, forming silica-rich deposits, as observed in geothermal areas of active volcanic environments (Newson, 1980). Fluid channels and degassing pipes have been reported from the Ries impact crater in Germany (Newsom et al., 1986). Hydrothermal convection cells from heated groundwater are then generated that can form hydrothermal mineral deposits.

Examples of hydrothermal ore deposits that can be related to impacts are numerous, and include lead, zinc, silver, and barium at Siljian in Sweden, lead–zinc associated with the Kardla Crater in Estonia (Puura et al., 2000), and copper, zinc, lead, and gold at Vermilion in the Sudbury structure (Grieve and Masaitis, 1994; Pirajno, 2000). Apart from hydrothermal mineral deposits, hydrocarbons can also be located in impact structures (Gorter, 1998). The Ames buried structure (450 Ma, 14 km diameter in Oklahoma, USA) contains important reserves of hydrocarbons (Donofrio, 1998). In Queensland, Australia, the 55 km-diameter Tookoonooka structure also contains hydrocarbons (Gorter, 1998). World-class oil and gasfields in the Gulf of Mexico are contained in Chicxulub impact breccia reservoirs (Grieve and Thierriault, 2000).

It is likely that the meteorite impact that created the Shoemaker impact structure formed a melt sheet that, together with heat generated by impact energy in the central uplift, gave rise to a hydrothermal convection system, within and around the central uplift zone. If a melt sheet was present, it would have acted as a magma-like heat source within the crater structure and would have formed several hot springs in the crater and surrounding areas. The thermal perturbation in the central uplift alone would have provided a significant heat source. In fact, it is estimated that the volume of water heated by the central uplift is twice that provided by the impact melt sheet (Crossey et al., 1993). The pods of quartz-jasperoidal material that are present along structural breaks (Plate 1) in the eastern rim of the Shoemaker impact structure may be the eroded remnants of fluid channels that fed thermal springs.

A hydrothermal system would have resulted in heated fluids circulating below the crater floor. Several studies have reported evidence of circulation of hydrothermal fluids heated by impact thermal energy. This evidence comes from fluid inclusion studies (Komor et al., 1988), petrography, and geochemistry (Puura et al., 2000; Short and Gold, 1996; Koeberl et al., 1996; McCarville and Crossey, 1996). The influence of impact-related hydrothermal activity in the Shoemaker structure could have extended well beyond the crater into the surrounding country rocks. Fluid inclusion studies suggest that the MVT mineralization hosted by the Sweetwaters Well Member appears to have undergone remobilization during a later heating event, with temperatures well above those generally attributed to circulation of basinal fluids. In the absence of recognized tectonothermal events in the region from 1600 Ma to about 500 Ma, it is tempting to speculate that the later heating event was induced by the Shoemaker impact.

Hydrothermal activity associated with impact events has been reported from the Ries (Germany, Newsom et al., 1986), Puchezh-Katunki (Russia, Naumov, 1993), Manson (McCarville and Crossey; 1996), Vredefort, and Sudbury structures (Canada, Grieve and Thierriault, 2000), and the Gosses Bluff structure in Australia (Milton et al., 1996). Newsom (1980) proposed a model of interaction of water and impact melt sheets. Commonly, impact-related hydrothermal systems result in the remobilization and deposition of sulfides in breccias or fracture zones. In the Ries impact structure, hydrothermal alteration minerals include illite, montmorillonite, analcite, calcite, siderite, K-feldspar, quartz, barite, and chlorite (Newsom et al., 1986). The 80 km-diameter Puchezh-Katunki impact crater is characterized by widespread hydrothermal alteration, mainly concentrated within the central uplift, which is composed of brecciated Archaean basement rocks (Naumov, 1993). Naumov (1993) recognized the following hydrothermal assemblages: chlorite–albite–epidote–calcite, associated with andradite, epidote, and prehnite in fractures; prehnite–calcite–pyrite, with an absence of Ca–Fe silicates; and zeolites–apophyllite–calcite–anhydrite–pyrite in vugs and fractures. Masaitis and Naumov (1993) modelled the hydrothermal convection for the Puchezh-Katunki structure and assumed that the fluids originated by infiltration of water from a crater lake towards a lens of hot impact breccia and basement rocks. These fluids would have reached the surface along the uplifted margins. On the basis of Naumov's (1993) mineral assemblages and their modelling, Masaitis and Naumov (1993) proposed three stages of hydrothermal activity: an initial stage, with temperatures of about 400–500°C, decreasing downward and outward from the impact site; a main stage, with maximum temperatures of 200–300°C, and fluids circulating at depths of 2.5 – 4 km; and a final stage, in which circulation is restricted to the uppermost parts of the basement rocks, with temperatures of 100–150°C.

In the Shoemaker impact structure, the effects of interaction of impact energy-induced hydrothermal convection within the impact aureole are evident in the granitoid rocks of the central uplift and in rocks of the Yelma and Frere Formations in the eastern inner ring (Fig. 23). Outcrops of Teague Granite in the east and southeast (*Ægte*) are fractured (Fig. 12), hydrothermally altered, and partially to pervasively silicified (Fig. 15a,b). The leucocratic granitoid rock (*Ægte*; Fig. 15) is probably the result of stages of silicification of the Teague Granite. This silicification was pervasive in places, whereby the entire granitoid is replaced by quartz (Fig. 15a,b). The silicified Teague Granite was also fractured (Fig. 15b) and overprinted with fracture-controlled sericitic alteration (Fig. 24c,d). A second-stage silicification of the leucogranite is suggested by the clear, anhedral, and almost unstrained quartz, and the absence of relic microcline (Fig. 24c). This silicification is associated with non-pervasive, fracture-controlled sericitic alteration (Fig. 24d). The two generations of hydrothermal quartz are characterized by euhedral and fluid inclusion-rich quartz, and fine-grained to microcrystalline quartz, filling fractures. In places, fibrous amphibole (actinolite–tremolite) infills microfractures in the rock and in a network of cracks in the garnet crystals that are locally

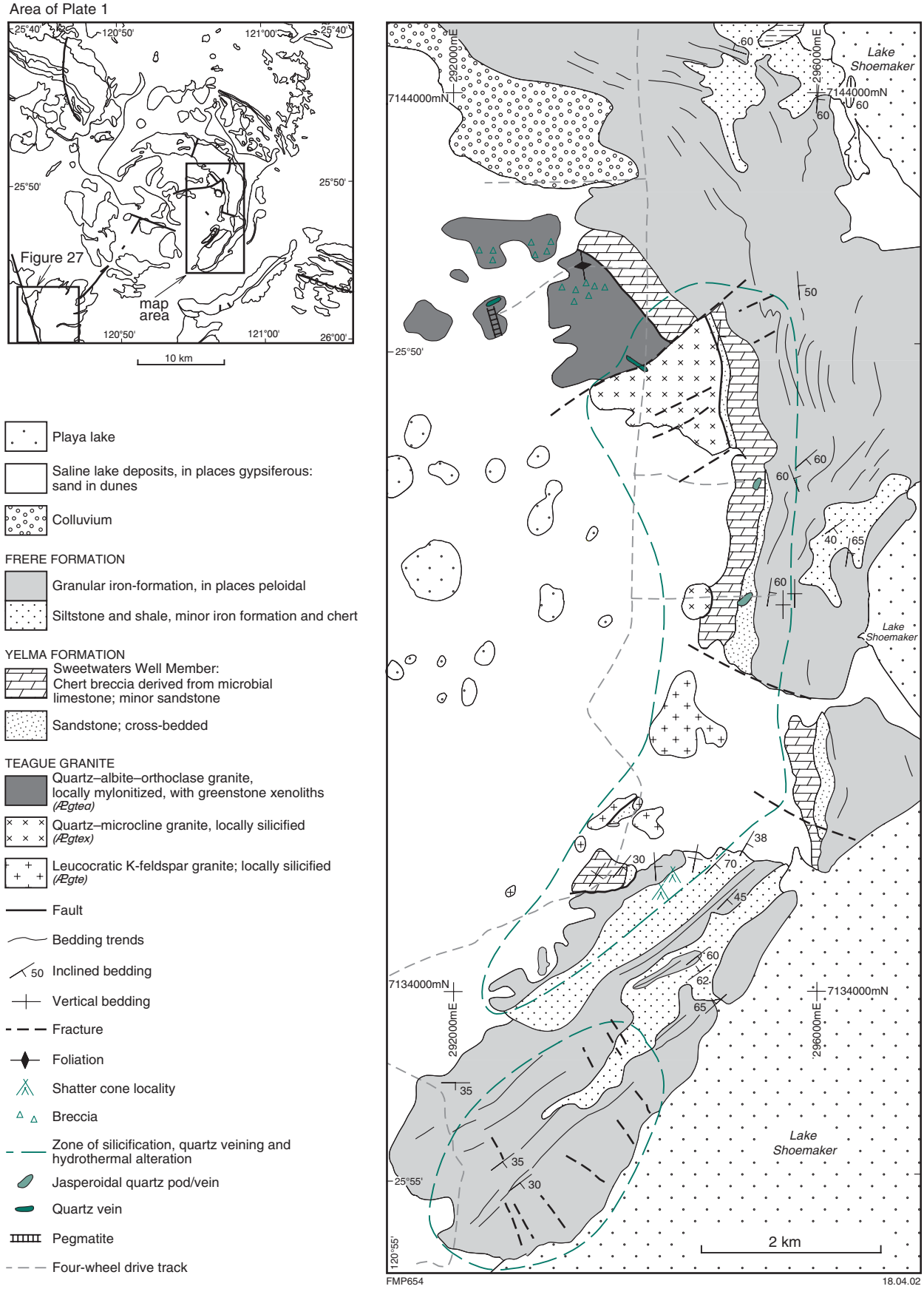

Figure 23. Geological map of the eastern inner ring of the Shoemaker impact structure, showing the extent of hydrothermal alteration

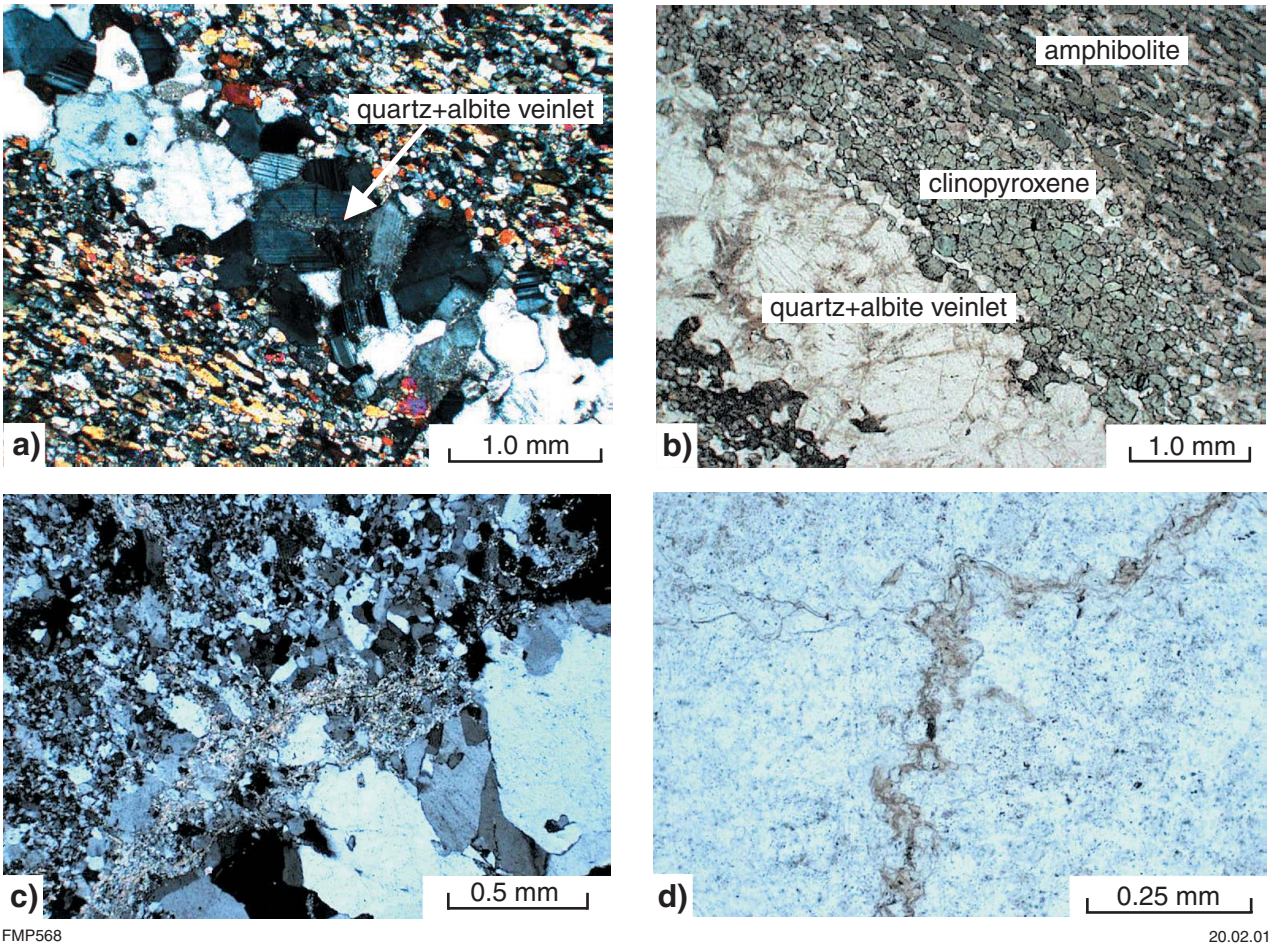

Figure 24. Alteration of the Teague Granite and greenstone enclaves: a and b) quartz–albite vein with a selvage of diopside cutting through an amphibolite xenolith; c) two phases of silicification (fine- and coarse-grained quartz), overprinted by sericite; d) silicified granite cut by a sinuous microfracture infilled with sericite; (b) to (d) with plane-polarized light, (a) with crossed polars

present in the Teague Granite (Fig. 25a). Andradite garnets have also been found in hydrothermally altered rocks in the Manson impact structure for which a reaction of the type given below is postulated (McCarville and Crossey, 1996):

$$3Ca_2 + 2Fe_3 + 3H_4SiO_4 + O_2 \rightarrow Ca_3Fe_2Si_3O_{12}\ \text{(andradite)} + 12H^+$$

White mica, quartz, sericite, and fibrous amphibole infill microfractures that may have been pseudotachylite veinlets (Fig. 14d). In addition, the results of alkali and calcium metasomatism on greenstone enclaves can be seen in Figure 24a,b in which a quartz–albite veinlet, associated with selvages of Ca-pyroxene (diopside), cuts through an amphibolite enclave in the Teague Granite. All these features indicate that hydrothermal minerals were precipitated during phases of post-impact hydrothermal activity. Some of the mineral phases associated with this hydrothermal activity are illustrated in Figures 24 and 25.

Pervasive silicification affected rocks of the Yelma Formation (Sweetwaters Well Member), whereas the granular iron-formation of the Frere Formation exhibits crosscutting quartz veining and is partially silicified (Fig. 26a). In the same area, pods of chert and jasperoidal quartz (*qc*) are present along the eastern margin of the central uplift (e.g. MGA 293644E 7135141N; Fig. 26b). The chert material consists mainly of brecciated microcrystalline quartz cemented by chalcedonic quartz. Open spaces are filled with euhedral quartz crystals. Dark-grey to opaque patches are possibly carbonaceous matter, and are associated with opaque spherules, 0.07 to 0.1 mm in diameter, and vermiform shapes, 0.25 to 0.2 mm long. Colourless and nearly isotropic rhombohedral crystals may be either dolomite or anglesite. These chert pods may have formed by precipitation from hydrothermal fluids that circulated along the boundaries of, or along faults in, the eastern sector of the Shoemaker impact structure.

Southwest of the Shoemaker impact structure, a number of northeast-trending, milky-white quartz veins are associated with, and parallel to, northeasterly and north-northeasterly trending fractures in hornblende–quartz–monzonite (*Agzq*; Fig. 27 and Plate 1). The attitude of the veins and associated fractures suggests a pattern that converges towards the centre of the Shoemaker impact structure. The quartz veins post-date the hornblende–quartz monzonite that was emplaced at 2664 ± 4 Ma

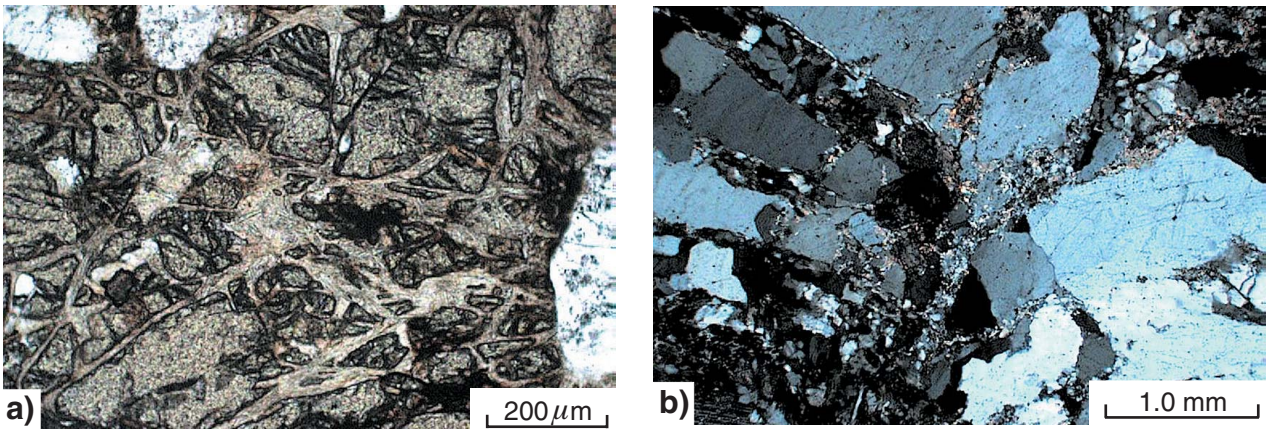

Figure 25. Hydrothermal alteration of the Teague Granite: a) sericite infilling fractures in garnet crystal (plane-polarized light); b) fracture-controlled sericitic alteration of leucogranite (crossed polars)

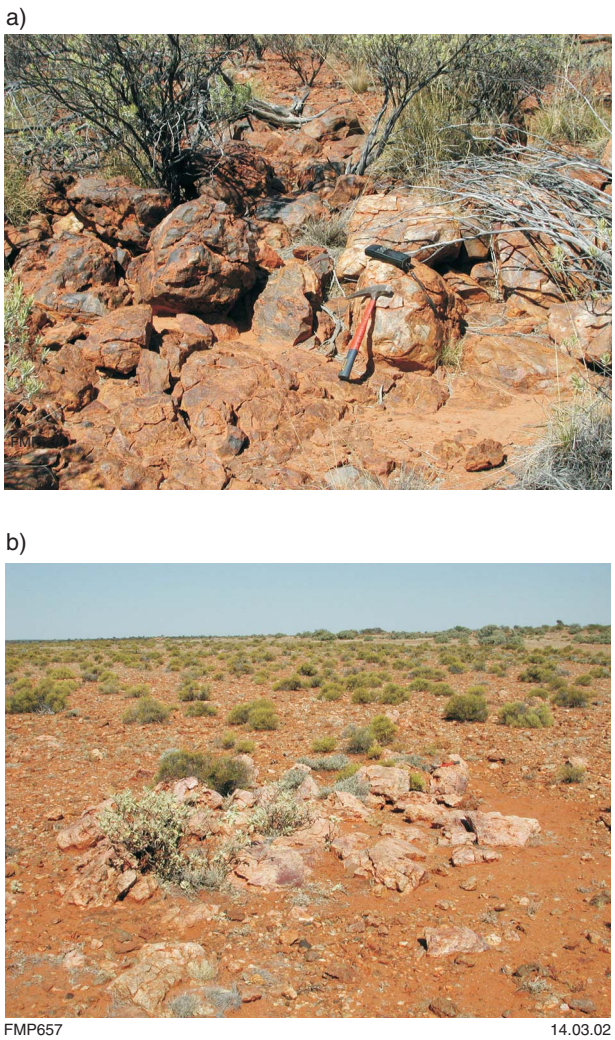

Figure 26. a) Outcrops of partially silicified granular iron-formation (Frere Formation); b) pod of jasperoidal chert

(Nelson, 1999) and indicate hydrothermal activity in the area. Other Archaean granitoid rocks in the region do not display the same regular pattern of quartz veins and fractures. It is possible, therefore, that the northeast-trending fractures are impact related and that their local infilling with quartz results from impact-induced circulation of hydrothermal fluids.

Mineralization

Although meteorite impacts are transient high-energy events, they trigger longer term processes such as hydrothermal convection cells. The consequences in terms of ore formation or modification of existing mineralization can be considerable. There is a substantial body of evidence to suggest that economically important mineral deposits owe their existence, directly or indirectly, to meteorite impact events. Grieve and Masaitis (1994) detailed the economic potential of impact structures and three types of mineral deposits associated with impact structures: pre-impact mineral deposits, subsequently modified during and after the impact; mineral deposits formed as a direct consequence of the impact; and mineral deposits formed by post-impact hydrothermal activity and flow of fluids (including hydrocarbons) into permeable lithologies, fractures, and faults. Examples of deposits that were formed as a consequence of a meteorite impact are those of the 1850 Ma Sudbury structure in Canada (Grieve and Therriault, 2000). These include world-class magmatic nickel–copper–PGE (platinum group element) deposits and hydrothermal zinc–copper–lead massive sulfide deposits.

The mineral deposits near the Shoemaker impact structure are an example of the first category. Spatially associated with the Shoemaker impact structure are deposits of massive iron oxides, and lead–zinc(–copper) sulfides hosted in stromatolitic carbonate rocks of the

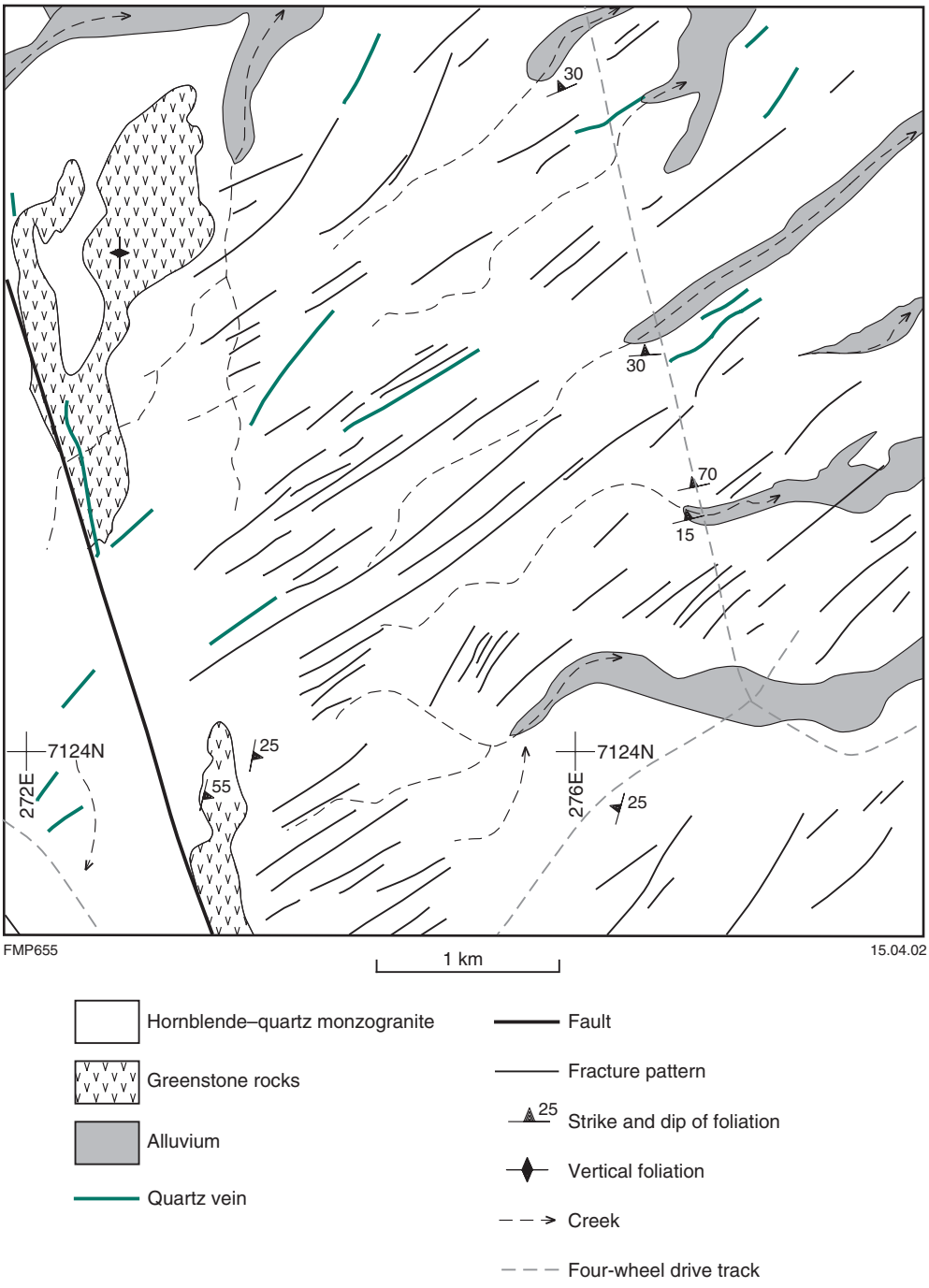

Figure 27. Simplified geological map of Archaean hornblende–quartz monzonite southwest of the Shoemaker impact structure, showing the northeast-trending fracture pattern and associated quartz veins. See Figure 23 for location

Sweetwaters Well Member (Yelma Formation). Evidence of hydrothermal activity and associated wallrock alteration was examined in the previous section.

Regolith geochemical anomaly

Anomalous abundances of gold (up to 6 ppb) in regolith materials (sheet wash) were recorded over an area about 30 to 40 km east-northeast of the centre of the Shoemaker impact structure (Morris et al., 1997). This area coincides with structures that are possibly related to the impact (Fig. 4). It is possible that fluids were mobilized from gold-bearing Archaean basement during impact-related hydrothermal activity.

Rare earth elements

The Teague Granite was investigated for rare earth element mineralization, but with no success (Metals Exploration Limited, 1983). During this exploration

program, Ce and La values of up to 1550 and 570 ppm respectively were obtained. Average Ce and La contents of the samples from this study are 150 and 100 ppm respectively (Table 3).

Iron oxides

Along the entire eastern part of the inner ring, prominent ridges are made up of folded outcrops of massive iron oxides (*PEfgi*), possibly due to supergene enrichment, within peloidal granular iron-formation rocks (Frere Formation). In the southeast of the inner ring, the granular iron-formation units form a lens, which is well defined on the TMI image (Plate 1) and characterized by abundant magnetite (*PEfgmi*). Although not uncommon in the Frere Formation (Adamides et al., 2000), these iron oxide-enriched rocks appear to be more common on the eastern inner ring of the Shoemaker impact structure. The trend of the outcrops indicates a type of small-scale folding (Plate 1; Fig. 23) that is not found elsewhere in the granular iron-formation of the Earaheedy Group. This deformation and iron-oxide enrichment in the eastern inner ring is consistent with the interpretation that the Shoemaker impact structure has a regional tilt to the east (see **Conclusion and discussion**), where the higher and therefore more fractured and altered levels of the structure are exposed.

Granular iron-formation units east-southeast of the Shoemaker impact structure on Granite Peak are cut by east-trending faults (Fig. 4). Along these faults the rocks are partly to pervasively silicified and contain abundant stilpnomelane. The stilpnomelane, a complex mica containing K, Na, Fe, Mg and Mn, is concentrated along microfractures (Fig. 28) suggesting that it was precipitated from alkali-rich hydrothermal fluids.

Zinc, lead, and copper sulfides

Carbonate-hosted sulfide and sulfate mineralization is present at a number of localities on the northwestern side of the Shoemaker impact structure (Fig. 4), over a strike length of 50 km. Except at the Sweetwater (on Merrie; Adamides, 2000) and Iroquois (on Nabberu; Pirajno and Jones, in prep.) prospects, the mineralization does not outcrop but was intersected in drillcore at depths ranging from 100 to 350 m, beneath the Frere Formation. The Iroquois prospect is closest to the Shoemaker impact structure (Fig. 4, Plate 1); another important prospect is Navajo, 6 km west-northwest of Mount Teague (outside the area of Plate 1; Fig. 4). These prospects have been investigated in detail by Renison Goldfields Consolidated, following a systematic diamond and reverse-circulation drilling program (Edgar, 1994; Feldtmann, 1995; Dörling, 1998).

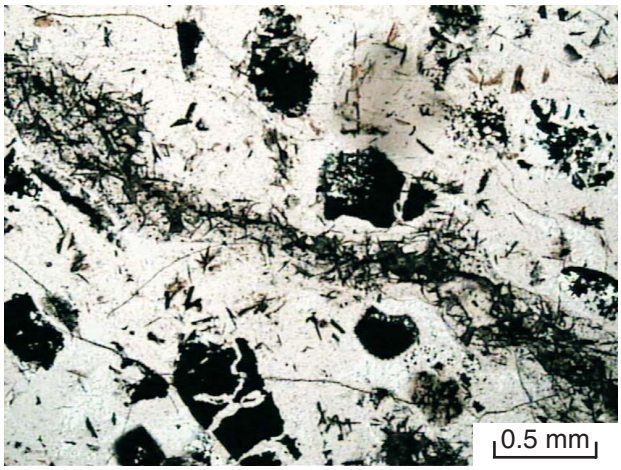

Figure 28. Stilpnomelane crystals along a microfracture in silicified iron-formation (plane-polarized light)

The carbonate rocks that host the mineralization belong to the newly defined Sweetwaters Well Member (Yelma Formation; Hocking et al., 2000), which is about 100 m thick and consists mainly of dolomite overlain and underlain by sandy dolomite and dolomitic feldspathic sandstone units. The dolomitic feldspathic sandstone unit at the top of the dolomite grades eastward to micaceous sandstone and is overlain by granular iron-formation of the Frere Formation. The Sweetwaters Well Member dolomite is light grey to grey, and massive to algal-laminated, commonly with stromatolite forms. Details of stromatolite taxa of the Earaheedy Basin can be found in Grey (1984, 1994).

Ore minerals include sphalerite with minor amounts of pyrite, galena, chalcopyrite, and tetrahedrite. These sulfides are associated with jigsaw breccias, open spaces, microfracture infills, and microbial laminae. Crosscutting barite veins are locally present. Sphalerite is typically zoned (Fig. 29), banded or colloform (or both), dark and therefore iron poor, and commonly contains inclusions of galena. Typically, sphalerite either replaces microbial laminae and columnar stromatolites (*Asperia digitata*) or fills open spaces (Fig. 29). The mineralization in open-space cavities indicates that sphalerite is the youngest ore mineral, followed by quartz and euhedral calcite (Fig. 29b). The euhedral calcite has growth zones rich in fluid inclusions, for which homogenization temperature measurements indicate high temperatures (see **Fluid inclusion studies**). In a sample of dolomitic feldspathic sandstone (GSWA 148362) from the base of the succession in the Navajo prospect, sericite, iron sulfides, and sphalerite infill microfractures (Fig. 29d). Pyrite is always of late generation and forms both euhedral crystals that replace sphalerite and fine disseminations. In other cases pyrite infills dissolution seams.

The best assay results of reported drillcore intersections gave 1.3% Zn and 0.2% Pb over 11 m, 2.3% Zn and 0.2% Pb over 3 m, 1.86% Zn and 0.23% Pb over 6 m, and 0.88% Zn and 0.1% Pb over 20 m. The best assay results reported from reverse circulation drilling gave 2.36% Zn and 0.72% Pb over 13 m. Barium values from mineralized rock chip samples range from 1000 to 4000 ppm (Dörling, 1996, 1997, 1998; Feldtmann, 1995).

Fluid inclusions studies

Fluid inclusion studies were carried out on behalf of Renison Goldfields Consolidated (Feldtmann, 1995) by

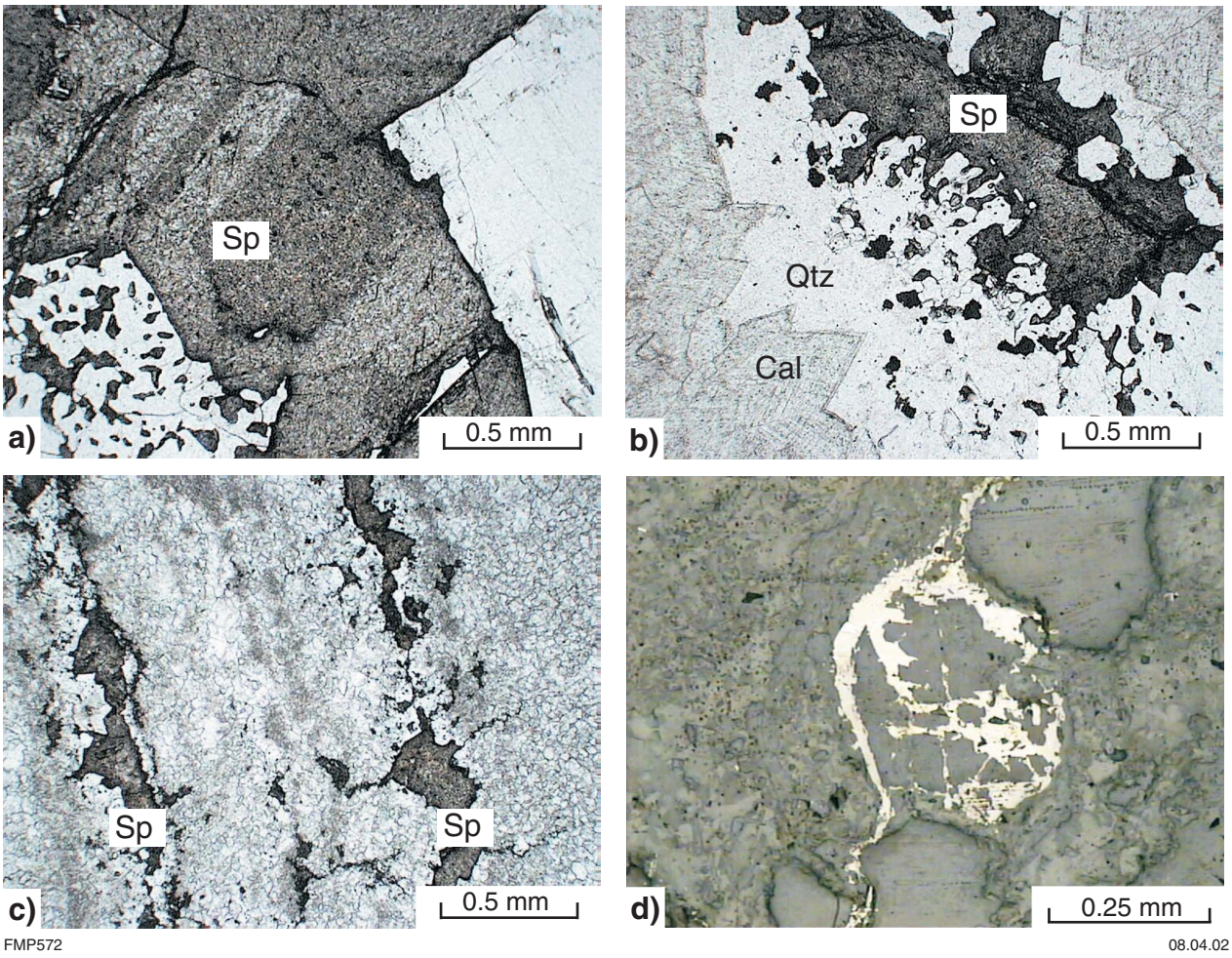

Figure 29. Sulfide mineralization in the Sweetwaters Well Member dolomite: a) zoned sphalerite; b) open-space filling by calcite, quartz, and zoned sphalerite (note fluid inclusions along growth zones in calcite crystals); c) sphalerite along microbial laminae; d) sphalerite around and along cracks of a quartz grain in sandy dolomite; (a) to (c) with plane-polarized light; (d) with reflected light

Seccombe and Jiang (1994) and Seccombe and Dellar (1995), and later by Teen (1996). These studies were conducted using an USGS-type heating–freezing stage on vein quartz and calcite from the sulfide-bearing dolomite of the Sweetwaters Well Member, obtained from drillcore at depths of 130–250 m. Homogenization temperature (T_h) and salinity (expressed as NaCl equivalent) data were obtained from two-phase (liquid + gas) primary and secondary inclusions. The regional variations of T_h and salinity are illustrated in Figure 30.

Seccombe and Jiang (1994) and Seccombe and Dellar (1995) noted that primary inclusions in quartz are generally liquid rich with vapour between 2 and 10% by volume; in exceptional cases the amount of gas may exceed 40%. Inclusions range in size from a few microns to about 10–15 µm and have polygonal, irregular, or negative shapes. Homogenization temperatures range widely from 19 to 262°C, with an average of 171°C, excluding the lowest temperatures of 19 to 21°C. Secondary inclusions in quartz, all confined to fracture planes within crystals and across adjacent crystals, have morphologies similar to the primary inclusions; they also contain between 2 and 10% by volume of gas bubbles. The T_h of secondary inclusions range from 121 to 361°C, averaging 194°C. Salinity calculations for both primary and secondary inclusions, based on freezing-point depression measurements ($T_{m\,ice}$) indicate moderate to high values ranging from 9.2 to 23.1 wt% NaCl equivalent.

Frequency plots of T_h in primary (quartz and calcite) and secondary (quartz) inclusions are shown in Figure 31. The T_h of secondary inclusions in quartz reveals two populations: 120–240°C and 320–360°C (Fig. 31b). This suggests that there were at least two hydrothermal episodes: one with lower temperature fluids up to 240°C, the other with substantially higher temperatures up to 361°C. Seccombe and Jiang (1994) commented on this feature and suggested that a late thermal event was responsible for the development of crosscutting quartz veinlets and associated euhedral calcite. Salinity measurements yielded values ranging from 2 to 12 wt% NaCl equivalent. Further measurements performed on primary inclusions in euhedral calcite crystals associated with quartz veining (Seccombe and Dellar, 1995) revealed a range of T_h from 237 to 302°C, with an average of

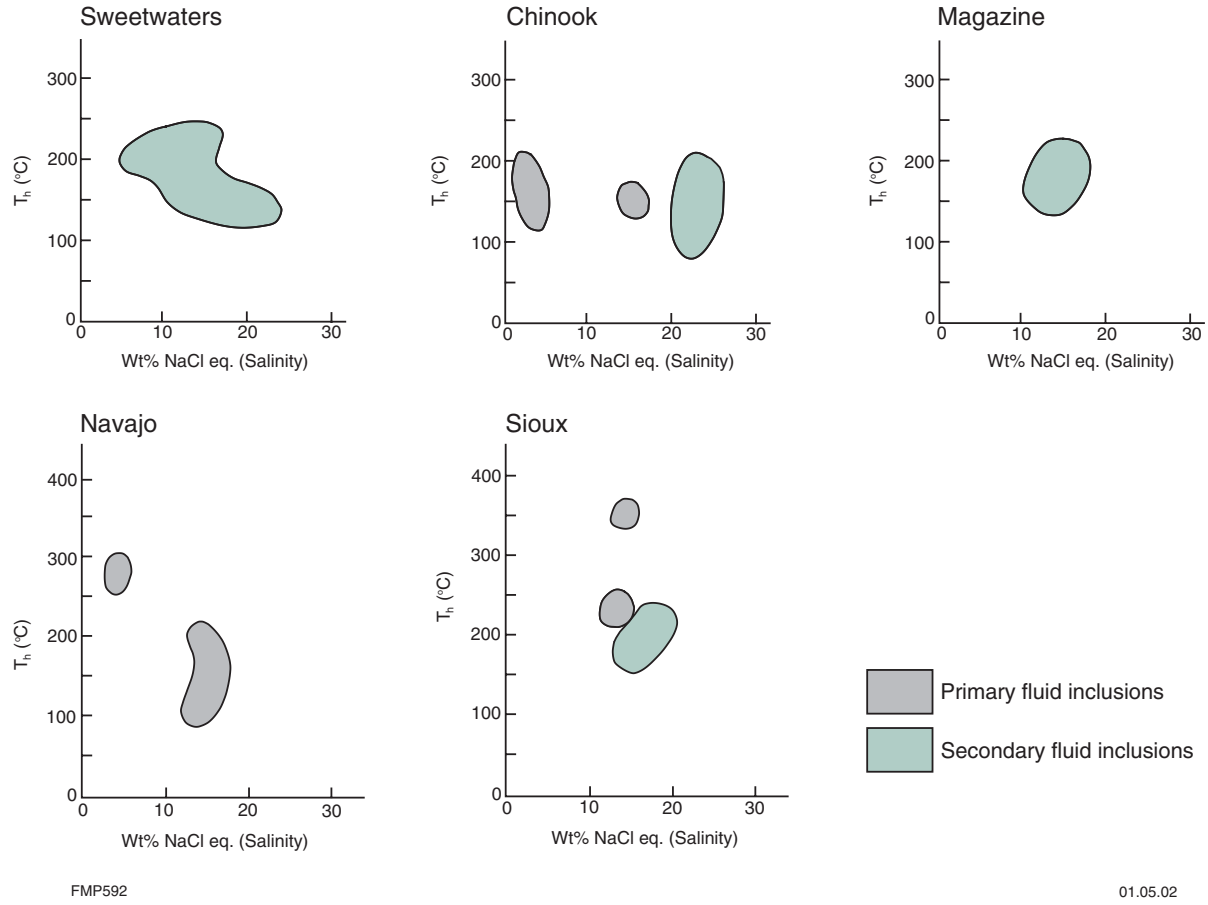

Figure 30. Homogenization temperatures of primary and secondary fluid inclusions for Mississippi Valley-type prospects near the Shoemaker impact structure (data from Seccombe and Jiang, 1994; Seccombe and Dellar, 1995; Teen, 1996; no information is available for the Iroquois prospect). Note anomalously high temperatures in prospects nearest the Shoemaker impact structure (Navajo and Sioux). See Figure 4 for location of prospects. See Figure 4 for location of prospects

265°C. Here too, the data indicate that at least two populations are present: one around 250–270°C, and the other around 300°C. The results of this study confirmed that there was a second thermal event with significantly higher temperatures (Seccombe and Dellar, 1995). It is also important to note that a peak T_h value (360°C) is reported from fluid inclusions closest to the Shoemaker impact structure (drillhole TDH 11, Sioux prospect; Edgar, 1994; Fig. 30).

Teen (1996) examined 126 fluid inclusions in 14 samples from the same five prospects west-northwest of the Shoemaker impact structure at distances ranging from 20 to 70 km from the centre of the structure. The fluid inclusions examined ranged in size from less than 5 to 100 µm. Primary fluid inclusions were two-phase with liquid:vapour ratios of between 10 and 20 vol. %, whereas secondary inclusions were much smaller (about 9 µm) but also two-phase, with liquid:vapour ratios also of 10–20 vol.%. Homogenization temperatures of primary inclusions ranged from 97 to 258°C, with a mean of 178°C; calculated salinities ranged from 2 to 24 NaCl wt% equivalent. Based on T_h and salinity data, Teen (1996) recognized four types of fluids in secondary inclusions:

- T_h 97–189°C, average 130°C, salinity 22–24 NaCl wt% equivalent;
- T_h 108–246°C, average 160°C, salinity 3 – 16.5 NaCl wt% equivalent;
- T_h 105–203°C, average 153°C, salinity 1.3 – 3.3 NaCl wt% equivalent;
- T_h 85–99°C, average 89°C, salinity not known.

Teen (1996) suggested that the second fluid type, which is found in late-stage quartz veins, could have remobilized earlier mineralization.

Discussion

The Sweetwaters Well Member sulfide and sulfate mineralization has many features consistent with carbonate-hosted Mississippi Valley-type ore deposits (MVT), such as colloform textures, a shelf carbonate host at the margins of a sedimentary basin (Garven and Raffensperger, 1997), and low-temperature and moderate-salinity fluids.

The fluid inclusion (primary and secondary) data briefly described above suggest that hydrothermal activity

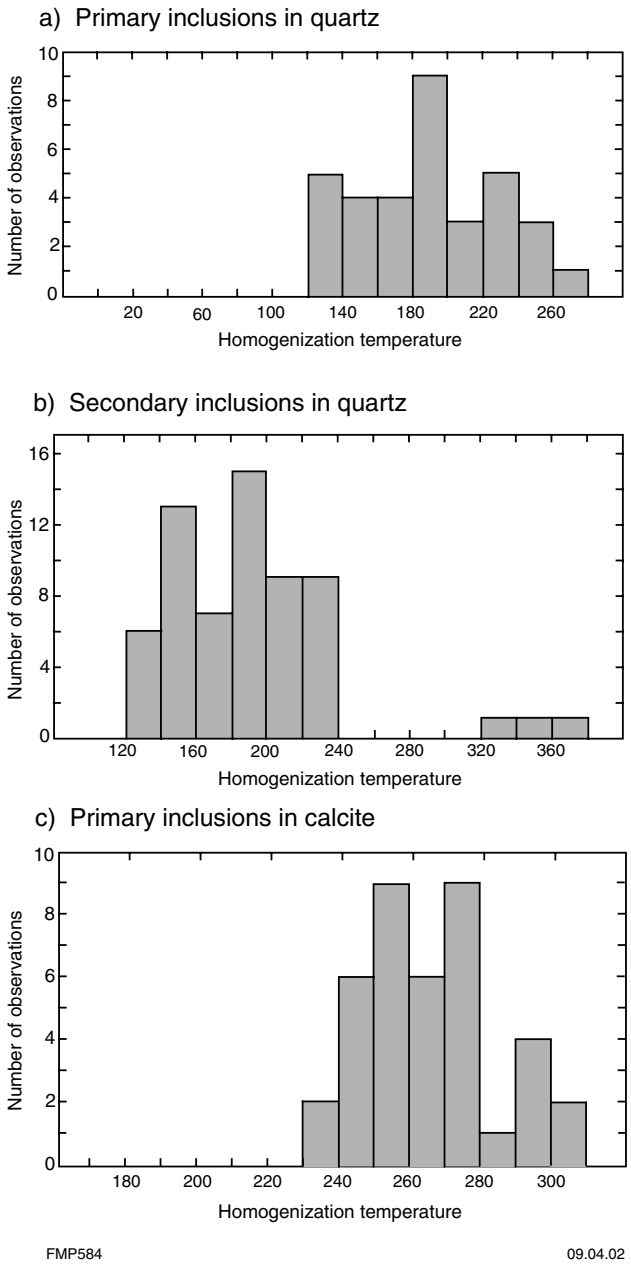

Figure 31. Histograms of homogenization temperature of fluid inclusions in quartz and calcite from the Sweetwaters Well Member mineralization: a) primary inclusions in quartz; b) secondary inclusions in quartz; c) primary inclusions in calcite. Data from Seccombe and Jiang (1994) and Seccombe and Dellar (1995)

in the region was multi-phase. The range of T_h and salinities are consistent with those usually found in MVT ore deposits (90–120°C; around 20% NaCl equivalent; Garven and Raffensperger, 1997; Wilkinson, 2001). However, evidence for temperatures in excess of 250°C near the Shoemaker impact structure suggests a heat source other than the basinal geothermal gradients considered responsible for fluid flow and hydrothermal systems in sedimentary basins (e.g. Garven and Raffensperger, 1997; Tóth and Almási, 2001).

Geochronology

The age of the Shoemaker impact structure is poorly constrained, and the available age data are presented in Table 4.

Bunting et al. (1980) obtained two whole-rock Rb–Sr isochron ages: 1630 Ma from a group of five samples of moderately fresh Teague Granite, and 1260 Ma from a group of four samples of altered and weathered Teague Granite. SHRIMP U–Pb dating of detrital zircons in sandstone of the Yelma Formation from the overturned eastern inner ring gave a maximum depositional age of 2027 ± 23 Ma for these sedimentary rocks (Nelson, 1997). A SHRIMP U–Pb age of 2648 ± 8 Ma from zircons extracted from the Teague Granite is interpreted as the magmatic crystallization age (Nelson, 1997).

An attempt was made at determining the age of the impact using the ^{40}Ar–^{39}Ar and K–Ar isotopic systems on K-feldspar and illite–smectite separates from three Teague Granite samples (GSWA 152613, 152614 and SIS-13). Details of the dating method of these samples are given in Appendices 3 and 4.

The ^{40}Ar–^{39}Ar system gave unreliable results because of disturbed apparent age spectra, indicative of partial argon loss due to a thermal overprinting event. The possibility that alteration and weathering were responsible for a portion of the low-temperature argon loss associated with GSWA 152614 complicated efforts to constrain the timing of the meteorite impact. The data from GSWA 152613 suggest a thermal signature after 1300 Ma, whereas the data from GSWA 152614 raises the possibility of a thermal event being even younger (<1100 Ma). Therefore, the ^{40}Ar–^{39}Ar system provides only broad constraints for the maximum age of the time of meteorite impact of less than 1300 Ma. A minimum age is difficult to estimate, but could be 1000 Ma or younger (Appendix 3). There is no evidence of a 1600 Ma 'event' as implied by the whole-rock Rb–Sr data (Bunting et al., 1980), suggesting that it could represent a mixed age (see Appendix 3).

The K–Ar system of illite and smectite in the Teague Granite gave two ages: 694 ± 25 Ma for SIS-13 and 568 ± 20 Ma for GSWA 152614. However, because the age of SIS-13 is based on K-feldspar, whereas the age of GSWA 152614 is based on illite–smectite and illite, the 568 ± 20 Ma age for the latter is considered more reliable.

The age data reported above are difficult to interpret. The 1630 Ma Rb–Sr isochron age may represent either resetting during a regional tectonothermal event or a mixed age resulting from a number of thermal events. The 1260 Ma Rb–Sr isochron age could be interpreted as a resetting due either to an episode of intense weathering (Pirajno and Glikson, 1998) or a mixed age due to the regional thermal events. In the Edmund and Collier Basins, west of the Shoemaker impact structure, two mafic magmatic events have been dated at 1460 and 1070 Ma (Wingate, 2002). The ^{40}Ar–^{39}Ar system on K-feldspar of the Teague Granite could provide a maximum age for the impact of less than 1000 Ma or, alternatively, it could represent a resetting due to a widespread thermal event

Table 4. Summary of geochronological data for the Teague Granite in the Shoemaker impact structure

GSWA sample	*Method*	*Whole rock or mineral*	*Age (Ma)*	*Reference*
118996	U–Pb	Zircon	2648 ± 8	Nelson (1997)
46301–46304	Rb–Sr	Whole rock	1630	Bunting et al. (1980)
46512–46515	Rb–Sr	Whole rock	1260	Bunting et al. (1980)
152613	^{40}Ar–^{39}Ar	K-feldspar	c. 1300	Appendix 3
152614	^{40}Ar–^{39}Ar	K-feldspar	c. 1000	Appendix 3
SIS-13	K–Ar	illite; K-feldspar	694 ± 25	Appendix 4
152614	K–Ar	illite, illite–smectite	568 ± 20	Appendix 4

(mafic magmatism) in the region at 1070 Ma. Indeed, evidence is mounting for the presence of a major c. 1000 Ma mafic igneous province, extending from the western Edmund Basin (Wingate, 2002) through to the north of the Earaheedy Basin (Glenayle Dolerite; Pirajno et al., in press, Nelson, in press; Compston, 1974) and about 350 km farther east (basalt in drillhole GSWA Empress 1/1A; Carlsen and Grey, 1998). The K–Ar illite–smectite system gives the age of a thermal event that formed illite and illite–smectite at 568 ± 20 Ma.

Given the above data and considerations and the fact that the Earaheedy Basin and surrounding areas have been thermally and tectonically stable from at least 1000 Ma, the younger K–Ar age of 560 Ma may belong to impact-related hydrothermal activity. If this assumption is correct, then the age of the impact must be close to the age of this hydrothermal activity, within dating errors.

Conclusions and discussion

Evidence for an impact origin for the Shoemaker impact structure include:

- a well-defined circular structure with surrounding rings of synclinal and anticlinal structures, which enclose a core of Archaean basement (Teague Granite and greenstone rocks);
- shatter cones in sedimentary rocks in both inner and outer rings;
- PDFs in quartz crystals of the Teague Granite;
- brecciation, fracturing, and hydrothermal alteration of the Teague Granite.

The circular structure of the Shoemaker structure could not have been caused by volcanic activity or by a cryptoexplosion, as advocated by earlier studies (e.g. Bunting et al., 1980), because there is no evidence of volcanic rocks in the region. Furthermore, the syenite in the core of the circular structure has an Archaean magmatic age and could not have been in any way implicated in cryptoexplosive activity, since the rocks deformed in the inner and outer rings are Palaeo-proterozoic in age.

The Shoemaker impact structure is a deeply eroded impact structure and for this reason the exposed diameter does not necessarily reflect its original extent (Plescia, 1999). Field geological observations, and magnetic and gravity data show that only the central structural uplift and the surrounding inner and outer rings to the east and northeast survived erosion. In addition, and for the reasons outlined previously, it is interpreted that the structure is tilted to the east, thus only exposing the altered portions of the central uplift in the east. This concept is schematically shown in Figure 32.

Traces of near-circular features in granite–greenstone basement rocks, up to 45–50 km from the centre of the Shoemaker impact structure, that are discernable on magnetic maps may be interpreted as ring faults or impact-induced crustal fractures (Fig. 7a,b). If this interpretation is correct, then the effects of the impact may have extended at least 45–50 km from the centre of the structure, in reasonably good agreement with calculations presented by Plescia (1999). A similar wider structure (a central ring about 30 km in diameter, surrounded by a 90 km-diameter ring fault) was inferred for the Acraman impact structure in South Australia (Williams et al., 1996).

Hypervelocity impacts result in instantaneous, extreme high-pressure (>10 GPa) shock-metamorphic effects in the target rocks. Shock metamorphism is manifested as physical effects on a wide range of scales, from mega-brecciation and shatter cone development to micron-scale PDFs and solid-state amorphization (destruction of the crystal structure), and the formation of central uplifts. These impact diagnostic features are present at the Shoemaker impact structure in sedimentary rocks of the inner and outer rings and in the Teague Granite.

The presence of PDFs in quartz, feldspar, zircon, and more rarely in other silicate crystals is considered one of the most important diagnostic criteria for the recognition of impact structures. These features form at pressures in excess of 7 GPa (commonly around 20–30 GPa; French, 1998), and consist of intracrystalline multiple sets of planar features a few microns apart, oriented along preferred crystallographic planes and therefore distinct from cleavages or fractures. The spacing between individual PDF planes is up to 10 μm (French, 1998). Because PDFs in target rocks form along crystallographic planes in the crystal lattice, it is desirable to measure the orientation of PDFs in individual grains and statistically establish their frequency along specific planes to obtain information on shock pressures (Stöffler and Langenhorst, 1994). The Shoemaker structure contains microbreccia veinlets with mineral fragments cemented by unidentified isotropic opaque material or iron oxides, or hydrothermal

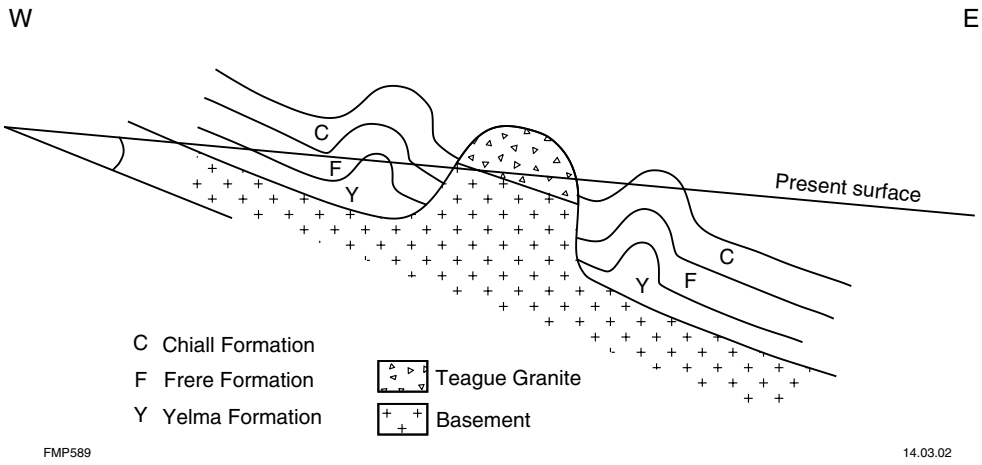

Figure 32. Schematic illustration of a model, mainly based on magnetic data, showing the postulated eastward tilting of the Shoemaker impact structure; the structure is deeply eroded and tilted so that the stratigraphically higher formations are exposed in the east, also most of the brecciated central basement uplift is eroded thereby only the easternmost and higher parts of the original uplift are now exposed (Teague Granite)

mineral phases, which texturally resemble pseudotachylites. Gravity and magnetic signatures are also consistent with an impact origin. The core of Archaean basement and the faulted contacts with the surrounding sedimentary rocks of the Earaheedy Group indicate that this basement was uplifted through the sedimentary cover.

The meteorite impact that created the Shoemaker impact structure probably formed a melt sheet which, together with heat generated by impact energy in the central uplift, gave rise to a hydrothermal convection system, within and around the central uplift zone. The melt sheet would have acted as a magma-like heat source within the crater structure and would have formed several hot springs in the crater and surrounding areas. The pods of quartz-jasperoidal material that are present along structural breaks (Plate 1) in the eastern rim of the Shoemaker impact structure may be the eroded remnants of fluid channels that fed thermal springs. The influence of impact-related hydrothermal activity in the Shoemaker structure could have extended well beyond the crater into the surrounding country rocks. Fluid inclusion studies suggest that the MVT mineralization hosted by the Sweetwaters Well Member was remobilized during a later heating event, with temperatures well above those generally attributed to circulation of basinal fluids. In the absence of recognized tectonothermal events in the region between 1600 and 1000 Ma, it is tempting to speculate that the later heating event was induced by the Shoemaker impact.

The Teague Granite is a key feature of the Shoemaker impact structure and is a remnant of the central structural uplift of the Archaean basement in the original crater. The magmatic age of the Teague Granite is 2648 Ma, which falls within the time span of 2650 and 2630 Ma for the emplacement of late- or post-tectonic felsic alkaline intrusions in the Yilgarn Craton (Smithies and Champion, 1999). These intrusions were emplaced along a broad northwest-trending belt across the craton, and comprise a range of syenitic rocks characterized by alkali feldspar and sodic clinopyroxene with or without quartz and amphibole, and accessory titanite, allanite, and apatite (Smithies and Champion, 1999; Johnson, 1991).

Two possibilities must be considered for the origin of the Teague Granite. Firstly, as noted above, the Teague Granite may be one of the alkaline plutons in the Yilgarn Craton, emplaced at 2650–2630 Ma (Smithies and Champion, 1999). If this is the case, then the mineralogy and texture of the Teague Granite indicate metasomatic processes related to the cooling of an alkaline melt, as detailed in Le Bas (1987). In terrestrial magmas, alkali metasomatism is the consequence of sodium-and potassium-rich fluids that emanate from carbonatite or ijolite intrusions (Le Bas, 1987). The associated alteration of country rocks is known as fenitization (McKie, 1966). Interestingly, Le Bas (1987, p. 74) states that 'products of fenitization are mineralogically syenitic, with the result that they are sometimes misidentified as igneous syenites'. Therefore such products can be syenitic fenite generated by ijolite, or fenitic syenite generated by carbonatite. Mineralogical changes in fenite zones depend on the distance from the causative intrusion, and therefore are temperature and depth dependent (Le Bas, 1987, fig. 13).

Alternatively, the metasomatic character of the Teague Granite could be linked to the meteorite impact that formed the Shoemaker impact structure. This hypothesis calls for metasomatic processes related to a heat source created by the transformation of kinetic energy into thermal energy in the target rocks. Alkali-rich high-temperature fluids were mobilized, resulting in the observed mineralogical, textural, and chemical features observed in the Teague Granite. Examples of impact-induced alteration have been reported in the literature (e.g. Puura et al., 2000).

Puura et al. (2000) studied impact-induced potassic metasomatism in sub-crater basement granitoids of the Kärdla Crater in Estonia, and found strong chemical and

mineralogical alteration of the subcrater lithologies. Chemical alteration includes potassic enrichment and sodium and calcium depletion, whereas the mineralogical alteration resulted in changes to the structural state of the feldspars (related to potassic enrichment and sodium and calcium removal) and decomposition of hornblende to iron-rich chlorite and quartz. Puura et al. (2000) concluded that these changes occurred as a result of post-impact alteration processes, but that the source of potassium is unknown. However, the authors also pointed out that geochemical studies of target rocks indicate selective mobility of alkalis with loss of potassium and sodium in strongly shocked rocks from large craters. The potassium and sodium lost from shocked rocks could be mobilized during phases of post-impact hydrothermal action, resulting in the enrichment of the surrounding or deeper lithologies (or both). Three possibilities are considered for the selective mobility of alkalis (Puura et al., 2000): action of a low-temperature post-impact hydrothermal system; ultra-high temperature and pressure mobilization of fluids; and an impact-induced high-temperature hydrothermal system.

The reddish-coloured Teague Granite exhibits a texture and mineralogical composition that supports intense alkali metasomatism of an original granitoid rock. The enrichment of sodium and potassium and depletion of silica deduced from the chemical data are consistent with this alkali metasomatism. The Teague Granite is characterized by a recrystallized anhedral granular or granoblastic assemblage of albite–quartz–microcline, with accessory aegirine-augite, biotite, fibrous amphibole, titanite, apatite, zircon, and garnet. Zircon and much of the biotite, however, are probably magmatic minerals of the precursor rock. 'Late-stage' hydrothermal activity was proposed by Johnson (1991) to account for the metasomatic texture and mineralogy of the 'Teague' syenite. If the metasomatic alteration of the Teague Granite is related to post-impact fluids, then it is reasonable to assume that the source of the metasomatizing fluids was from above and that a downward pattern or zoning of mineralogical and textural changes recording decreasing temperatures should exist.

Paucity of outcrops around the Shoemaker impact structure hinders detailed studies and only through drilling can direct information be obtained. It would then be possible to further test the hypothesis that meteorite impacts forming complex structures can result in localized metasomatic, and perhaps also localized magmatic, activity. In addition to being scientifically challenging, this possibility also has implications for the formation of mineral deposits.

The precise age of Shoemaker impact structure remains uncertain. A possible age could be close to the 568 Ma K–Ar age of illite–smectite, which indicates a hydrothermal event, perhaps linked to thermal energy released after the impact. Further and more systematic analyses are necessary to constrain the age of the impact.

References

ADAMIDES, N. G., 2000, Geology of the Merrie 1:100 000 sheet: Western Australia Geological Survey, 1:100 000 Geological Series Explanatory Notes, 37p.

ADAMIDES, N. G., PIRAJNO, F., and HOCKING, R. M., 2000, Geology of the Fairbairn 1:100 000 sheet: Western Australia Geological Survey, 1:100 000 Geological Series Explanatory Notes, 26p.

ALBRITTON, C. C., 1989, Catastrophic episodes in Earth history: London, Chapman and Hall, 221p.

ALVAREZ, L. W., ALVAREZ, W., ASARO, F., and MICHEL, H. V., 1980, Extraterrestrial cause for the Cretaceous–Tertiary extinction: Science, v. 208, p. 1095–1108.

ALVAREZ, L. W., ASARO, F., MICHEL, H. V., and ALVAREZ, W., 1982, Iridium anomaly approximately synchronous with terminal Eocene extinctions: Science, v. 216, p. 886–888.

BUNTING, J. A., 1986, Geology of the eastern part of the Nabberu Basin: Western Australia Geological Survey, Bulletin 131, 130p.

BUNTING, J. A., BRAKEL, A. T., and COMMANDER, D. P., 1982, Nabberu, W.A.: Western Australia Geological Survey, 1:250 000 Geological Series Explanatory Notes, 27p.

BUNTING, J. A., COMMANDER, D. P., and GEE, R. D., 1977, Preliminary synthesis of Lower Proterozoic stratigraphy and structure adjacent to the northern margin of the Yilgarn block: Western Australia Geological Survey, Annual Report 1976, p. 43–48.

BUNTING, J. A., de LAETER, J. R., and LIBBY, W. G., 1980, Evidence for the age and cryptoexplosive origin of the Teague ring structure, Western Australia: Western Australia Geological Survey, Annual Review 1980, p. 81–85.

BUTLER, H., 1974, The Lake Teague ring structure, Western Australia: an astrobleme?: Search, v. 5, p. 536–537.

CARLSEN, G. M., and GREY, K., 1998, GSWA Empress 1A and the petroleum evaluation of the western Officer Basin: Western Australia Geological Survey, Annual Review 1997–98, p. 119–125.

CHAMPION, D. C., and SHERATON, J. W., 1997, Geochemistry and Sm–Nd isotope systematics of Archaean granitoid of the Eastern Goldfields Province, Yilgarn Craton, Australia: constraints on crustal growth: Precambrian Research, v. 83, p. 109–132.

CHAPPELL, B. W., 1991, Trace element analysis of rocks by X-ray spectrometry, *in* Advances in X-ray analyses *edited by* C. S. BARRETT, J. W. GILFRICH, T. C. HUANG, and P. K. PREDECKI: New York, Plenum Press, v. 34, p. 263–276.

CHAPPELL, B. W., and HERGT, J. M., 1989, The use of known Fe content as a flux monitor in neutron activation analysis: Chemical Geology, v. 78, p. 151–158.

COMMANDER, D. P., MUHLING, P. C., and BUNTING, J. A., 1982, Stanley, W.A.: Western Australia Geological Survey, 1:250 000 Geological Series Explanatory Notes, 19p.

COMPSTON, W., 1974, The Table Hill volcanics of the Officer Basin — Precambrian or Palaeozoic?: Geological Society of Australia, Journal, v. 21, p. 403–411.

CORNER, B., REIMOLD, W. U., BRANDT, D., and KOEBERL, C., 1997, Morokweng impact structure, Northwest Province, South Africa: geophysical imaging and shock petrographic studies: Earth and Planetary Science Letters, v. 146, p. 351–364.

CROSSEY, L. J., CAMPANA, M. E., GATES, T. J., and McCARVILLE, P., 1993, Post-impact fluid flow and alteration: Manson impact structure, Manson: Geological Society of America, Abstracts with Programs, v. 25, p. A-23.

DEER, W. A., HOWIE, R. A., and ZUSSMAN, J., 1966, An introduction to the rock-forming minerals: London, Longman, 528p.

DONOFRIO, R. R., 1998, North American impact structures hold giant field potential: Oil and Gas Journal, May issue, p. 69–83.

DÖRLING, S. L., 1996. Teague Project, E69/562, 856, 857, 858, 975, 987, 988, 1012, 1014, 1036, 1059, 1060: Western Australia Geological Survey, Statutory mineral exploration report, Item 10603 A49642 (unpublished).

DÖRLING, S. L., 1997, Partial surrender report, Canning Gap Project, E69/597: Western Australia Geological Survey, Statutory mineral exploration report, Item 9769 A51110 (unpublished).

DÖRLING, S. L., 1998, Teague Project, E69/562, 856, 857, 858, 975, 987, 988, 1012, 1014, 1036, 1059, 1060: Western Australia Geological Survey, Statutory mineral exploration report, Item 10603 A53279 (unpublished).

DRESSLER, B. O., REIMOLD, W. U., 2001, Terrestrial impact melt rocks and glasses: Earth-Science Reviews, v. 56, p. 205–284.

EDGAR, W., 1994, Teague Project, Annual Report, E69/562, 855, 856, 857, 858, 975, vols 1 and 2: Western Australia Geological Survey, Statutory mineral exploration report, Item 10603 A42560 (unpublished).

FARRELL, T. R., and WYCHE, S., 1999, Geology of the Millrose 1:100 000 sheet: Western Australia Geological Survey, 1:100 000 Geological Series Explanatory Notes, 29p.

FELDTMANN, R., 1995, Teague Project, E69/562, 855, 856, 857, 858, 975, 987, 988, 1012, 1013, 1014, 1031, 1059, 1060, 1036: Western Australia Geological Survey, Statutory mineral exploration report, Item 10603 A45916 (unpublished).

FRENCH, B. M., 1998, Traces of catastrophe — a handbook of shock-metamorphic effects in terrestrial meteorite impact structures: Houston, Lunar and Planetary Science Institute, LPI Contribution No. 954, 120p.

GARVEN, G., and RAFFENSPERGER, J. P., 1997, Hydrogeology and geochemistry of ore genesis in sedimentary basins, *in* Geochemistry of ore deposits *edited by* H. L. BARNES: New York, J. Wiley and Sons, p. 125–189.

GLIKSON, A. Y., 1993, Asteroids and early Precambrian crustal evolution: Earth-Science Reviews, v. 35, p. 285–319.

GLIKSON, A. Y. (ed.), 1996, Australian impact structures: Australian Geological Survey Organisation, Journal of Australian Geology and Geophysics, Thematic Issue, v. 16, no. 4, 625p.

GLIKSON, A. Y., EGGINS, S., MERNAGH, T. P., PIRAJNO, F., IASKY, R. P., and MORY, A. J., in prep., Evidence of vapor-mediated chemical fractionation and siderophile element enrichment in shock-metamorphosed granitoids of a central basement uplift, Woodleigh impact structure, Western Australia: Meteoritics and Planetary Science.

GORTER, J. D., 1998, The petroleum potential of Australian Phanerozoic impact structures: Australian Petroleum Exploration Association, Journal, v. 38, p. 159–187.

GRADY, M. M., HUTCHISON, R., McCALL, G. J. H., and ROTHERY, D. A., (eds), 1998, Meteorites: flux with time and impact effects: London, Geological Society, Special Publication no. 140, 278p.

GREY, K., 1984, Biostratigraphic studies of stromatolites from the Proterozoic Earaheedy Group, Nabberu Basin, Western Australia: Western Australia Geological Survey, Bulletin 130, 123p.

GREY, K., 1994, Stromatolites from the Palaeoproterozoic Earaheedy Group, Earaheedy Basin, Western Australia: *Alcheringa*, v. 18, p. 187–218.

GRIEVE, R. A. F, 1987, Terrestrial impact structures: Annual Review of Earth and Planetary Sciences, v. 15, p. 245–270.

GRIEVE, R. A. F., 1990, Impact cratering on the Earth: Scientific American, April, p. 44–52.

GRIEVE, R. A. F., 1994, Impact: a natural hazard in planetary evolution: Episodes, v. 17, p. 9–17.

GRIEVE, R. A. F., 1997, Extraterrestrial impact events: the record in the rocks and the stratigraphic column: Palaeogeography, Palaeoclimatology, Palaeoecology, v. 132, p. 5–23.

GRIEVE, R. A. F., and HEAD, J. W., 1983, The Manicouagan impact structure: an analysis of its original dimension and form: Journal of Geophysical Research v. 88, p. A807–A818.

GRIEVE, R. A. F., LANGENHORST, F., and STÖFFLER, D., 1996, Shock metamorphism of quartz in nature and experiment: II. Significance in geoscience: Meteoritics and Planetary Science, v. 31, p. 6–35.

GRIEVE, R. A. F., and MASAITIS, V. L., 1994, The economic potential of terrestrial impact craters: International Geology Review, v. 36, p. 105–151.

GRIEVE, R. A. F., and PILKINGTON, M., 1996, The signatures of terrestrial impacts: Australian Geological Survey Organisation, Journal of Australian Geology and Geophysics, v. 16, p. 373–376.

GRIEVE, R. A. F., and THIERRIAULT, A., 2000, Vredefort, Sudbury and Chixculub: three of a kind?: Annual Review of Earth and Planetary Sciences, v. 28, p. 305–338.

GRIFFIN, T. J., 1990, Eastern Goldfield Province, *in* Geology and mineral resources of Western Australia: Western Australia Geological Survey, Memoir 3, p. 77–119.

GUPPY, D. J., and MATHESON, R. S., 1949, Wolfe Creek meteorite crater: Australia BMR, Report 1949/13, Geological Series no. 8, 5p.

HALL, W. M., GOODE., A. D. T., BUNTING, J. A., and COMMANDER, D. P., 1977, Stratigraphic terminology of the Earaheedy Group, Nabberu Basin: Western Australia Geological Survey, Annual Report 1976, p. 40–43.

HAWKE, P., in prep., Interpretation of geophysical data over the Shoemaker impact structure, Earaheedy Basin, Western Australia: Western Australia Geological Survey, Record.

HOCKING, R. M., JONES, J. A., PIRAJNO, F., and GREY, K., 2000, Revised lithostratigraphy for Proterozoic rocks in the Earaheedy Basin and nearby areas: Western Australia Geological Survey, Record 2000/16, 22p.

IASKY, R. P., MORY, A. J., BLUNDELL, K., 2001, The geophysical interpretation of the Woodleigh impact structure, Southern Carnarvon Basin, Western Australia: Western Australia Geological Survey, Report 79, p. 41.

JACKSON, J. A., 1997, Glossary of geology (4th edition): Virginia, U.S.A., American Geological Institute, 769p.

JOHNSON, G. I., 1991, The petrology, geochemistry and geochronology of the felsic alkaline suite of the eastern Yilgarn block, Western Australia: South Australia, University of Adelaide, PhD thesis (unpublished).

JONES, J. A., 2000, Granite Peak, W.A. Sheet 3146: Western Australia Geological Survey, 1:100 000 Geological Series.

JONES, J. A., PIRAJNO, F., and HOCKING, R. M., 2000a, Stratigraphy, tectonic evolution and mineral potential of the Earaheedy Basin: Western Australia Geological Survey, Record 2000/8, p. 11–13.

JONES, J. A., PIRAJNO, F., and HOCKING, R. M., 2000b, Revised stratigraphy for the Earaheedy Group: implications for the tectonic evolution and mineral potential of the Earaheedy Basin: Western Australia Geological Survey, Annual Review 1999–2000, p. 57–64.

KOEBERL, C., and ANDERSON, R. R., 1996, The Manson impact structure, Iowa: anatomy of an impact crater: Geological Society of America, Special Paper 302, 457p.

KOEBERL, C., REIMOLD, W. U., KRACHER, A., TRÄXLER, B., VORMAIER, A., and KÖRNER, W., 1996, Mineralogical, petrological and geochemical studies of drill core samples from the Manson Impact Structure, Iowa: Geological Society of America, Special Paper 302, p. 145–220.

KOMOR, S. C., VALLEY, J. W., and BROWN, P. E., 1988, Fluid-inclusion evidence for impact heating at the Siljan Ring, Sweden: Geology, v. 16, p. 711–715.

KRING, D. A., 1995, The dimension of the Chicxulub impact crater and impact melt sheet: Journal of Geophysical Research, v. 100, p. 16 979 – 16 986.

LE BAS, M. J., 1987, Nephelinites and carbonatites, *in* Alkaline igneous rocks *edited by* J. G. FITTON, and B. G. J. UPTON: London, Geological Society, Special Publication no. 30, p. 53–83.

LIU, S.-F., 1997, Solid geology of the Nabberu 1:250 000 map sheet, Western Australia: Australian Geological Survey Organisation, Research Newsletter, v. 27, p. 23–24.

LIU, S.-F., and MACKEY, T., 1998, Using images in a geological interpretation of data: Australian Geological Survey Organisation, Research Newsletter, v. 28, p. 17–19.

MARTIN, D. McB., and THORNE, A. M., 2001, New insights into the Bangemall Supergroup: Western Australia Geological Survey, Record 2001/5, p. 1–2.

MASAITIS, V. L., and NAUMOV, M. V., 1993, Puchezh-Katunki impact crater: preliminary model of hydrothermal circulation system: Meteoritics, v. 28, p. 390–391.

McCARVILLE, P., and CROSSEY, L. J., 1996, Post-impact hydrothermal alteration of the Manson impact structure: Geological Society of America, Special Paper 302, p. 347–376.

McKIE, D., 1966, Fenitization, *in* Carbonatites, *edited by* D. F. TUTTLE and J. GITTENS: New York, Wiley Interscience, p. 261–294.

MELOSH, H. J., 1989, Impact cratering — a geological process: United Kingdom, Oxford Monographs on Geology and Geophysics, no. 11, 245p.

METALS EXPLORATION LIMITED, 1983, Annual report, October 1983: Western Australia Geological Survey, Statutory mineral exploration report, Item 1836 A12894 (unpublished).

MILTON, D. J., GLIKSON, A. Y., and BRETT, R., 1996, Gosses Bluff — a latest Jurassic impact structure, central Australia. 1. Geological structure, stratigraphy and origin: Australian Geological Survey Organisation, Journal of Geology and Geophysics, v. 16, p. 453–486.

MORGAN, J., WARNER, M. R., COLLINS, G. S., MELOSH, H. J., and CHRISTESON, G. L., 2000, Peak-ring formation in large impact craters: geophysical constraints from Chicxulub: Earth and Planetary Science Letters, v. 183, p. 347–354.

MORGAN, J., WARNER, M., THE CHICXULUB WORKING GROUP, BRITTAN, J., BUFFLER, R., CAMARGO, A., CHRISTESON, G., DENTON, P., HILDEBRAND, A., HOBBS, R., MACINTYRE, H., MACKENZIE, G., MAGUIRE, P., MARIN, L., NAKAMURA, Y., PILKINGTON, M., SHARPTON, V., SNYDER, D., SUAREZ, G., and TREJO, A., 1997, Size and morphology of the Chicxulub impact crater: Nature, v. 390 (6659), p. 472–476.

MORRIS, P. A., SANDERS, A. J., and FAULKNER, J. A., 1997, Geochemical mapping of the Nabberu 1:250 000 sheet: Western Australia Geological Survey, 1:250 000 Regolith Geochemistry Series Explanatory Notes, 63p.

MORRIS, P. A., PIRAJNO, F., and SHEVCHENKO, S., in press, Proterozoic mineralization identified by integrated regional geochemistry, geophysics and bedrock mapping in Western Australia: Geochemistry: Exploration, Environment, Analysis.

MORY, A. J., IASKY, R. P., GLIKSON, A. Y., and PIRAJNO, F., 2000a, Woodleigh, Carnarvon Basin, Western Australia: a new 120 km-diameter impact structure: Earth and Planetary Science Letters, v. 177 (1–2), p. 119–128.

MORY, A. J., IASKY, R. P., GLIKSON, A. Y., and PIRAJNO, F., 2000b, Response to 'Critical comment on A. J. Mory et al., 2000, Woodleigh, Carnarvon Basin, Western Australia: a new 120 km-diameter impact structure', by W. U. REIMOLD and C. KOEBERL: Earth and Planetary Science Letters, v. 184 (1), p. 359–365.

MORY, A. J., PIRAJNO, F.,. GLIKSON, A. Y., and COKER, J., 2001, GSWA Woodleigh 1, 2, and 2A well completion report, Woodleigh impact structure, Southern Carnarvon Basin, Western Australia: Western Australia Geological Survey, Record 2001/6, 147p.

NAUMOV, M. V., 1993, Zonation of hydrothermal alteration in the central uplift of the Puchezh-Katunki astrobleme: Meteoritics and Planetary Science, v. 28, p. 408–409.

NELSON, D. R., 1997, Compilation of SHRIMP U–Pb zircon geochronology data, 1996: Western Australia Geological Survey, Record 1997/2, 189p.

NELSON, D. R., 1999, Compilation of geochronology data, 1998: Western Australia Geological Survey, Record 1999/2, 222p.

NELSON, D. R., 2001, Compilation of geochronology data, 2000: Western Australia Geological Survey, Record 2001/2, 205p.

NELSON, D. R., in prep., Compilation of geochronology data, 2001: Western Australia Geological Survey, Record 2002/2.

NESBITT, R. W., and STANLEY, J. (eds), 1980, Analytical geochemistry — a compilation of reports 1973–1979: South Australia, University of Adelaide, Center for Precambrian Research, Research Report 3.

NEWSOM, H. E., 1980, Hydrothermal alteration of impact melt sheets with implications for Mars: Icarus, v. 44, p. 207–216.

NEWSOM, H. E., GRAUP, G., SEWARDS, T., and KEIL, K., 1986, Fluidization and hydrothermal alteration of the suevite deposit at the Ries Crater, West Germany, and implications for Mars: Journal of Geophysical Research, v. 91, p. E239–E251.

NICHOLSON, K., 1983, Fluorine determination in geochemistry: errors in the electrode method of analysis: Chemical Geology, v. 38, p. 1–22.

NICOLAYSEN, L., and FERGUSON, J., 1990, Cryptoexplosion structures, shock deformation and siderophile concentrations related to explosive venting of fluids associated with alkaline ultramafic magmas: Tectonophysics, v. 171, p. 303–335.

NORRISH, K., and HUTTON, J. T., 1969, An accurate X-ray spectrographic method for the analysis of a wide range of geological samples: Geochimica et Cosmochimica Acta, v. 33, p. 431–453.

PASSCHIER, C. W., and TROUW, R. A. J., 1996: Micro-tectonics: Berlin, Springer-Verlag, 287p.

PERNICKA, E., KAETHER, D., and KOEBERL, C., 1996, Siderophile element concentrations in drill core samples from the Manson Crater: Geological Society of America, Special Paper 302, p. 325–330.

PILKINGTON, M., and GRIEVE, R. A. F., 1992, The geophysical signature of terrestrial impact craters: Reviews of Geophysics, v. 30, p. 161–181.

PIRAJNO, F., 1992, Hydrothermal mineral deposits — principles and fundamental concepts for the exploration geologist: Berlin, Springer-Verlag, 702p.

PIRAJNO, F., 1998, Nabberu, W.A. Sheet 3046: Western Australia Geological Survey, 1:100 000 Geological Series.

PIRAJNO, F., 2000, Ore deposits and mantle plumes: Durdrecht, Holland, Kluwer Academic Publishers, 576p.

PIRAJNO, F., and GLIKSON, A. Y., 1998, Shoemaker impact structure, Western Australia: Celestial Mechanics and Dynamical Astronomy, v. 69, p. 25–30.

PIRAJNO, F., and HOCKING, R. M., 2001, Mudan, W.A. Sheet 3247: Western Australia Geological Survey, 1:100 000 Geological Series.

PIRAJNO, F., HOCKING, R. M., and JONES, J. A., 1999, Geology, mineralization and geodynamic evolution of the Palaeoproterozoic Yerrida and Earaheedy Basins, W.A.: Geological Society of Australia, Abstracts no. 56, p. 30–33.

PIRAJNO, F., and JONES, J. A., in prep., Geology of the Nabberu and Granite Peak 1:100 000 sheets: Western Australia Geological Survey, 1:100 000 Geological Series Explanatory Notes.

PIRAJNO, F., JONES, J. A., and HOCKING, R. M., 2000, Revised stratigraphy of the Palaeoproterozoic Earaheedy Group: implications for the tectonic evolution of the Earaheedy Basin, Western Australia: Geological Society of Australia, Abstracts no. 51, p. 391.

PIRAJNO, F., JONES, J. A., HOCKING, R. M., and HALILOVIC, J., in press, Geology and geodynamic evolution of Palaeoproterozoic basins of the eastern Capricorn Orogen, Western Australia: Precambrian Research.

PLESCIA, J. B., 1999, Gravity signature of the Teague Ring Impact Structure, Western Australia: Geological Society of America, Special Paper 339, p. 165–175.

PUURA, V., KÄRKI, A., KIRS, J., KIRSIMÄE, K., KLEESMENT, A., KONSA, M., NIIN, M., PLADO, J., SUUROJA, K., and SUUROJA, S., 2000, Impact-induced replacement of plagioclase by K-feldspar in granitoids and amphibolites at the Kärdla Crater, Estonia, *in* Impacts and the early Earth *edited by* I. GILMOUR and C. KOERBERL: Berlin, Springer-Verlag, p. 417–445.

REIMOLD, W. U., and GIBSON, R. L., 1996, Geology and evolution of the Vredefort Impact Structure: South African Journal of Earth Sciences, v. 23, p. 125–162.

REIMOLD, W. U., KOEBERL, C., BRANDSATTER, F. J., KRUGER, F. J., ARMSTRONG, R. A., and BOOTSMAN, C., 1999, Morokweng impact structure, South Africa: petrographic and isotopic results and implications for the size of the structure: Geological Society of America, Special Paper 339, p. 61–90.

SECCOMBE, P. K., and DELLAR, A., 1995, Fluid inclusion investigation of five samples: Teague Project, *in* Teague Project, E69/562, 855, 856, 857, 858, 975, 987, 988, 1012, 1013, 1014, 1031, 1059, 1060, 1036 *edited by* R. FELDTMANN: Western Australia Geological Survey, Statutory mineral exploration report, Item 10603 A45916 (unpublished).

SECCOMBE, P. K., and JIANG, Z., 1994, Fluid inclusion investigation of eight samples: Teague Project, *in* Teague Project, E69/562, 855, 856, 857, 858, 975, 987, 988, 1012, 1013, 1014, 1031, 1059, 1060, 1036 *edited by* R. FELDTMANN: Western Australia Geological Survey, Statutory mineral exploration report, Item 10603 A45916 (unpublished).

SHEPPARD, S., OCCHIPINTI, S. A., TYLER, I. M., and NELSON, D. R., 1999, The nature of the c. 2.0 Ga crust along the southern

margin of the Gascoyne Complex: Western Australia Geological Survey, Annual Review 1998–99, p. 56–61.

SHEVCHENKO, S., 2001, Gravity data — Kingston and Stanley 1:250 000 sheets, Western Australia: Western Australia Geological Survey, Record 2000/19, 29p.

SHOEMAKER, E. M., 1963, Impact mechanics at Meteor Crater, Arizona, *in* The Solar System, volume 4 *edited by* B. MIDDLEHURST and G. P. KUIPER: Chicago University Press, p. 301–336.

SHOEMAKER, E. M., and SHOEMAKER, C. S., 1996, The Proterozoic impact record of Australia: Australian Geological Survey Organisation, Journal of Australian Geology and Geophysics, v. 16, p. 379–398.

SHORT, N. M., and GOLD, D. P., 1996, Petrography of shocked rocks from the central peak at the Manson impact structure: Geological Society of America, Special Paper 302, p. 245–265.

SMITH, M., and WU, C., 2000, The geology and genesis of the Bayan Obo Fe–REE–Nb deposit: a review, *in* Hydrothermal iron oxide copper–gold and related deposits: a global perspective *edited by* T. M. PORTER: Australian Mineral Foundation, p. 271–281.

SMITHIES, R. H., and BAGAS, L., 1997, High pressure amphibolite–granulite facies metamorphism in the Paleoproterozoic Rudall Complex, central Western Australia: Precambrian Research, v. 83, p. 243–265.

SMITHIES, R. H., and CHAMPION, D. C., 1999, Late Archaean felsic alkaline igneous rocks in the Eastern Goldfields, Yilgarn Craton, Western Australia: a result of lower crustal delamination?: London, Geological Society, Journal, v. 156, p. 561–576.

SPRAY, J. G., 1998, Localised shock and friction-induced melting in response to hypervelocity impact: London, Geological Society, Special Publication 240, p. 195–204.

STÖFFLER, D., and LANGENHORST, F., 1994, Shock metamorphism of quartz in nature and experiment. I. Basic observation and theory: Meteoritics and Planetary Science, v. 29, p. 155–181.

SUN, S.-S., 1982, Chemical composition and origin of the Earth's primitive mantle: Geochimica et Cosmochimica Acta, v. 46, p. 179–192.

TEEN, M. T., 1996, Silicification and base metal mineralization within the Earaheedy Basin, Western Australia: University of Tasmania, Centre for Ore Deposit and Exploration Studies, BSc (Hon) thesis (unpublished).

TÓTH, J., and ALMÁSI, I., 2001, Interpretation of observed fluid potential patterns in a deep sedimentary basin under tectonic compression, Hungarian Great Plain, Pannonian basin: Geofluids, v. 1, p. 11–36.

TYLER, I. M., 1999, Palaeoproterozoic orogeny in Western Australia: Geological Society of Australia, Abstracts no. 56, p. 47–49.

TYLER, I. M., 2000, Palaeoproterozoic orogeny in Western Australia, *in* GSWA 2000 extended abstracts: Geological data for WA explorers in the new millennium: Western Australia Geological Survey, Record 2000/8, p. 7–8.

TYLER, I. M., PIRAJNO, F., BAGAS, L., MYERS, J. S., and PRESTON, W., 1998, The geology and mineral deposits of the Proterozoic in Western Australia: Australian Geological Survey Organisation, Journal of Geology and Geophysics v. 17, p. 223–224.

TYLER, I. M., and THORNE, A. M., 1990, The northern margin of the Capricorn Orogen, Western Australia — an example of an Early Proterozoic collision zone: Journal of Structural Geology, v. 12, p. 685–701.

WANG, K., GELDSETZER, H. H. J., and CHATTERTON, B. D. F., 1994, A late Devonian extraterrestrial impact and extinction in eastern Gondwana: geochemical, sedimentological and faunal evidence: Geological Society of America, Special Paper 293, p. 111–120.

WILLIAMS, G. E., SCHMIDT, P. W., and BOYD, D. M., 1996, Magnetic signature and morphology of the Acraman impact structure, South Australia: Australian Geological Survey Organisation, Journal of Australian Geology and Geophysics, v. 16, p. 431–442.

WILKINSON, J. J., 2001, Fluid inclusions in hydrothermal ore deposits: Lithos, v. 55, p. 229–272.

WINGATE, M. T. D., 2002, Age and palaeomagnetism of dolerite sills intruded into the Bangemall Supergroup on the Edmund 1:250 000 sheet, Western Australia: Western Australia Geological Survey, Record 2002/4, 48p.

WITT, W. K., and DAVY, R., 1997, Geology and geochemistry of Archaean granites in the Kalgoorlie region of the Eastern Goldfields, Western Australia: a syn-collisional tectonic setting?: Precambrian Research, v. 83, p. 133–183.

WOODHEAD, J. D., and HERGT, J. M., 1997, Application of the 'double spike' technique to Pb-isotope geochronology: Chemical Geology, v. 138, p. 311–321.

WYCHE, S., and FARRELL, T., 2000, Regional geological setting of the Yandal greenstone belt, northeast Yilgarn Craton: Australian Institute of Geoscientists, Bulletin 32, p. 41–49.

Appendix I

Morphometric analysis and estimates of the original dimensions of the Shoemaker impact structure

by

A. Y. Glikson*

Estimates of the original dimensions of eroded impact structures can be either observed directly from relic structures or, in complex structures, derived from relations deduced from experimental data (Pilkington and Grieve, 1992; French, 1998). In the case of impact structures plugged by a central basement uplift, as in the Shoemaker impact structure, comparisons need to be made with other impact structures containing a central basement uplift.

Different criteria have been applied to determine the outer diameter (Ds) of impact structures, which in some instances is based on the presence of external ring faults or geophysical signatures (or both). Such an approach has been taken, for example, in connection with the Acraman impact structure, in South Australia, where a 90 km-diameter ring fault surrounds a 30 km-diameter inner zone (Williams et al., 1996). For the Vredefort impact structure in South Africa, Ds is suggested as 300 km, where an approximately 90–100 km-diameter central uplift (Du) is surrounded by concentric mildly folded volcanic and sedimentary rocks of the Witwatersrand Basin (Therriault et al., 1997). At the Morokweng impact structure in the southern Kalahari, a 340 km-diameter magnetic and Bouguer gravity anomaly ring surrounds a 70 km-diameter deformed and brecciated crater zone (Corner et al., 1997), although according to other views a diameter of about 200 km is defined by a ring syncline (Reimold et al., 1999). At Chicxulub, Yucatan in Mexico, a well defined ring fault corresponds to a diameter of 180 km (Hildebrand et al., 1991), whereas drilling of melt breccia and megabreccia at distances of 125 and 150 km south of the centre respectively suggests an original crater as large as 310 km in diameter (Sharpton et al., 1997).

The impact-deformed aureole in the Shoemaker impact structure is best defined between the intersections of the outer circular zone with the regional west-northwesterly striking ridge of the Frere Formation (Fig. 4, Plate 1). This intersection is sharply defined in the west-northwest, whereas to the east-southeast it is demarcated by a flexure, yielding an overall diameter (Ds) of 29–30 km (Fig. 4, Plate 1). A possible ring fault, defined by magnetic data, about 45 km north of the centre of the Shoemaker impact structure, may conceivably imply an original 90-km diameter of the Shoemaker impact structure, by analogy with the relationships postulated for Chicxulub by Sharpton et al. (1997) and for the Acraman impact structure by Williams et al. (1996). However, pending further definition of an outer ring or ring fault at the Shoemaker impact structure, in the following discussion we assume a diameter of 30 km. Other relevant parameters at the Shoemaker impact structure include a central basement uplift (Du) of 12 km in diameter, a gravity model suggesting that the density contrast extends to a depth of 5 km (Plescia, 1999), and an assumed Proterozoic sedimentary sequence at the impact site, about 2 – 2.3 km thick, unconformably overlying the Archaean granitoid–greenstone basement (Fig. 4, Plate 1).

Grieve and Pilkington (1996) formulated the observed relations between the overall structural diameter (Ds) and vertical structural uplift (Su) in 15 complex impact structures in terms of the formula: $Su = 0.06Ds^{1.1}$.

Accordingly, the vertical basement uplift for Ds = 30 km at the Shoemaker impact structure would be 1.91 km — a value close to that estimated from the stratigraphic thickness. A revised relationship based on the study of 24 impact structures (Grieve and Pilkington, 1996) is: $Su = 0.086Ds^{1.03}$.

Thus, the central uplift value for Shoemaker impact structure would be 2.84 km. However, the above formulas are deduced mostly from the study of impact structures formed in layered rocks. In so far as different relations may pertain to the rebound of basement plugs, comparisons between the Shoemaker impact structure and centrally plugged impact structures such as Strangways (Northern Territory; Shoemaker and Shoemaker, 1996), Woodleigh (Carnarvon Basin; Mory et al., 2000), Vredefort (South Africa; Therriault et al., 1997) and Araguinha (Brazil; Von Engelhardt et al., 1992) are more pertinent (Table 4).

The calculated vertical movement of central uplift at the Shoemaker impact structure (2.84 km) exceeds the inferred stratigraphic thickness at the impact site (2 – 2.3 km) by about 550 m, but is less than the displacement suggested by the gravity model value (4–5 km; Plescia, 1999). Assuming the stratigraphic estimate is correct, this calculation would place an upper limit of 550 m on the amount of erosion of the basement plug. The inferred density differences at depths greater than 2 – 2.3 km may be due to fracturing of the basement underlying the central granitoid uplift.

As shown in Table 1.1, the morphometric parameters of the Shoemaker impact structure and the Strangways

* Research School of Earth Sciences, Australian National University, Canberra, A.C.T.

Table 1.1. Morphometric parameters of impact structures containing basement uplift plugs

Impact structure, location	*Reference*	*Age (Ma)*	*Ds (km)*	*Du (km)*	*model Dum (km)*	*model Su (km)*	*Du/Ds*	*Su/Du*	*Ts (km)*
Strangways, Northern Territory	Shoemaker and Shoemaker (1996)	646 ± 42	26	11	8.6	2.5	0.42	0.23	–
Shoemaker, Earaheedy Basin, Western Australia	This study	?568–694	30	12	9.9	2.8	0.4	0.24	>2.3
Araguinha, Brazil	Von Engelhardt et al. (1992)	247	42	4	14	4.0	0.095	1.0	>0.5
Woodleigh, Carnarvon Basin, Western Australia	Mory et al. (2000)	364 ± 8	120	25	41	12	0.21	0.48	>3.6
Vredefort, Orange Free State, South Africa	Therriault et al. (1993)	2023 ± 4	300	54	104	30.6	0.18	0.57	>11

NOTES: Ds: overall structural diameter
Du: diameter of basement uplift
Dum: model diameter of basement uplift; $Dum = 0.13Ds^{1.02}$
Su: vertical structural uplift (model $Su = 0.086\ Ds^{1.03}$)
Ts: minimum sedimentary thickness overlying the basement–cover unconformity and penetrated by the impact

SOURCE: Grieve and Pilkington (1996)

impact structure are very similar. In contrast, the ratios between the diameter of the central basement uplift and the overall structure (Du:Ds) at Woodleigh, Vredefort, and Araguinha are lower by factors of about 2 to 4. The ratios between the calculated vertical uplift (Su) and the observed diameter of the basement plug (Du) are higher at Woodleigh and Vredefort by about a factor of 2 compared to the Shoemaker and Strangways impact structures. Because the central basement uplifts have a cone-shaped structure, the lower Du:Ds ratios of the larger Woodleigh and Vredefort structures conceivably correspond to the greater sedimentary thicknesses (Ts) pierced by the basement plugs, with consequent narrowing of their cross sections (Du).

References

CORNER, B., REIMOLD, W. U., BRANDT, D., and KOEBERL, C., 1997, Morokweng impact structure, Northwest Province, South Africa: geophysical imaging and shock petrographic studies: Earth and Planetary Science Letters, v. 146, p. 351–364.

FRENCH, B. M., 1998, Traces of catastrophe — a handbook of shock-metamorphic effects in terrestrial meteorite impact structures: Houston, Lunar and Planetary Science Institute, LPI Contribution No. 954, 120p.

GRIEVE, R. A. F., and PILKINGTON, M., 1996, The signatures of terrestrial impacts: Australian Geological Survey Organisation, Journal of Australian Geology and Geophysics, v. 16, p. 373–376.

HILDEBRAND, A. R., PENFIELD, G. T., KRING, D. A., PILKINGTON, M., CAMARGO, A., JACOBSEN, S. B., and BOYNTON, W. V., 1991, Chicxulub crater, a possible Cretaceous/Tertiary boundary impact crater on the Yucatan Peninsula, Mexico: Geology, v. 19, p. 867–871.

MORY, A. J., IASKY, R. P., GLIKSON, A. Y., and PIRAJNO, F., 2000, Woodleigh, Carnarvon Basin, Western Australia: a new 120 km-diameter impact structure: Earth and Planetary Science Letters, v. 177 (1–2), p. 119–128.

PILKINGTON, M., and GRIEVE, R. A. F., 1992, The geophysical signature of terrestrial impact craters: Reviews of Geophysics, v. 30, p. 161–181.

PLESCIA, J. B., 1999, Gravity signature of the Teague Ring Impact Structure, Western Australia: Geological Society of America, Special Paper 339, p. 165–175.

REIMOLD, W. U., KOEBERL, C., BRANDSATTER, F. J., KRUGER, F. J., ARMSTRONG, R. A., and BOOTSMAN, C., 1999, Morokweng impact structure, South Africa: petrographic and isotopic results and implications for the size of the structure: Geological Society of America, Special Paper 339, p. 61–90.

SHARPTON, V. L., MARIN, L. E., CORRIGAN, C. M., and DRESSLER, B. O., 1997, Impact deposits from the southern inner flank of the Chicxulub impact basin: Lunar and Planetary Science Contribution, v. 922, p. 53–54.

SHOEMAKER, E. M., and SHOEMAKER, C. S., 1996, The Proterozoic impact record of Australia: Australian Geological Survey Organisation, Journal of Australian Geology and Geophysics, v. 16, p. 379–398.

THERRIAULT, A. M., GRIEVE, R. A. F., and REIMOLD, W. U., 1997, Original size of the Vredefort Structure: implications for the geological evolution of the Witwatersrand basin: Meteoritics and Planetary Sciences, v. 32, p. 71–77.

VON ENGELHARDT, W., MATTHAI, ST K., and WALZEBUCK, J., 1992, Araguahinha impact crater, Brazil: 1. The interior part of the uplift: Meteoritics and Planetary Science, v. 27, p. 442–457.

WILLIAMS, G. E., SCHMIDT, P. W., and BOYD, D. M., 1996, Magnetic signature and morphology of the Acraman impact structure, South Australia: Australian Geological Survey Organisation, Journal of Australian Geology and Geophysics v. 16, p. 431–442.

Appendix 2

Scanning electron microscopy and energy dispersive spectrometric study of the Teague Granite

by

A. Y. Glikson*

Scanning electron microscopy (SEM) and energy dispersive spectrometric (EDS) analyses were carried out on three samples of Teague Granite (GSWA 152612, 152613 and 152614) from the Shoemaker impact structure, over areas of up to 6 mm^2.

Energy dispersive spectrometry analyses (EDS) were conducted on the Jeol6400 at the Research School of Biological Studies, Australian National University. The study included reconnaissance X-ray mapping at centimetre scale, involving semi-quantitative EDS scanning of element concentrations of more than about 0.5% (Brink, 1993). In this method, X-ray counts are read at 15 KeV accelerating voltage, with spectra collection time of 80 seconds (~120 seconds real time) at about 8000 cps. Semi-quantitative whole-rock analysis was performed by scanning analyses over areas ranging from 40 × 50 µm to 140 × 200 µm. Spot analyses were carried out with an approximately 1 µm-size beam. Accuracy and precision were monitored using reference standards by Astimex Scientific Limited MINM25-53 (Serial Number 95-050). Estimate of precision values (standard deviation of replicate within-grain analyses) for the different elements in different minerals are as follows: SiO_2: 0.15 – 0.44%; Al_2O_3: 0.16 – 0.19%; MgO: 0.11 – 0.42%; FeO: 0.12 – 0.24%; MnO: 0.11% (almandine); NiO: 0.15% (olivine); CaO: 0.03 – 0.20%; Na_2O: 0.07% (albite); K_2O: 0.01 (albite); BaO: 0.48%; SO_3: 0.24%. Estimates of accuracy, expressed in percentage of the amount present, not including abundances near detection limits, are: SiO_2: 0.4 – 2.0%; Al_2O_3: 0.33 – 0.60%; MgO: 0.2 – 2.5%; FeO: 1.96 – 13%; CaO: 0.69 – 2.95%; Na_2O: 1.1%; BaO: 0.2%; SO_3: 1.8% (Tables 2.1, 2.2, and 2.3).

These analyses reveal local whole-rock compositions consistent with altered, very low calcium, potassium-rich to sodium-rich material of syenitic composition, with very high differentiation indices (DI > 87), low colour indices (CI < 3.7), and low An (An < 13.26). Silica is intermediate to low, as reflected by the presence of normative corundum in GSWA 152612. Feldspar and mica analyses are presented in Tables 2.2 and 2.3 respectively. Details for each sample examined are given below.

* Research School of Earth Sciences, Australian National University, Canberra, A.C.T.

Table 2.1. Scanning electron microscope and energy dispersive spectrometric analyses of areas less than 6 mm^2 of the Teague Granite

Rock type	*Alkali-feldspar granite*		*Quartz syenite*		*Syenite*	
GSWA sample	*152612/1*	*152612/2*	*152613/1*	*152613/2*	*152614/1*	*152614/2*
			Percentage			
SiO_2	65.4	68.05	79.45	74.33	66.10	64.84
TiO_2	0.11	0.06	0.12	0.11	0.09	0.15
Al_2O_3	20.74	19.27	11.14	14.96	18.40	19.09
FeO(t)	0.63	0.60	0.64	0.122	0.52	1.42
MnO	–	0.05	0.12	–	–	–
CaO	2.03	1.79	0.25	0.31	0.49	0.26
Na_2O	7.73	6.89	4.21	6.23	6.290	5.45
K_2O	2.36	3.08	4.05	3.81	6.89	8.67
P_2O_5	0.49	–	–	–	–	–
CIPW norm						
Qz	7.83	11.53	39.11	22.71	0.76	–
C	2.96	1.34	–	0.03	–	0.27
Or	13.96	18.20	23.92	22.50	40.69	51.21
Ab	65.40	58.33	34.75	52.69	53.24	43.47
An	6.83	8.90	–	1.53	1.62	1.30
Differentiation index	87.20	88.06	97.78	97.90	94.68	96.11

Table 2.2. Scanning electron microscope and energy dispersive analyses of feldspars from the Teague Granite

Rock type	*Alkali-feldspar granite*		*Quartz syenite*		*Syenite*	
GSWA *sample*	*152612/1*	*152612/2*	*152613/1*	*152613/2*	*152614/1*	*152614/2*
			Percentage			
SiO_2	64.62	64.43	4.80	64.69	68.42	63.86
TiO_2	0.18	0.30	0.12	0.11	0.09	0.15
Al_2O_3	18.63	18.96	18.55	18.61	20.07	18.59
FeO(t)	–	–	–	–	–	1.25
CaO	–	0.07	–	–	0.27	–
Na_2O	0.29	1.51	0.23	0.32	11.01	0.40
K_2O	16.27	14.72	16.42	16.38	0.23	15.83

GSWA 152612

GSWA 152612 contains K-feldspar, albite, quartz, mica, hydrated iron oxide, and zircon. Normatively the rock is dominated by Ab (58–65%) and has moderate Or (14 – 18.2%), and low Qz (7.8 – 11.53%). The high Al_2O_3 (19.27 – 20.74%) in part reflects micaceous alteration products and this is represented by normative corundum (1.3 – 2.96%) in two analyses (Table 2.1). The rock may be termed 'altered sodium-rich quartz syenite', but is probably a desilicified metasomatized granitoid–fenite.

GSWA 152613

GSWA 152613 contains K-feldspar, albite, quartz, mica (with exsloved iron-oxide lamella), hydrated iron oxide, and zircon. Normatively, the rock has higher Qz (22.71 – 39.11%) than the other samples, and has Ab:Or ratios of about 1.5 to 2.5. The rock may be termed albite–K-feldspar–quartz syenite, and may represent a lesser degree of metasomatism and desilicification of an original granitoid relative to GSWA 152612.

GSWA 152614

GSWA 152614 contains K-feldspar, albite, altered mica, and chlorite, and zircon. Normatively, the rock has similar Ab and Or abundances to the other samples and little or no Qz. The rock can be defined as an albite–K-feldspar syenite, and may represent a metasomatized granitoid.

Table 2.3. Scanning electron microscope and energy dispersive spot analyses of biotites from the Teague Granite

Rock type	*Alkali-feldspar granite*	*Quartz syenite*
GSWA sample	*152612*	*152613*
	Percentage	
SiO_2	41.36	48.85
TiO_2	2.79	0.85
Al_2O_3	16.88	29.83
MnO	0.29	0.15
FeO	18.22	6.27
Na_2O	0.24	0.18
K_2O	9.38	11.18

Reference

BRINK, F. J., 1993, A review of X-ray mapping: Melbourne, Victoria, La Trobe University (unpublished report).

Appendix 3

^{40}Ar–^{39}Ar analyses of K-feldspar separates from samples GSWA 152613 and 152614, Shoemaker impact structure

by

D. Phillips*

Introduction

This appendix describes ^{40}Ar–^{39}Ar analytical results obtained on K-feldspar separates from two samples (GSWA 152613 and 152614) from the Shoemaker impact structure, Western Australia, supplied by F. Pirajno of the Geological Survey of Western Australia (GSWA). The objective of the study was to provide constraints on the timing of the meteorite impact.

The Shoemaker impact structure is in the Earaheedy Basin and consists of upturned Earaheedy Group (Yelma and Frere Formation) rocks with a central uplift of Archaean basement (Pirajno and Glickson, 1998). The age of the Earaheedy Group sedimentary rocks range from 1950 to 1830 Ma, which provides a maximum age constraint for the timing of the impact event. Shoemaker and Shoemaker (1996) suggested that the impact may have occurred at c. 1630 Ma, based on whole-rock Rb–Sr analyses of quartz syenites from the central uplift (Bunting et al., 1980). A second Rb–Sr isochron age of c. 1260 Ma may represent an intense weathering event (Pirajno and Glickson, 1998).

Sample descriptions

Three granitoid samples containing K-feldspar were submitted to the Precise Radiogenic Isotope Services (PRISE), Australian National University, Canberra, for ^{40}Ar–^{39}Ar step-heating analyses. Examination of thin sections of the samples resulted in the selection of the two least altered samples (GSWA 152613 and 152614) for dating.

The two samples contain abundant medium-grained K-feldspar (microcline). The K-feldspar grains are somewhat turbid and variably altered, often exhibiting a reddish iron-oxide staining. GSWA 152613 contains the least altered feldspar grains. There is little evidence to suggest that the K-feldspar grains have been recrystallized as a result of impact; however, K-feldspar is characterized by a relatively low blocking temperature for argon diffusion (<250°C), and it is possible that heating during impact reset the argon isotopic systematics of the feldspar grains.

* School of Earth Sciences, University of Melbourne, Melbourne, Victoria.

Analytical procedures

Mineral separations and isotopic analyses were carried out at the Research School of Earth Sciences, Australian National University, Canberra. K-feldspar mineral separates were prepared using standard crushing, de-sliming, heavy liquid, and paramagnetic techniques. Several grains with relatively clear interiors were individually hand picked from each sample. The grains were washed in distilled water and acetone before being shipped for irradiation. Approximately 3 mg of each sample was wrapped in aluminium packets and placed into an aluminium irradiation canister together with interspersed aliquots of the flux monitor 77-600 (age = 414.2 Ma; MacDougall and Harrison, 1981). Packets containing degassed potassium glass were placed at either end of the canister to monitor the ^{40}Ar production from potassium. The irradiation canister was irradiated for 48 hours in position B2W of the SAFARI1 reactor in Pelindaba, Pretoria, South Africa. After irradiation, the samples were removed from their packaging and 0.1 – 0.3 mg aliquots were loaded into tin foil packets for analysis. The samples were individually dropped into a tantalum resistance furnace and heated to progressively higher temperatures, with temperatures maintained for 15 minutes per step. ^{40}Ar–^{39}Ar step-heating analyses were carried out on a VG MM12 mass spectrometer using an electron multiplier detector. Mass discrimination was monitored by analyses of standard air volumes. Correction factors (Phillips et al., 1998) for interfering reactions are as follows:

- $(^{36}Ar/^{37}Ar)_{Ca} = 3.20 (\pm 0.01) \times 10^{-4}$;
- $(^{39}Ar/^{37}Ar)_{Ca} = 7.5 (\pm 0.3) \times 10^{-4}$;
- $(^{40}Ar/^{39}Ar)_{K} = 0.035 (\pm 0.005)$.

The K:Ca ratios were calculated as follows:
$K/Ca = 1.90 \times {}^{39}Ar/{}^{37}Ar$.

The reported data have been corrected for system backgrounds, mass discrimination, radioactive decay, and fluence gradients. Errors associated with the age determinations are one sigma (1σ) uncertainties and exclude errors in the J-value estimates. The error on the J-value is ± 0.4%, excluding the uncertainty in the age of 77-600 hornblende (which is about 1%). Decay constants are those of Steiger and Jager (1977). The ^{40}Ar–^{39}Ar dating technique is described in detail by MacDougall and Harrison (1999).

Table 3.1. ^{40}Ar–^{39}Ar analytical data for feldspar from the Teague Granite

Temperature (°C)	*Cumulative ^{39}Ar*	*$^{40}Ar/^{39}Ar$*	*$^{37}Ar/^{39}Ar$*	*$^{36}Ar/^{39}Ar$*	*Volume ^{39}Ar × 10^{-15}mol*	*% Atmospheric ^{40}Ar*	*Ca/K*	*$^{40}Ar^*/^{39}Ar$*	*Age (Ma)*	*± 1 s.d. (Ma)*
GSWA 152613 K-feldspar										
Mass = 0.25 mg										
J-value = 0.02474 ± 0.00010										
650	0.008	85.84	0.0081	0.0071	0.637	97.5	0.0154	83.72	2 024	6
700	0.017	43.53	0.0002	0.0026	0.706	98.2	0.0003	42.74	1 301	5
750	0.033	46.95	0.0053	0.0012	1.247	99.2	0.0101	46.57	1 383	5
800	0.059	48.75	0.0012	0.0007	2.020	99.5	0.0037	48.52	1 423	3
850	0.093	51.42	0.0002	0.0006	2.595	99.6	0.0004	51.20	1 476	3
900	0.143	52.94	0.0003	0.0012	3.887	99.3	0.0006	52.55	1 502	5
950	0.191	54.30	0.0004	0.0012	3.763	99.3	0.0007	53.91	1 529	5
1 000	0.235	55.63	0.0101	0.0020	3.396	98.9	0.0193	55.02	1 550	3
1 050	0.291	57.77	0.0003	0.0015	4.363	99.2	0.0005	57.28	1 592	3
1 100	0.382	61.38	0.0045	0.0012	7.076	99.4	0.0085	60.99	1 659	4
1 150	0.547	64.39	0.0005	0.0012	12.840	99.4	0.0009	63.99	1 712	4
1 150	0.652	65.74	0.0001	0.0009	8.147	99.6	0.0003	65.45	1 737	4
1 200	0.793	68.10	0.0025	0.0007	10.940	99.6	0.0047	67.84	1 777	3
1 225	0.926	71.59	0.0001	0.0011	10.350	99.5	0.0002	71.23	1 833	6
1 250	0.986	78.36	0.0021	0.0013	4.703	99.5	0.0040	77.94	1 938	6
1 275	0.996	80.72	0.0135	0.0058	0.765	97.8	0.0257	78.97	1 954	8
1 325	0.999	86.24	0.0090	0.0184	0.275	93.7	0.0172	80.76	1 981	13
1 400	1.000	144.48	0.0569	0.2254	0.028	53.9	0.1081	77.86	1 937	27
GSWA 152614 K-feldspar										
Mass = 0.15 mg										
J-value = 0.02470 ± 0.00010										
650	0.009	156.28	0.0251	0.0148	0.187	97.2	0.0477	151.87	2 811	4
700	0.022	34.78	0.0105	0.0058	0.253	95.0	0.0199	33.03	1 076	4
750	0.039	35.30	0.0190	0.0064	0.348	94.6	0.0361	33.38	1 085	6
800	0.060	38.36	0.0094	0.0029	0.436	97.7	0.0178	37.48	1 182	4
850	0.079	43.30	0.0109	0.0030	0.367	97.9	0.0208	42.39	1 292	4
900	0.095	45.55	0.0151	0.0033	0.331	97.8	0.0287	44.56	1 339	6
950	0.113	45.54	0.0008	0.0031	0.357	97.9	0.0015	46.39	1 377	4
1 000	0.136	46.26	0.0084	0.0021	0.478	98.6	0.0160	44.60	1 340	4
1 050	0.171	47.43	0.0169	0.0049	0.694	96.9	0.0322	45.95	1 368	6
1 100	0.241	48.09	0.0130	0.0032	1.420	98.0	0.0246	47.11	1 392	5
1 125	0.326	48.25	0.0193	0.0036	1.715	97.7	0.0366	47.15	1 393	7
1 150	0.444	49.20	0.0106	0.0012	2.395	99.2	0.0201	48.80	1 427	5
1 175	0.598	50.67	0.0121	0.0014	3.100	99.1	0.0230	50.24	1 456	5
1 200	0.769	53.38	0.0039	0.0018	3.459	99.0	0.0073	52.82	1 506	4
1 225	0.922	58.69	0.0078	0.0018	3.097	99.0	0.0147	58.12	1 606	4
1 250	0.989	72.58	0.0027	0.0022	1.354	99.1	0.0052	71.89	1 842	8
1 300	0.998	74.22	0.0022	0.0162	0.177	93.5	0.0042	69.40	1 801	7
1 400	1.000	200.32	0.2930	0.4552	0.047	32.8	0.5568	65.81	1 741	51

NOTES: Errors are one sigma (1σ) uncertainties and exclude uncertainties in the J-value
Data are corrected for mass spectrometer backgrounds, discrimination, and radioactive decay
Interference corrections are: $(^{36}Ar/^{37}Ar)_{Ca}$ = 3.2E–4; $(^{39}Ar/^{37}Ar)_{Ca}$ = 7.54E–4; $(^{40}Ar/^{39}Ar)_{K}$ = 3.50E–2
J-value is based on an age of 414.2 Ma for 77-600 hornblende monitor
$^{40}Ar^*$ = radiogenic ^{40}Ar
s.d. = standard deviation

^{40}Ar–^{39}Ar step-heating results

Analytical results for GSWA 152613 and 152614 are presented in Table 3.1 and displayed in Figure 3.1.

GSWA 152613

A 0.25 mg hand-picked aliquot of K-feldspar from this sample was step-heated in 14 increments (Fig. 3.1a). The resulting age spectrum is discordant, with apparent ages generally increasing with increasing temperature, from 1301 ± 5 Ma to a maximum of 1981 ± 13 Ma. The old apparent age associated with the lowest temperature step is due either to the release of excess ^{40}Ar from fluid inclusions hosted by the feldspar grains or to recoil loss of ^{39}Ar from micro-structurally complex feldspar. This apparent 'age' (2024 ± 6 Ma) has no age significance. The pattern exhibited by the remaining increments is consistent with partial argon loss, caused by thermal overprinting. If correct, this result implies crystallization of the feldspar before 1840 Ma and partial resetting at some time after 1300 Ma.

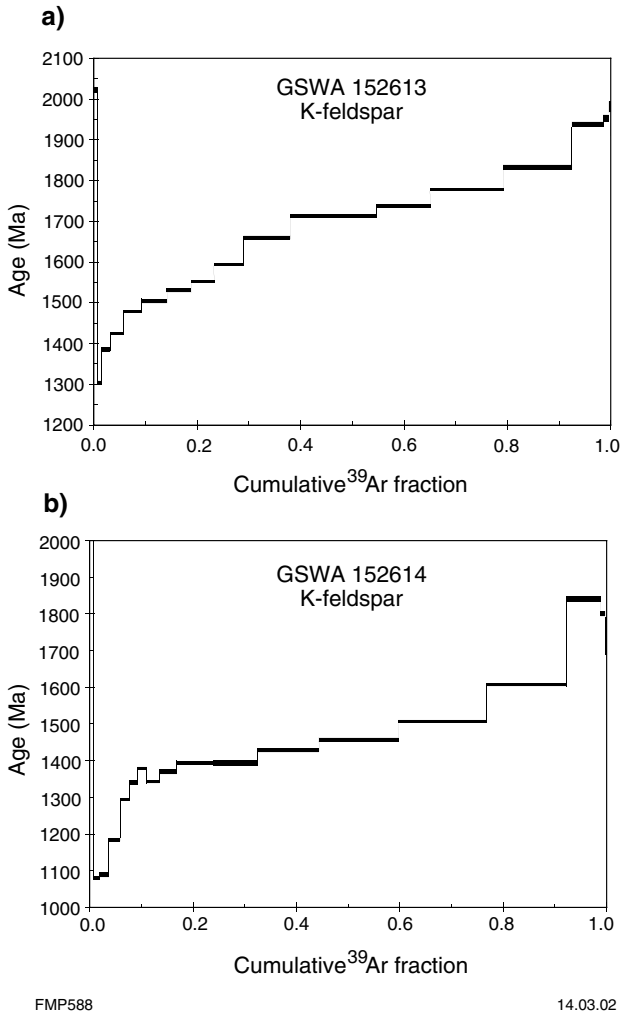

Figure 3.1. ^{40}Ar–^{39}Ar step-heating results for GSWA 152613 and 152614

GSWA 152614

A 0.15 mg K-feldspar separate from this sample was analysed in 18 heating increments (Fig. 3.1b). The age spectrum obtained is again discordant, with apparent ages increasing from 1076 ± 4 Ma to a maximum of 1842 ± 8 Ma. As above, the old apparent age associated with the lowest temperature step is due either to the release of excess ^{40}Ar from fluid inclusions hosted by the feldspar grains or to recoil loss of ^{39}Ar from micro-structurally complex feldspar. The remainder of the spectrum suggests extensive resetting of the feldspar argon isotopic systematics by a thermal event. If all argon loss is due to impact heating, then the current results imply overprinting before 1100 Ma. However, the feldspar grains from this sample are more altered than those from the previous sample, suggesting that some portion of the low-temperature loss could be due to more recent alteration or ?weathering.

Discussion

The two K-feldspar samples exhibit similarly disturbed apparent age spectra indicative of partial argon loss due to a thermal overprinting event. The fact that the oldest apparent ages (>1950 Ma) are older than the inferred time of formation of the Earaheedy Basin (1950–1830 Ma) suggests that the partial resetting event is likely to be impact heating. Despite the high temperatures associated with meteorite impact events, impact heating is of very short duration and may not totally reset the argon isotopic systematics of affected minerals. This situation has been observed in some rocks associated with the Vredefort impact structure in South Africa and is not totally unexpected.

The possibility that alteration or weathering is responsible for a portion of the low-temperature argon loss associated with GSWA 152614 complicates efforts to constrain the timing of meteorite impact. The data from GSWA 152613 suggest that the impact occurred earlier than 1.3 Ga, while that from GSWA 152614 raises the possibility of the event being even younger (younger than 1.1 Ga). Therefore, the current data provide only broad constraints for the upper limit of the time of meteorite impact at younger than 1.3 Ga. There is no evidence of a 1.6 Ga 'event' as implied by some of the Rb–Sr data, suggesting that this 'age' could represent a mixed age.

Recommendations

If the K-feldspar data reflect partial resetting due to impact heating at some time after 1.3 Ga, then fission track analyses may yield additional information. Alternatively, other feldspar samples from areas that may have experienced more severe heating should be sought for further ^{40}Ar–^{39}Ar studies. Ideally, samples that have experienced complete recrystallization during impact heating would provide the best estimates for the time of meteorite impact.

References

BUNTING, J. A., de LAETER, J. R., and LIBBY, W. G., 1980, Evidence for the age and cryptoexplosive origin of the Teague Ring structure, Western Australia: Western Australia Geological Survey, Annual Report 1980, p. 125–129.

MacDOUGALL, I., and HARRISON, T. M., 1981, Geochronology and thermochronology by the $^{40}Ar/^{39}Ar$ method (1st edition): New York, Oxford University Press.

MacDOUGALL, I., and HARRISON, T. M., 1999, Geochronology and thermochronology by the $^{40}Ar/^{39}Ar$ method (2nd edition): New York, Oxford University Press.

PHILLIPS, D., MACHIN, K. J., KIVIETS, G. B., ROBERTS, M. A., SKINNER, E. M. W., and FOURIE, L. F., 1998, A petrographic and $^{40}Ar/^{39}Ar$ geochronological study of the Voorspoed kimberlite, South Africa: implications for the origin of Group II kimberlite magmatism: South African Journal of Geology, v. 101 (4), p. 299–306.

PIRAJNO, F., and GLIKSON, A. Y., 1998, Shoemaker impact structure, Western Australia: Celestial Mechanics and Dynamical Astronomy, v. 69, p. 25–30.

SHOEMAKER, E. M., and SHOEMAKER, C. S., 1996, The Proterozoic impact record of Australia, *in* Australian impact structures *edited by* A. Y. GLIKSON: Australian Geological Survey Organisation, Journal, v. 16, p. 379–398.

STEIGER, R. H., and JAGER, E., 1977, Subcommission on geochronology: Convention on the use of decay constants in geo- and cosmochronology: Earth and Planetary Science Letters, v. 36, p. 359–362.

Appendix 4

K–Ar age dating of illite–smectite

by

T. Uysal*

Method

To prepare a sample for separation of the clay-sized fraction, rock chips were gently crushed to sand-sized particles followed by disaggregation in distilled water using an ultrasonic bath. Different clay-sized fractions were obtained by centrifugation.The decanted clay suspension was placed on a glass slide. Following the X-ray diffraction (XRD) analysis of air-dried samples, the oriented clay-aggregate mounts were placed in an ethylene-glycol atmosphere at 30–40°C overnight prior to additional XRD analysis. These analyses were performed on a Philips PW1130 XRD unit operated at 40 kV and 40 mA at a scanning rate of 1°2θ/min with CuKα radiation.

The argon isotopic composition was determined by isotope dilution using ^{38}Ar as a tracer. Mineral separates were fused in a molybdenum crucible under vacuum, using a radio-frequency generator positioned around the crucible and enclosing vacuum line. The gases produced were purified by getters and analysed on a VG Gas Analysis 8-80 mass spectrometer operated in the static mode at 2 kV accelerating voltage. The extraction and purification line together with samples were baked under vacuum for at least 12 hours at 100°C to remove absorbed argon of atmospheric origin. Ages were calculated from data corrected for machine mass discrimination and system blanks using the decay constants of Steiger and Jäger (1977). The K_2O content of the samples was determined using an inductively coupled plasma optical emission spectrometer (ICP-OES), with accuracy better than 1%. The errors include all uncertainties in the measurement of the isotope ratios and potassium contents. Argon isotopic results were controlled by analysing international GLO-glauconite standard, with averages of 11.13×10^{-10} mole/g (n = 6; cf. 11.09×10^{-10} mole/g).

* Stable Isotope Geochemistry Laboratory, Department of Earth Sciences, The University of Queensland, Brisbane, Queensland 4072.

Results

The results are presented in Table 4.1.

GSWA 152614 contained an insiginificant amount of feldspar and therefore the illite–smectite age (568 ± 20 Ma) of this sample is considered more reliable.

Reference

STEIGER, R. H., and JAGER, E., 1977, Subcommission on Geochronology: convention on the use of decay constants in geochronology and cosmochronology: Earth and Planetary Science Letters, v. 36, p. 359–362.

Table 4.1. K–Ar analytical data

Sample number	*Grain size*	*Mineralogy*	*K_2O wt%*	*^{40}Ar rad. (%)*	*Age*
SIS-13	<0.5 µ	Illite–smectite, feldspar	1.57	48.15	694 ± 25
GSWA 152614	<0.5 µ	Illite–smectite, illite	1.09	30	568 ± 20

NOTE: ^{40}Ar rad. (%) = percent radiogenic ^{40}Ar

The Shoemaker impact structure is about 110 km northeast of Wiluna, on the southern margin of the Palaeoproterozoic Earaheedy Basin. The structure is about 30 km in diameter, deeply eroded, and consists of a ring syncline and a ring anticline with a core of Archaean granite–greenstone rocks that is interpreted as the central uplift. The structure is well defined by circular aeromagnetic anomalies and a negative Bouguer gravity anomaly coincident with the central uplift. The geophysical data also suggest that the original diameter of the structure could have been 45–50 km. The age of the Shoemaker structure is not well constrained, but dating of the Teague Granite in the central uplift indicates a maximum age of c. 1300 Ma (Ar–Ar) and a minimum age of c. 568 Ma (K–Ar). Shock metamorphic features include shatter cones and planar deformation features in quartz crystals. Rocks on the eastern rim of the structure exhibit pervasive to nonpervasive hydrothermal alteration, such as quartz veining and silicification.

Further details of geological publications and maps produced by the Geological Survey of Western Australia can be obtained by contacting:

Information Centre
Department of Mineral and Petroleum Resources
100 Plain Street
East Perth WA 6004
Phone: (08) 9222 3459 Fax: (08) 9222 3444
www.mpr.wa.gov.au

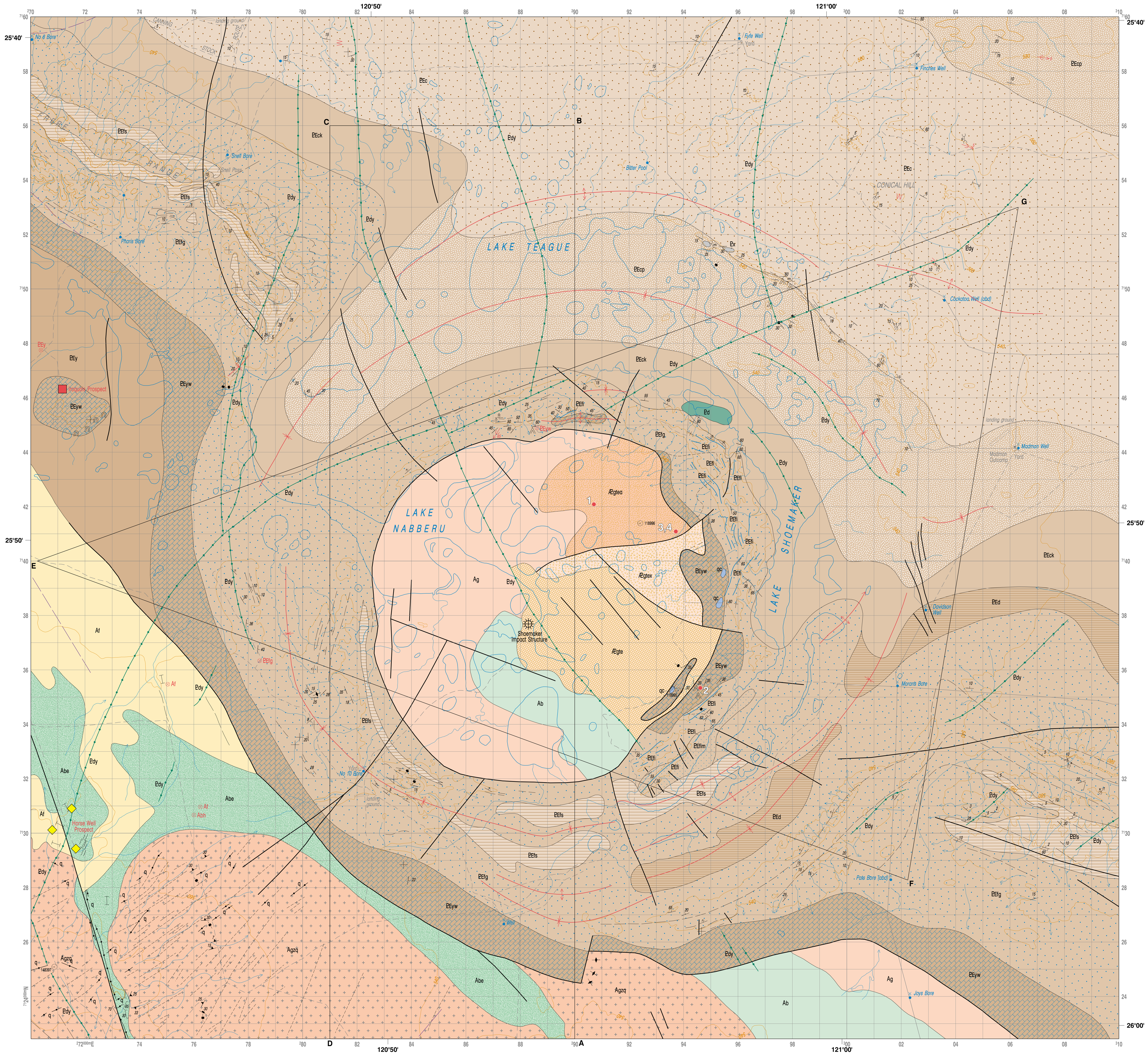

SCALE 1:100 000

1000 0 1 2 3 4 5 6 7 8 9 10
Metres Kilometres

BLOCK DIAGRAMS

Not to scale. Oblique profiles foreshortened

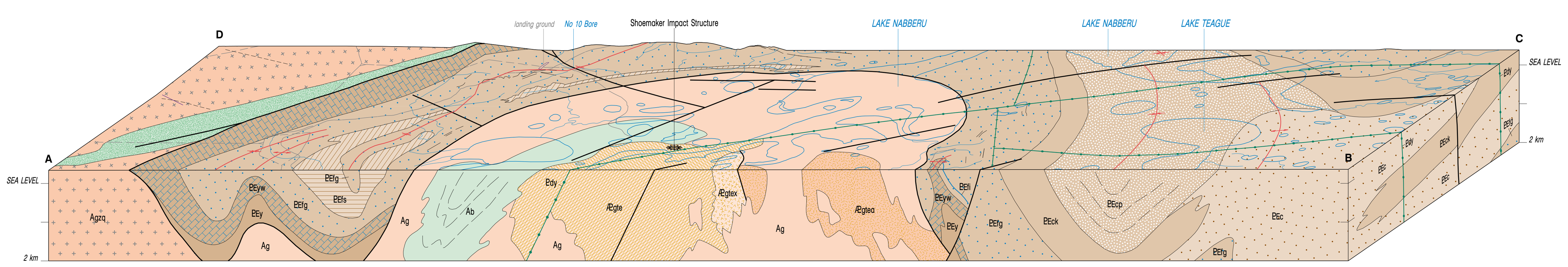

Vertical exaggeration of surface profile V/H = 5

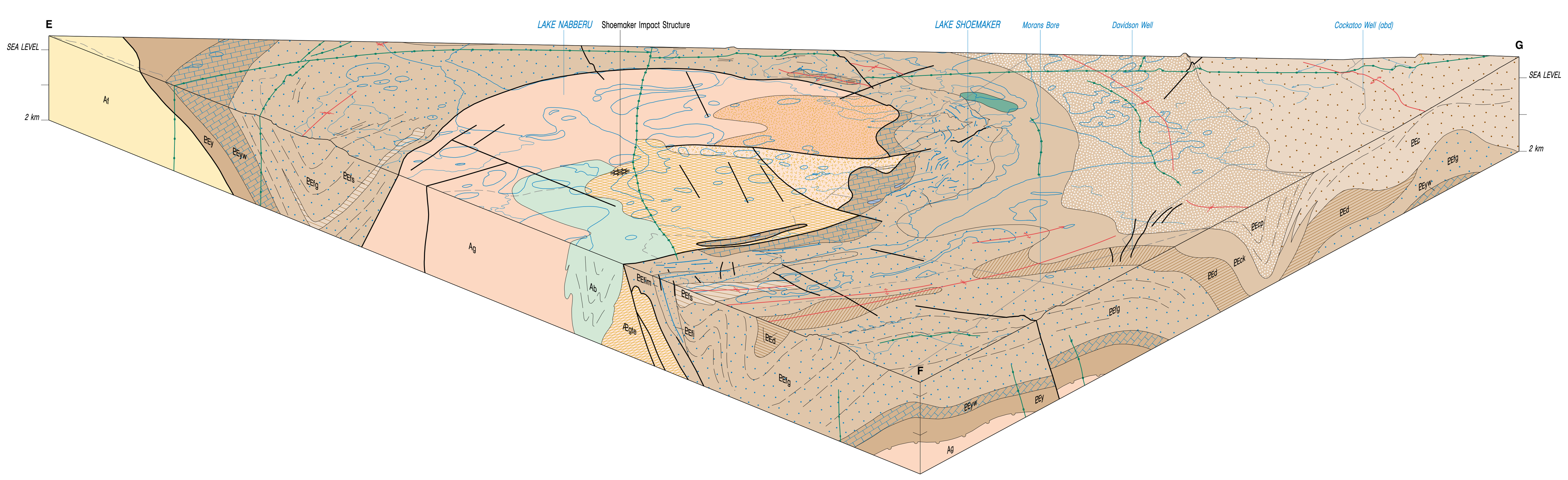

Vertical exaggeration of surface profile V/H = 5 — Unconformity

q — Quartz vein

qc — Hydrothermal chert pod; uncertain age

PROTEROZOIC — PALAEOPROTEROZOIC

- Pdy — Mafic dyke; interpreted from aeromagnetic data
- Pd — Dolerite sill
- Px — Megabreccia; probably reworked impact allochthonous breccia; predominantly sandstone clasts

Earaheedy Group — EARAHEEDY BASIN

Miningarra Subgroup

- PEc — **CHIALL FORMATION:** quartzose sandstone and interbedded siltstone
  - PEcp — **Princess Ranges Member:** sandstone and minor siltstone
  - PEck — **Karri Karri Member:** laminated shale and siltstone
- PEd — **WINDIDDA FORMATION:** laminated siltstone and shale

Tooloo Subgroup

- PEfg — **FRERE FORMATION:** granular iron-formation, in places peloidal, with interbedded shale bands
  - PEfs — Shale and siltstone
  - PEfi — Supergene-enriched granular iron-formation
  - PEfim — Granular iron-formation; locally with magnetite-rich ironstone of possible hydrothermal origin
- **YELMA FORMATION**
  - PEyw — **Sweetwaters Well Member:** stromatolitic and cryptalgal banded dolomite (*Asperia digitata, Ephyaltes edigunensis, and Pilbara deverella*); minor chert breccia and chert layers derived from stromatolitic dolomite; locally with cross-bedded sandstone
  - PEy — Sandstone, shale, and siltstone

c. 2648[1] Ma

ARCHAEAN — YILGARN CRATON

TEAGUE GRANITE: Archaean granite (*c.* 2648 Ma) altered by post-impact metasomatism during the Palaeoproterozoic

- ÆPgte — Leucocratic alkali granite, locally silicified
- ÆPgtex — Quartz–microcline–albite granite; brecciated and locally silicified, locally with pseudotachylite veinlets and planar deformation features on quartz crystals
- ÆPgtea — Quartz–albite–orthoclase(–aegirine–augite–garnet) granite, locally with pseudotachylite veinlets and planar deformation features on quartz crystals

c. 2648[1] Ma
c. 2664[1] Ma

- Ag — Granitoid rock, generally monzogranite; undivided
- Agzq — Hornblende–quartz monzonite
- Af — Metamorphosed felsic volcanic rock
- Ab — Metamorphosed mafic and ultramafic rock; undivided
- Abe — Metabasalt with epidote, garnet–epidote, or clinopyroxene–epidote–chlorite alteration
- Abh — Quartz–actinolite hornfels (subsurface only)

Geological boundary
- exposed
- concealed

Fault
- concealed
- concealed, position uncertain

Strongly foliated rock

Fold
- anticline, showing trend direction, exposed
- syncline, exposed
- syncline, concealed
- mesoscale folding

Small-scale fold axis, showing trend and plunge
- anticline
- syncline

Bedding, showing strike and dip
- inclined
- vertical
- horizontal
- strike and dip estimated from aerial photography
  - 0–15°
  - 15–45°
  - trend of bedding

Palaeocurrent, showing trend and sense of direction
- from fluting, direction known
- from asymmetrical ripple marks, direction known
- from cross-bedding, direction known
- from current lineation, direction not known
- from megaripple marks, direction not known

Metamorphic foliation, showing strike and dip
- inclined
- vertical

Cleavage, showing strike and dip
- inclined
- vertical

Fracture or joint, showing strike and dip
- inclined
- vertical

Airphoto lineament
- unspecified
- fracture pattern in granitoid rock

Aeromagnetic lineament

Meteorite impact structure

Shatter cone

Stromatolite fossil locality

Isotopic age determination site with identification number — 148397

Field site location for photographic samples

Track

Fence, generally with track

Yard

Breakaway

Contour line, 20 metre interval — 540

Watercourse with ephemeral pool

Lake

Bore, well — Bore, Well

Windpump

Subsurface data from drillhole, costean, or shallow shaft — PEy

Mineral occurrence or prospect
- Stratabound sedimentary mineralization — lead, zinc
- Vein and hydrothermal mineralization — gold
- Sedimentary — calcrete and uranium

Outcrops of Teague Granite

Shatter cone in chert of the Yelma Formation

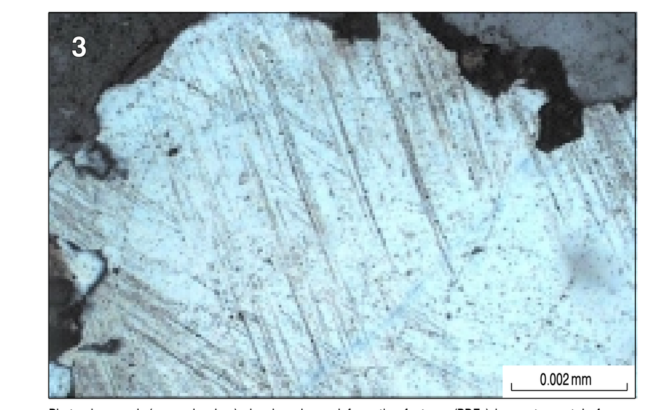

Photomicrograph (crossed polars) showing planar deformation features (PDFs) in quartz crystal of Teague Granite

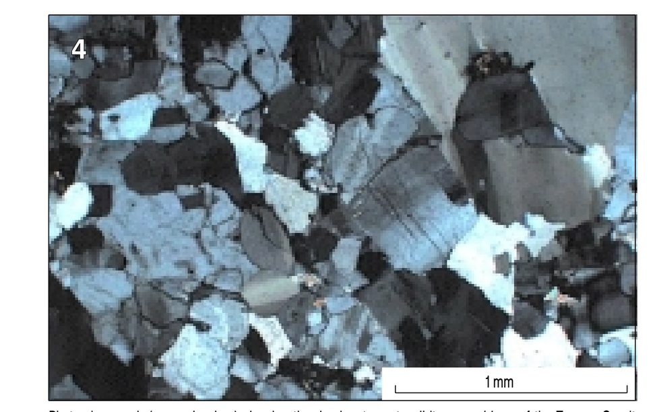

Photomicrograph (crossed polars) showing the dominant quartz–albite assemblage of the Teague Granite

AERIAL OBLIQUE VIEW LOOKING SOUTH

View looking south at an elevation of approximately 1000 metres above ground level

LANDSAT THEMATIC MAPPER MOSAIC — BANDS 1, 2, 3, 4, 5, 7. Date of imagery: 1 June 1997

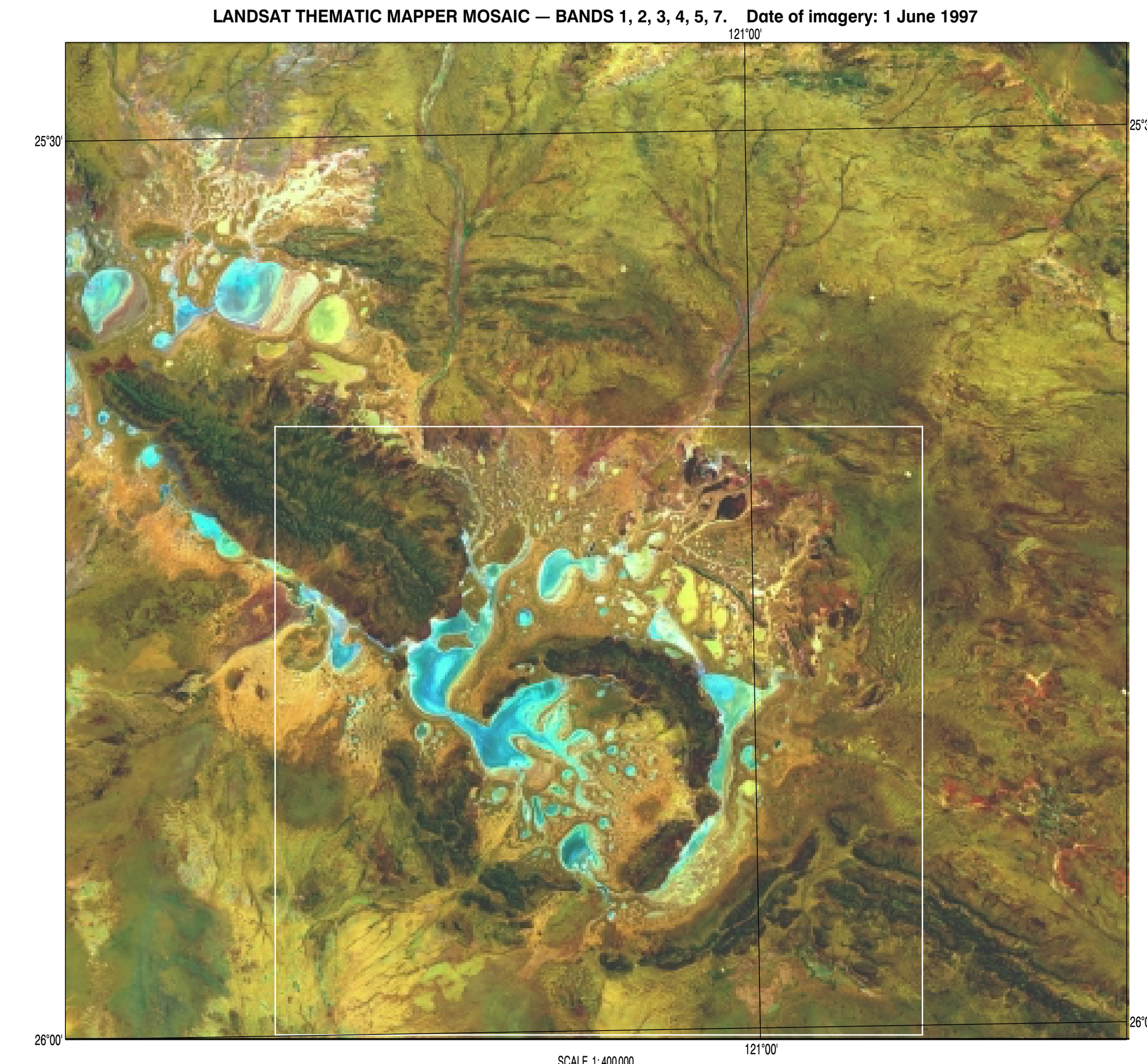

SCALE 1:400 000
0 10 20
Kilometres

SIMPLIFIED OUTCROP GEOLOGY

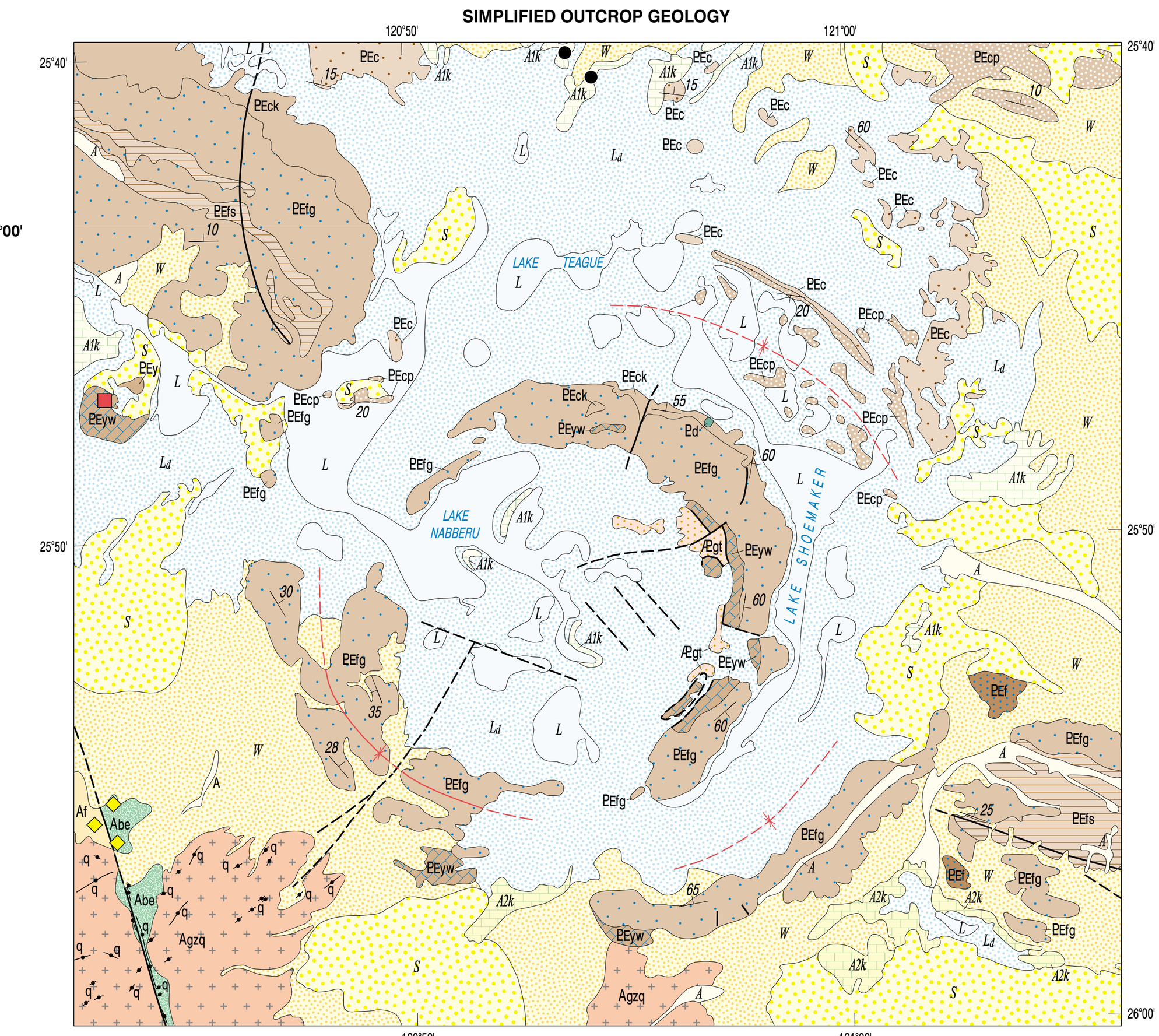

SCALE 1:250 000
0 5 10
Kilometres

PHANEROZOIC — CAINOZOIC — QUATERNARY

- W — Sheetwash deposits
- A — Alluvium
- A1k — Calcrete
- L — Lacustrine deposits in playa lakes
- Ld — Sand dunes, minor gypsiferous and saline beds
- S — Sandplain and dunes
- A2k — Calcrete

q — Quartz vein

PROTEROZOIC — PALAEOPROTEROZOIC

- Pd — Dolerite

Earaheedy Group — EARAHEEDY BASIN

- PEc — Chiall Formation
  - PEcp — Princess Ranges Member
  - PEck — Karri Karri Member
- PEf — Frere Formation
  - PEfg — Granular iron-formation
  - PEfs — Siltstone, shale, and minor chert
- Yelma Formation:
  - PEyw — Sweetwater Well Member
  - PEy — Sandstone, shale, and stromatolitic carbonate

ARCHAEAN — YILGARN CRATON

- ÆPgt — Teague Granite, undifferentiated
- Agzq — Hornblende-quartz monzonite
- Abe — Metabasalt with epidote alteration
- Af — Metamorphosed felsic volcanic rock

TOTAL MAGNETIC INTENSITY IMAGE — AGSO–GSWA 1996

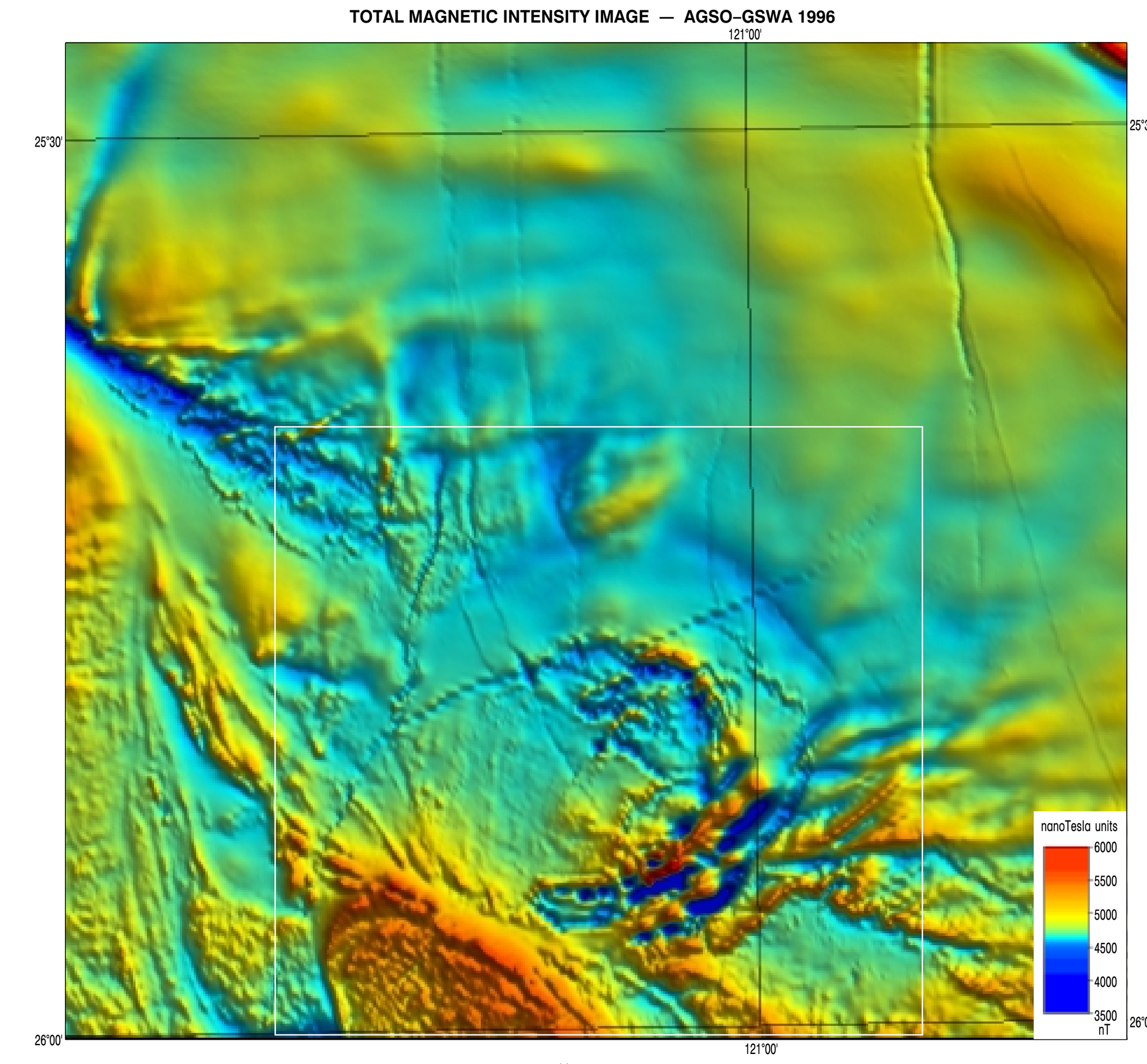

SCALE 1:400 000
0 10 20
Kilometres

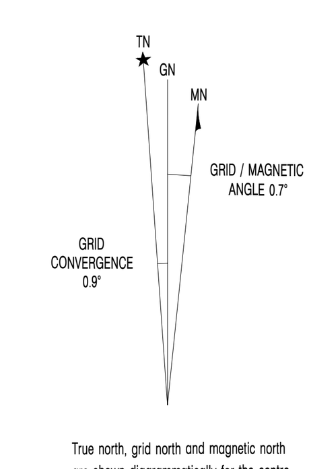

True north, grid north and magnetic north are shown diagrammatically for the centre of the map. Magnetic north is correct for 2001 and moves easterly by about 0.1° in 3 years.

Geology by F. Pirajno and J. A. Jones 1998

Compiled by F. Pirajno, 2000

Geochronology by: (1) D. R. Nelson, 1997, GSWA Record 1997/2

Edited by D. Ferdinando and G. Loan

Cartography by S. Collopy, S. Coldicutt, and B. Williams

Topography from the Department of Land Administration Sheet SG 51-5, 3046, SG 51-5, 3146, SG 51-9, 3045, and SG 51-9, 3145 with modifications from geological field survey

Landsat imagery supplied by Remote Sensing Services, Department of Land Administration

Published by the Geological Survey of Western Australia. Digital and hard copies of this map are available from the Information Centre, Department of Minerals and Energy, 100 Plain Street, East Perth, WA, 6004. Phone (08) 9222 3459, Fax (08) 9222 3444

Printed by Frank Daniels Pty. Ltd., Western Australia

The recommended reference for this map is:
PIRAJNO, F., 2001, Interpreted geology of the Shoemaker impact structure (1:100 000 scale), in Shoemaker Impact Structure, Western Australia Geological Survey, Report 82, plate 1.

SHEET INDEX

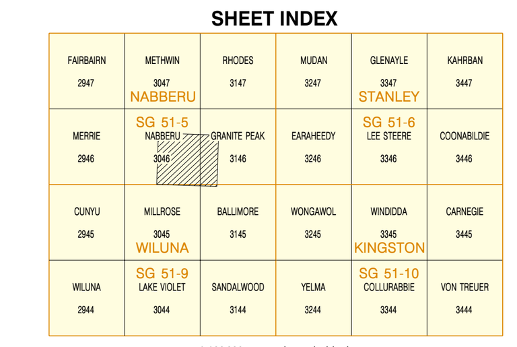

1:100 000 maps shown in black
1:250 000 maps shown in brown

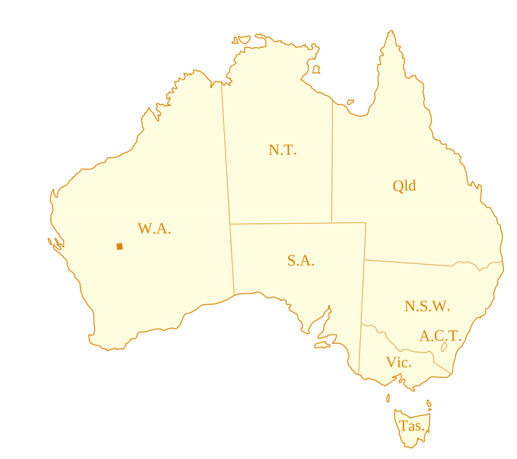

DEPARTMENT OF MINERALS AND ENERGY
L. C. RANFORD, DIRECTOR GENERAL

GOVERNMENT OF WESTERN AUSTRALIA
CLIVE BROWN, M.L.A.
MINISTER FOR STATE DEVELOPMENT; TOURISM; SMALL BUSINESS; GOLDFIELDS–ESPERANCE

GEOLOGICAL SURVEY OF WESTERN AUSTRALIA
TIM GRIFFIN, DIRECTOR

SCALE 1:100 000

1000 0 1 2 3 4 5 6 7 8 9 10
Metres Kilometres

UNIVERSAL TRANSVERSE MERCATOR PROJECTION
HORIZONTAL DATUM: GEOCENTRIC DATUM OF AUSTRALIA 1994
VERTICAL DATUM: AUSTRALIAN HEIGHT DATUM

Grid lines indicate 1000 metre interval of the Map Grid Australia Zone 51

The Map Grid Australia (MGA) is based on the Geocentric Datum of Australia 1994 (GDA94)
GDA94 positions are compatible within one metre of the datum WGS84 positions

Reference points to align maps based on the previous datum, AGD84, have been placed near the map corners

GEOLOGICAL SURVEY OF WESTERN AUSTRLIA
REPORT 82 PLATE 1

INTERPRETED GEOLOGY OF THE SHOEMAKER IMPACT STRUCTURE